UNRAVELING THE REGULATION MECHANISM OF NON-CODING SMALL RNA00203 ON BIOFILM FORMATION IN *ACINETOBACTER BAUMANNII*

GEBRELIBANOS DANIEL KAHASE

PhD

The Hong Kong Polytechnic University

2026

The Hong Kong Polytechnic University

Department of Health Technology and Informatics

Unraveling the regulation mechanism of non-coding small RNA00203 on biofilm formation in *Acinetobacter baumannii*

GEBRELIBANOS Daniel Kahase

A thesis submitted in partial fulfilment of the requirements for the degree of Doctor of Philosophy

August 2025

CERTIFICATE OF ORIGINALITY

I hereby declare that this thesis is my own work and that, to the best of my knowledge and belief, it reproduces no material previously published or written, nor material that has been accepted for the award of any other degree or diploma, except where due acknowledgement has been made in the text.

_____ (Signed)

Gebrelibanos Daniel Kahase (Name of student)

Abstract

Acinetobacter baumannii is the most prevalent and clinically relevant member of the *A. baumannii* complex and a priority pathogen for the search for new antimicrobials. Biofilm formation and antimicrobial resistance are the key attributes that enable the bacterium to circulate within healthcare institutions. Moreover, biofilm-related infections usually tend to be chronic and refractory to antibiotic treatments and immune responses, complicating patient management. To disarm the biofilm, a deep understanding of its regulatory dynamics is crucial. In our previous work, we demonstrated that a novel regulatory small RNA00203 (sRNA00203) plays a major role in biofilm formation and biofilm-related antimicrobial resistance in *A. baumannii* ST1894. However, the underlying regulatory networks remain unexplored. Thus, the current study aims to (1) identify genome-wide influenced genes and pathways by sRNA00203; (2) identify and validate the primary target mRNAs of sRNA00203 in biofilm cells, and (3) identify proteins that potentially interact with sRNA00203.

We conducted comparative transcriptomics and proteomics studies on the sRNA00203 deletion mutant and wild-type *A. baumannii* ST1894 strains to identify genes that are potentially influenced by sRNA00203. The results revealed that a total of 816 genes and 600 proteins were significantly influenced in biofilm cells (absolute value of log2 fold change ≥ 1, $q < 0.05$). Of the 816 differentially expressed genes in the sRNA00203-deleted strain, 406 were upregulated and 410 were downregulated. Functional annotation showed that major facilitator superfamily efflux pump, type IV pili(T4P), quorum sensing, and iron acquisition systems were repressed. In contrast, genes related to ribosomal proteins, Csu pili, Ade IJK efflux pumps, and porins (CarO type IV, OmpW, and OmpH) were induced. Whole-cell proteome analysis reaffirmed consistent findings, with the exception of the ribosomal proteins and Csu pili. Remarkably, the genes that encode the protein translocase subunit SecE and UDP-3-O-(3-hydroxymyristoyl) glucosamine N-acyltransferase (*lpxD*) were found to be influenced at the translation level. Phenotypically, the majority of the sRNA-deleted strain displayed a reduction of T4P under transmission electron microscope.

The combined omics studies uncovered the genome-wide potential targets of sRNA00203, but could not distinguish the base-pairing primary targets. To address this gap, we designed a tag-based RNA-RNA interactome capture assay. The 24-nucleotide tag was integrated into sRNA00203 through PCR, and a tagged sRNA00203-expressing strain was constructed using Gibson assembly. Then, using tag antisense sequences as biotin-labelled riboprobes, we were able to retrieve the bound RNA from the tagged sRNA00203-expressing strain and sRNA00203-overexpressing (control) biofilm cell lysate. RNA-seq of the retrieved RNA revealed significant enrichment of 219 genes. Of these genes, genes encoding Class I SAM-dependent methyltransferase (E5A72_RS16120), preprotein translocase subunit SecE, and lipid A hydroxylase LpxO were confirmed to bind at predicted sites with sRNA00203 by electrophoretic mobility shift assay (EMSA).

To further investigate the involvement of chaperone proteins in the regulatory process of sRNA0203, we performed an RNA-protein pulldown assay using *A. baumannii* biofilm cell lysate. The retrieved proteins were subjected to label-free proteomics. We observed that 32 of the 155 identified proteins were differentially expressed (DEPs) between sRNA00203 and control RNA. Predominantly, proteins such as ribosomal proteins, RNA polymerase subunit, and elongation factors were included in the DEPs, which are annotated as RNA-binding proteins. The known sRNA-modulating chaperone proteins like Hfq and CsrA were not significantly enriched. Instead, UPF0234 protein and chaperone protein DnaK were identified as putative sRNA00203 binding proteins.

Collectively, this study explores regulatory circuits of the novel sRNA00203 for the first time. The sRNA promotes biofilm formation in *A. baumannii* by inducing the formation of pili, a secretion system, cell wall components, and iron acquisition pathways. Besides, sRNA00203 expression also negatively influences the expression of efflux pumps and porins, which may in turn alter susceptibility of *A. baumannii* to antimicrobial agents in the biofilm state. The biofilm-related genes such as E5A72_RS16120, *secE*, and *lpxO* have been confirmed to interact directly with the sRNA. Furthermore, the regulatory process mediated by the sRNA00203 could potentially be independent of the Hfq chaperone protein. However, new candidate interacting proteins identified in this study could facilitate the sRNA to act on the target mRNAs.

Publications

1. **Daniel Kahase GEBRELIBANOS**, Abebe Mekuria SHENKUTIE, Franklin Wang CHOW, Polly Hang Mei LEUNG. Integrated transcriptomic and proteomic investigation of biofilm cells elucidated genome-wide targets of novel non-coding small RNA00203 in *Acinetobacter baumannii.* (Prepared manuscript for submission).
2. Abebe Mekuria SHENKUTIE, **Daniel Kahase GEBRELIBANOS**, Mianzhi Yao, Gadissa Bedada Hundie, Franklin Wang CHOW, Polly Hang Mei LEUNG. (2023). Impairment of novel non-coding small RNA00203 inhibits biofilm formation and reduces biofilm-specific antibiotic resistance in *Acinetobacter baumannii*. *International Journal of Antimicrobial Agents*, 62(3), 106889.

Presentation

1. **Daniel Kahase GEBRELIBANOS**, Abebe Mekuria SHENKUTIE, Franklin Wang CHOW, Polly Hang Mei LEUNG. Influence of non-coding small RNA00203 in biofilm cells of *Acinetobacter baumannii*: Transcriptomic and phenotypic. Oral Presentation, 35th European Congress of Clinical Microbiology and Infectious Diseases (ESCMID) Global 2025, held from 11-15 April 2025, Vienna, Austria.

Acknowledgements

I would like to express my immense gratitude to my supervisor, Prof. Polly Leung, for her unwavering support since I contacted her to pursue my Ph.D. study. Her constant, insightful feedback and invaluable mentorship have played a pivotal role in my PhD journey.

I would also like to thank my co-supervisor, Dr. Franklin Chow, for providing valuable guidance and support on the experimental setup.

I want to deliver my warmest appreciation to Prof. Polly's research team members, namely Dr. Abebe Mekuria SHENKUTIE, Mr. ZHANG Zhipeng, Mrs. Ayesha, Ms. ZHANG Jiaying, Mr. Tilaye Shibbiru MENGISTU, Mr. Abera Abdeta KITABA, Mr. Tadesse Lejisa GAROMSA, Ms. JIANG Bei, Dr. Ying NI, and Mr. ZHENG Zhihang, for their insightful discussions on experiment outcomes.

I am also grateful to Department of Health Technology and Informatics, the Hong Kong Polytechnic University, for providing a conducive academic environment, and the Hong Kong PhD Fellowship Scheme of the Research Grants Council, Government of the Hong Kong Special Administrative Region, China, for providing valuable resources to support my study.

My heartfelt thanks go to my wife (Eskedar Demssie) and my mother (Abrhatsion Tesfayohannes), brothers, and sisters, whose patience, understanding, and constant motivation have been the foundation of my accomplishments.

Above all, I am deeply grateful to Almighty God for his blessings, guidance, and strength in every phase of my life.

Table of Contents

List of Figures

List of Tables

List of Abbreviations

AHL	N-acyl homoserine lactone
AMR	Antimicrobial resistance
cDNA	Complementary DNA
CLSI	Clinical Laboratory Standard Institute
DEG	Deferentially expressed gene
DEP	Differentially expressed protein
DNA	Deoxyribonucleic acid
EPS	Extracellular polymeric substance
FPKM	Fragments per kilobase per million base pairs
GO	Gene ontology
HCAI	Healthcare-associated infections
ICU	Intensive care unit
KEGG	Kyoto Encyclopedia of Genes and Genomes
LPS	Lipopolysaccharide
MBC	Mutant biofilmcells cell
MBEC	Minimum biofilm eradication concentration
MBIC	Minimum biofilm inhibition concentration
MDR	Multi-drug resistance
MFS	Major facilitator superfamily
MIC	Minimum inhibitory concentration
MPC	Mutant planktonic cell
OMP	Outer membrane protein
PBS	Phosphate-buffered saline
PCR	Polymerase Chain Reaction
QS	Quorum sensing
RNA	Ribonucleic acid
RND	Resistance-nodulation-cell division
SDS	Shine-Dalgarno sequence
sRNA	Small RNA
T4P	Type four pili
TCSs	Two-component systems
TEM	Transmission electron microscopy
TFs	Transcription factors
WBC	Wild-type biofilm cell
WPC	Wild-type planktonic cell

1. Introduction

1.1 Properties of *Acinetobacter baumannii*

Acinetobacter is an aerobic, gram-negative, and rod-shaped bacterium. The organism lacks oxidase activity, displays positive catalase reaction, does not produce indole, utilizes citrate as a carbon source, and is both non-motile and non-fermentative (Kurcik-Trajkovska, 2009; Peleg et al., 2008).

As of 2021, the genus *Acinetobacter* encompasses 144 species, with only 68 validly named (Qin et al., 2021). Species categorized in the *Acinetobacter calcoaceticus–Acinetobacter baumannii* complex are priority pathogens of healthcare-associated infections (HCAI) (Howard et al., 2012). The complex includes five clinically important species: *Acinetobacter baumannii*, *A. pittii*, *A. nosocomialis*, *A. seifertii*, and *A. dijkshoorniae*. Additionally, there is a species named *A. calcoaceticus* that is not significantly associated with human disease (Vijayakumar et al., 2019). Among the five species, *A. baumannii* has the highest clinical significance (Harding et al., 2018). Unlike the medically less important *Acinetobacter* spp., the natural habitat of *A. baumannii* is still undefined (Novović & Jovčić, 2023). Reports indicate occasional identification of *A. baumannii* from soil, vegetables, surface water, lice (Antunes et al., 2014; Peleg et al., 2008), and paleosol (Hrenovic et al., 2014). The isolation of the pathogen from the environmental samples was predicted to be due to contamination from health care institutions, infected humans, and animals (Antunes et al., 2014; Peleg et al., 2008).

1.2 Clinical significance of *A. baumannii*

Due to the widespread utilization of broad-spectrum antibiotics, presence of implantable devices, and the presence of immunocompromised patients, *A. baumannii* has become endemic in healthcare settings nowadays (M.-F. Lin, 2014). The ability of *A. baumannii* to retain virulence and form biofilms, along with its high propensity for incorporating foreign genetic materials into its genome, further enhances its endemicity (Antunes et al., 2014; Chapartegui-González et al., 2018).

A. baumannii caused nearly 2% of healthcare-associated infections in Europe and USA (D. Wong et al., 2017). Globally, the pathogen contributed to 20% of all infections that occurred in the intensive care units (ICUs) (J. Kim et al., 2017). The most predominant types of

infections are ventilator-associated pneumonia and bloodstream infections, which are associated with high mortality rates (Antunes et al., 2014). Apart from the lungs and bloodstream, *A. baumannii* also causes infections in other body tissues, including meninges, skin, and urinary tract. The overall mortality irrespective of the infection site is 54% in ICUs and 5% in general medical wards (Bianco et al., 2016).

Furthermore, the infection burden is higher when the infection is caused by an antimicrobial-resistant *A. baumannii* isolate. In 2019, *A. baumannii* was estimated to be responsible for over 300,000 deaths worldwide, with a significant association with antimicrobial resistance (AMR) (Murray et al., 2022). In addition, the mortality rate of nosocomial pneumonia caused by multidrug-resistant (MDR) bacteria was reported to be 43% (Mohd Sazlly Lim et al., 2019).

Although *A. baumannii* mainly causes HCAI, the pathogen is also responsible for community-acquired infections. Such types of infections primarily occur in individuals with co-morbidities such as diabetes mellitus and chronic lung diseases. Community-acquired pneumonia caused by *A. baumannii* presents a fulminant disease course characterized by an immediate onset of fever and multi-organ failure, resulting in a mortality rate of over 60% (Dexter et al., 2015; Morris et al., 2019).

1.3 Virulence determinants and pathogenesis of *A. baumannii*

In recent years, significant efforts have been devoted to understanding the complex factors leading to the pathogenesis of *A. baumannii*. Unlike other nosocomial bacterial species, such as *E. coli* and *P. aeruginosa,* with specific molecular determinants or toxins responsible for diseases, pathogenesis of *A. baumannii* is attributed to multiple factors acting together to cause infection (Mea et al., 2021). Indeed, tracing out each underlying mechanism or confirming the putative virulence factors for disease causation remains elusive.

Virulence determinants are attributes that enable a bacterium to adhere, enter a host, evade host defenses, acquire micronutrients from the environment, multiply in a host, and sense alterations in the surroundings (Casadevall & Pirofski, 2009). *A. baumannii* possesses a wide array of virulence factors comprising outer membrane proteins, glycoconjugates, protein secretion systems, along with several other molecular factors known for their role in

pathogenicity and survival within its ecological niche (Tiku, 2022). The following subsections elaborate on the contributions of the main virulence factors to pathogenesis.

1.3.1 Porins

One of the key tools that enable *A. baumannii* to counteract harmful conditions imposed by the external environment and host, such as stress from antibiotics and immunological defense, is the presence of outer membrane proteins (OMPs). These proteins encompass various porin protein variants, including OprD, CarO, OmpA, Omp33-36, and Omp22, which are characterized as beta barrel-shaped outer membrane channel proteins (Tiku, 2022; Uppalapati et al., 2020).

Outer membrane protein A (OmpA) is considered a major porin protein that promotes bacterial adhesion to host cells and biofilm formation (Choi et al., 2005; Gaddy et al., 2009). Other factors, such as BapA and fimbrial-like protrusions, are also important in the adhesion of the pathogen (Uppalapati et al., 2020). Adhesion of *A. baumannii* to host cells is the priming stage in pathogenesis. Then, OmpA, after entering and localizing to the mitochondria, causes epithelial cells to undergo caspase 3-mediated mitochondrial fragmentation and apoptosis (Choi et al., 2005). Consistent with the diverse roles of OmpA, studies have demonstrated that substances targeting OmpA affect adhesion, motility (M. F. Lin, Tsai, et al., 2015), and biofilm formation of *A. baumannii* (Na et al., 2021). Furthermore, disruption of OmpA made the pathogen more susceptible to colistin (Parra-Millán et al., 2018).

The other type of porin protein with polymorphic variants found in *A. baumannii* is CarO, which is linked to ornithine transport, cell adherence, and carbapenem susceptibility (Uppalapati et al., 2020). The relationship between its expression and susceptibility is a subject of controversy. One suggestion is that CarO serves as a route for drug influx (Mussi et al., 2005), while other challenge this (Zahn et al., 2015). Additional OMPs such as OmpW and heat-modifiable protein HMP-AB also facilitate the transportation of β-lactams across the bacterial cytoplasmic membrane (M. H. yin Wong et al., 2019). However, the loss of CarO polypeptide resulted in an imipenem resistance phenotype (Limansky et al., 2002).

1.3.2 Polysaccharide capsule

Similar to other bacterial capsules, *A. baumannii* capsule is composed of a highly variable, hydrophilic exopolysaccharide, which offers protection of the bacterial cell against desiccation and disinfectants (Geisinger et al., 2019). Besides, the capsule is also responsible for immune evasion due to the presence of negative charges on the capsular surface and prevents the adherence of phagocytes to the bacterial cells (Cress et al., 2014; Harding et al., 2018).

The majority of *A. baumannii* strains possess capsules and have mucoid phenotypes, which are associated with multidrug resistance (Hu et al., 2020). On the other hand, non-capsular strains are more susceptible to peptide antibiotics(Geisinger & Isberg, 2015; Tiku, 2022), disinfectants, and are unable to survive inside the host based on a mouse model (Bjånes et al., 2024; Tipton et al., 2018).

1.3.3 Lipooligosaccharide

Lipopolysaccharide (LPS) is a major part of the gram-negative bacterial cell wall. LPS plays a vital role in the virulence and host fitness of Gram-negative bacteria. This component consists of the endotoxic lipid A unit, an oligosaccharide core, and a repetitive O-antigen unit (Lee et al., 2017). However, *A. baumannii* lacks the O-antigen component but possesses a similar immunogenic structure called lipooligosaccharide (LOS) (Harding et al., 2018). The endotoxic lipid A is the biosynthetic product of Lpx enzymes, which are encoded by the genes *lpxA*, *lpxC*, *lpxD*, *lpxH*, *lpxB*, *lpxK,* and *lpxM* (Powers & Trent, 2018). This anchor unit is the target for polymyxin E, the last-resort antibiotic for treating carbapenem-resistant pathogens (Harding et al., 2018). Modifications in the LOS are associated with resistance to colistin (Ko et al., 2023; Pelletier et al., 2013). Conversely, LOS-deficient isolate due to mutation in *lpxD* was reported to exhibit lower biofilm formation capability (Farshadzadeh et al., 2018).

During *A. baumannii* infections, the LOS, a known immunogenic component, plays a crucial role by interacting with the host immune system. LOS binds to toll-like receptor 4 (TLR4) along with CD14 on host immune cells, leading to activation of mitogen-activated protein kinase (MAPK) and nuclear factor kappa B (NF-κB). This further stimulates production of pro-inflammatory cytokines such as tumor necrosis factor-alpha (TNF-α), interleukin-1 beta (IL-

1β), interleukin-6 (IL-6), and chemokines like interleukin-8 (IL-8). Finally, the cytokines recruit and activate immune cells, resulting in inflammation and elimination of the organism (Chen, 2020; García-Patiño et al., 2017; F. J. Li et al., 2018). If *A. baumannii* can resist the clearance and multiply, it will cause septic shock in the host (D. Wong et al., 2017). However, strains lacking LOS have been reported to induce less production of these pro-inflammatory immune mediators (L. Lin et al., 2012).

1.3.4 Pili

The two adhesive filamentous appendages identified on *A. baumannii* surface are chaperone-usher (Csu) pili and type IV pili (Harding et al., 2018). Many of the *A. baumannii* strains possess the type I Csu pilus system. This system includes different pilin subunits, namely CsuA/B, CsuA, CsuB, CsuC, CsuD, and CsuE, each of which has distinct roles in the process of pilin polymerization at the outer membrane. These pilin subunits contribute substantially to the structural integrity and function of the pili (Ahmad et al., 2023; Harding et al., 2018). Csu pili play a role in attachment and biofilm formation on abiotic surfaces (Ahmad et al., 2023; Harding et al., 2018).

Type IV pili consist of major (PilA) and minor pilin (PIlW, PilE, and PilX) subunits, as well as other biogenesis machinery. Type IV pili are essential for twitching motility, natural competence, and adherence to epithelial cells (Ahmad et al., 2023; Harding et al., 2018). The major subunit PilA was shown to play a critical role in the adhesion of *A. baumannii* onto human A549 and Detroit 562 cell lines (Piepenbrink et al., 2016; Ronish et al., 2019). Apart from adhesion, C-terminal glycosylation of type IV pili subunit also facilitates evasion of host immunity via masking effect (Harding et al., 2018; Piepenbrink et al., 2016) and biofilm development (Tucker et al., 2014).

1.3.5 Iron metabolism and acquisition system

In order to survive inside the host, a pathogen must obtain iron and other essential metals from the invaded host. Virulence of *A. baumannii* is diminished if it lacks the capability to scavenge and metabolize iron and zinc within the host (Harding et al., 2018).

Iron is usually found in the host in the form of heme, ferritin, transferrin, and lactoferrin, which limit its free availability. During infection, *A. baumannii* utilizes several strategies to cope with the limited iron (Law & Tan, 2022). The primary way of scavenging iron is through

the release of a high-affinity iron-binding molecule named a siderophore. The gene cluster, *basA*-J is responsible for encoding enzymes that are involved in the biosynthesis of acinetobactin, which is the most prominent among the three forms of siderophore (fimsbactins A-F and baumannoferrins A and B) (Shapiro & Wencewicz, 2016). Disruption of some of these genes caused attenuation of *A. baumannii* survival in bacteremia and pneumonia animal models (Conde-Pérez et al., 2021; Sheldon & Skaar, 2020). However, fimsbactin and baumannoferrin mutant strains did not exhibit similar attenuation of virulence (Sheldon & Skaar, 2020). The isomerization forms of the acinetobactin enable it to function properly in a wide range of pH, including in serum (Shapiro & Wencewicz, 2016). All of this suggests acinetobactin as a critical virulence factor and a possible target for new therapy formulations (Conde-Pérez et al., 2021; Sheldon & Skaar, 2020).

Once chelated to the iron, the bacterium transports the siderophore-iron (III) complex into the cytoplasm via outer and inner membrane-associated receptors. Interruption in transportation has also been reported to reduce the survival rate of *A. baumannii* in murine and *Galleria mellonella* infection models. For instance, infection of the animal model with a BauA-deleted strain showed an 80% increase in survival compared to infection by parental strains (10%) (Conde-Pérez et al., 2021). In addition, the TonB3 mutant, among the three conserved TonB genes linked to iron transport found in *A. baumannii* isolates, demonstrated reduced pathogenicity (Runci et al., 2019).

1.3.6 Phospholipase

Gram-negative pathogens possess various classes of phospholipases that play a role in phospholipid catabolism. The release of these lipolytic enzymes can lead to cell membrane instability (Lee et al., 2017). Similarly, *A. baumannii* encodes phospholipase C and D enzymes that specifically target eukaryotic membranes. These enzymes have also been reported to contribute to iron acquisition by lysing erythrocytes, and their presence has been reported to be conserved in diverse strains (Morris et al., 2019). Consistent with these functions, studies have confirmed that the loss of the encoding gene results in impaired survival of the strain in human serum (Jacobs et al., 2010), invasion of host cells, and reduced virulence in animal models (Jacobs et al., 2010; Kareem et al., 2017; Stahl et al., 2015).

1.3.7 General secretory (Sec) system

Bacteria use general secretory (Sec), twin-arginine translocation (TAT) pathway, and secretion system type I up to VI to transport a variety of proteins across their cytoplasmic membrane. The proteins contribute to their survival, pathogenicity, and communication with other microbes (Jamali et al., 2025). Secretion systems have been identified in *A. baumannii*; specifically, the type II secretion system (T2SS) is found in the majority of its isolate genomes. The functions of this system are relatively well studied (P. Li et al., 2023; Weber et al., 2017). However, due to limited data in *A. baumannii*, most studies infer the role of the Sec pathway from other bacteria.

The Sec system, universally conserved in bacteria, is essential to export unfolded proteins through the cytoplasmic membrane (Gupta et al., 2024). This system comprises the SecB chaperone, SecA ATPase, and SecYEG translocon, which are coordinated to export the unfolded polypeptides across the inner membrane (IM) into the periplasm. The SecB is a chaperone protein that maintains preproteins in an unfolded state. It binds to nascent polypeptides and prevents their premature folding in the cytoplasm before they engage with SecA (Crane & Randall, 2017). Then, SecA, an ATPase, provides the energy needed for protein translocation through the SecYEG translocon. The SecYEG complex form is a membrane-embedded protein-conducting channel in the IM. Specifically, SecY forms the core channel, SecE stabilizes the complex, and SecG enhances translocation efficiency (Govindarajan & Amster-Choder, 2017; Jon Beckwith, 2013; Winkler et al., 2020). Finally, the processed proteins in the periplasm move across the outer membrane by type II or type V secretion system (Lucidi et al., 2023). The proteins secreted into the extracellular milieu have been reported to support *M. tuberculosis* survival in the human host (Miller et al., 2017) and to facilitate surface attachment and synthesis of matrix components in *S. mutans* biofilm (Huang et al., 2008).

1.4 Biofilm formation

Bacterial species can survive in the form of biofilm, a community of bacterial cells enclosed within a self-produced matrix of extracellular polymeric substance (EPS). Here, the bacterial cells adhere to one another and/or to a surface (Flemming et al., 2016). The transition of bacteria from a planktonic to biofilm lifestyle passes through different steps. A new model

has classified the steps into aggregation, maturation/growth, and disaggregation events, which may not occur sequentially (Sauer et al., 2022).

The well-established sessile life form enables a bacterium to survive under harsh conditions, potentially leading to persistent infections. Thus, biofilm formation is considered a potent virulence determinant (Zhao et al., 2023). Moreover, it has been reported that over 80% of chronic human infections are possibly caused by biofilm-forming bacteria (Chambers & Sauer, 2013).

Likewise, *A. baumannii* has the capacity to form biofilms on both tissue and abiotic surfaces. (Zeighami et al., 2019). Globally, more than half of the clinical isolates (65.63%) are biofilm formers, with strong biofilm formers accounting for 41.34% (Gedefie et al., 2023). This is largely attributed to the increasing prevalence of nosocomial infections caused by *A. baumannii*. Environmental factors (e.g., surface hydrophobicity, growth media, and temperature) and inherent features of the pathogen are important for initiating and sustaining the biofilm formation (Eze et al., 2018). Type I chaperone-usher pilus system (Csu pili), capsule, adhesin, biofilm-associated proteins (BapAb), repeats in toxins (RTX)-like domain-containing protein, poly-β-1,6-N-acetylglucosamine (PNAG), and autotransporter system are reported to be common inherent factors that facilitate biofilm formation in *A. baumannii* (Harding et al., 2018).

1.4.1 Stages of biofilm formation

The biofilm development of *A. baumannii* strains under the influence of hydrodynamic forces, which better simulate the natural environment, has been depicted in four stages (Feng et al., 2013). Based on these findings, the merged three-step cycle of *A. baumannii* includes cell adherence, growth, and maturation of biofilm, and finally dispersion (Figure 1.1).

The first stage of bacterial cell adherence of freely moving planktonic bacteria initiates biofilm formation by coming into contact with biotic and abiotic surfaces. This contact is usually maintained by non-specific physical forces, but bacterial cells can readily detach. After some time, cells accumulate, and bacterial appendages such as pili facilitate stable and irreversible adhesion by minimizing repulsive forces exerted (Garrett et al., 2008). Cease of motility, activation of quorum-sensing, increase in polysaccharide production, and cells

alignment along their axis are indicators of the shift from loose to irreversible surface attachment (Petrova & Sauer, 2012; Sauer et al., 2002).

Following irreversible attachment, bacterial biofilms grow and mature through surface proliferation and the production of more extracellular polymeric substance (EPS), forming microcolonies and three-dimensional structures (Ahmad et al., 2023; Barraud et al., 2015; Kaplan, 2010). Proteins, polysaccharides, lipids, and DNA of the EPS facilitate bacterial cohesion and gene expression, leading to the establishment of water channels for metabolic flux (Kaplan, 2010; Zhao et al., 2023). Lastly, detachment and relocation of planktonic cells to new surfaces (dispersion/disaggregation) occur. Dispersion is a crucial process in the survival of pathogens and disease transmission (Barraud et al., 2015). Signals from internal and external sources initiate the process, either passively through erosion or sloughing or actively through seeding and degrading of the biofilm matrix (Guilhen et al., 2017; Kaplan, 2010).

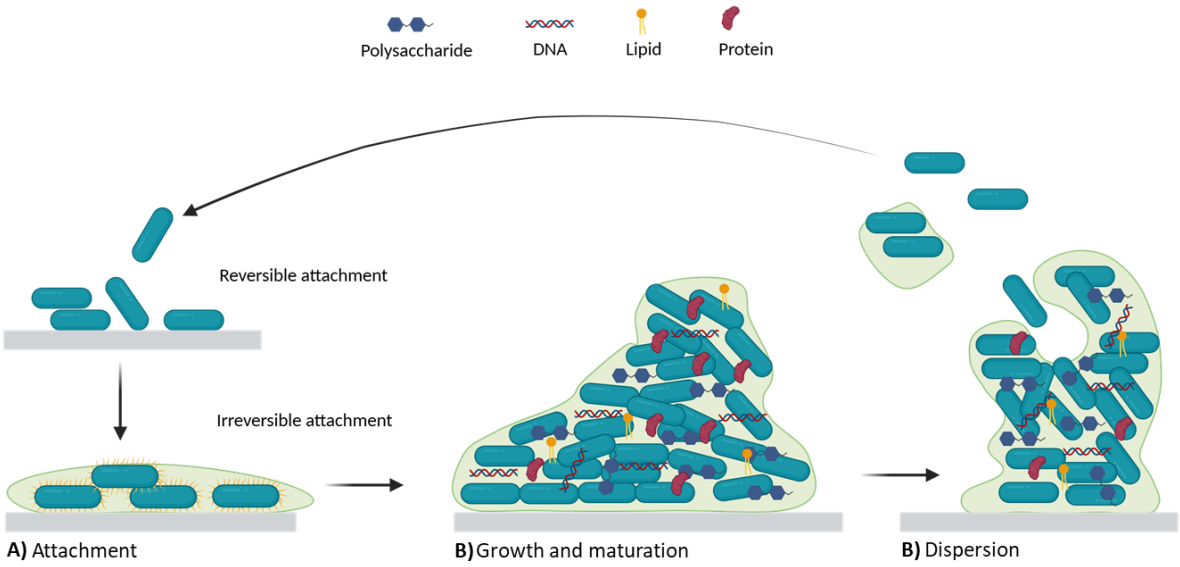

Figure 1.1 Diagrammatic illustration of the biofilm development lifecycle.
The process of biofilm formation primarily consists of three stages: (A) At the first stage, planktonic cells initially adhere reversibly to an abiotic/biotic surface. Then it proceeds to irreversible attachment, characterized by the firm adherence of cells through the use of pili, other surface structures, and polysaccharides. (B) Growth and maturation, during which the biofilm develops a complex, three-dimensional mountain-like structure with increased cell density and EPS accumulation. (C) Finally, during dispersion, cells or cell clusters are released

from the mature biofilm, allowing them to colonize new surfaces. EPS: extracellular polymeric substance. The Figure was modified from (Grygiel et al., 2024) using the Biorender tool.

1.4.2 Biofilm-related infections

National Institutes of Health of the USA notify that most microbial infections are linked with biofilms (Lewis, 2001). The infections tend to be chronic and refractory to antibiotics due to the bacterial sessile form of living, which is also often difficult to eliminate by the human immune effector cells. Potentially, biofilm causes device-related, non-device-related infections and biofilm-related device malfunction (Del Pozo, 2018; Jamal et al., 2018).

Although medical devices are indispensable in medicine, they are associated with a high risk of infections. For instance, in USA, device-associated infections account for 25.6% of all HCAI and implant-related biofilm infections, costing over one billion dollars for hospitalization annually (Magill et al., 2014; Rabih O. Darouiche, 2004). Contact lenses, mechanical heart valves, central venous catheters, peritoneal dialysis catheters, pacemakers, prosthetic joints, and urinary catheters are among the devices on which biofilms grow (Del Pozo, 2018; Jamal et al., 2018). The implants, once inserted into the body, are conditioned by body tissue and secretions, which can facilitate the adherence of planktonic bacteria and the establishment of well-structured bacterial communities (biofilm) (Donlan & Costerton, 2002). This consequently able to causes bloodstream infection, urinary tract infection, chronic wound infection, and ventilator-associated pneumonia (VAP) (Del Pozo, 2018; Jamal et al., 2018; Pompilio et al., 2021).

A. baumannii is one of the common pathogens isolated from device-related biofilm infections (Ciofu et al., 2022). For instance, examinations of catheter surfaces from ICU patients reveal dense adherence of the bacteria due to catheter indwelling for extended periods (Djeribi et al., 2012). It is not limited to attachment and may spread to sterile anatomic sites. Detachment of portions of biofilms from endotracheal tubes could reach the lungs via aspiration and exacerbate respiratory infections (Ferreira et al., 2016). Moreover, the biofilms exhibited high resistance rates to fluoroquinolones (up to 90%), third-generation cephalosporins (over 80%), and carbapenems (around 70%) (Mishra et al., 2024). These biofilms led to severe ventilator-associated pneumonia, with survival rates dropping

significantly in cases involving biofilm-producing strains compared to non-producers (Chukamnerd et al., 2024).

1.5 Underlying antimicrobial resistance mechanisms

The capacity of *A. baumannii* to acquire antibiotic resistance greatly enhances its capacity to thrive as a pathogen in medical settings. Many of the clinical isolates are resistant to multiple antimicrobial agents (M.-F. Lin, 2014). Thus, the World Health Organization categorizes this bacterial species as a priority for new antibiotic research and discovery (World Health Organization (WHO), 2017). The accumulation of underlying resistance mechanisms, such as the production of degrading and modifying enzymes, efflux pumps, impermeability, and alteration of antibiotic target sites, are the reasons for the limited antibiotic choices available for the management of infected patients (Lee et al., 2017; M.-F. Lin, 2014). Biofilm formation is also another layer of machinery to evade antibiotics in *A. baumannii* (Roy et al., 2022). These mechanisms broadly could be included in either acquired by horizontal gene transfer or intrinsic (Kyriakidis et al., 2021). The mechanisms are detailed below, and the summary is illustrated in Figure 1.2.

1.5.1 Production of degrading and modifying enzymes

The production of degrading enzymes, such as β-lactamases, is widely prevalent in gram-negative pathogens. These enzymes are classified based on protein homology into three serine-dependent classes (A, C, and D) and one zinc-dependent class (B, metallo-β-lactamases (MBLs)) (Queenan & Bush, 2007). *A. baumannii* possesses all the four classes of β-lactamases, which are the predominant resistance mechanism against β-lactam antibiotics (Jahan et al., 2021). Carbapenemases are a functional category that belongs to classes A, B, and D that can hydrolyze the β-lactam ring of carbapenems, penicillins, cephalosporins, and monobactams (Queenan & Bush, 2007).

Among the four classes, class D β-lactamases (OXA-type) are highly prevalent and the major way of carbapenem resistance in *A. bauamannii*. Five OXA-type categories, such as OXA-23, OXA-24/33/40, OXA-51, OXA-58, and OXA-134, are designated as carbapenemases (Périchon et al., 2014; M. H. yin Wong et al., 2019). A study has reported more than 90% of the clinical isolates of *A. baumannii* harbour OXA-23-like gene (Lowe et al., 2018). Another study has identified *blaOXA*–24 and *blaOXA*–58 as major contributors to carbapenem

resistance (M. H. yin Wong et al., 2019). Insertion sequences, such as ISAba9 and ISAba1, have been found to enhance the activity of the intrinsic *blaOXA*-51 and acquired *bla*OXA–23, respectively, by providing stronger promoter regions (Figueiredo et al., 2009; M. H. yin Wong et al., 2019).

Bacterial pathogens also release modifying enzymes that deactivate aminoglycosides, which is the prevailing resistance mechanism observed in clinical isolates against aminoglycoside antibiotics. These enzymes are categorized as *N*-acetyltransferases (AACs), nucleotidyltransferases (ANTs), and phosphotransferases (APHs). It is common for isolates to harbor multiple genes encoding the aminoglycoside-modifying enzymes (AMEs) (Serio et al., 2018). A similar situation is observed in *A. baumannii*. Studies have demonstrated that the *aph(3)-VIa* AME gene was predominantly identified in *A. baumannii* isolates from Egypt (Saleh et al., 2023) and Iran (Jouybari et al., 2021). Other AME genes, such as *ant(2")-Ia*, *aac(6')-Ib*, and *armA*, were also detected (Jouybari et al., 2021). The plasmid encoded AMEs AAC (6')-Ib-cr also appeared in modifying ciprofloxacin and norfloxacin (Kyriakidis et al., 2021). Regional variations exist in the distribution of AME genes within this pathogen (Saleh et al., 2023).

1.5.2 Efflux pumps

Gram-negative pathogens resist antibiotics through the direct extrusion of drugs using efflux pumps embedded in the cell membrane. Additionally, these proteins can indirectly reduce bacterial susceptibility to numerous antimicrobials by facilitating biofilm formation, quorum sensing, and a two-component system (Amaral et al., 2014). In *A. baumannii,* experimentally characterized efflux pumps, such as the resistance-nodulation-cell division (RND), toxic compound extrusion (MATE), and major facilitator superfamily (MFS) transporters, function to reduce the amount of medicines that can reach cellular targets (Abdi et al., 2020; Geisinger et al., 2019).

The major efflux pump in *A. baumannii* is the RND efflux system, which comprises the AdeABC, AdeIJK, and AdeFGH chromosomal operons. Both the AdeABC and AdeIJK pumps exhibit relatively broader substrate ranges (Geisinger et al., 2019). Mutations in the AdeRS regulatory system result in enhanced expression of AdeABC, leading to increased acquired resistance to carbapenems, aminoglycosides, and fluoroquinolones (Yoon et al., 2013). Conversely, the AdeIJK operon contributes to intrinsic resistance against Imipenem,

cefotaxime, erythromycin, chloramphenicol, fluoroquinolones, tetracycline, lincosamides, rifampin, and trimethoprim (Damier-Piolle et al., 2008). RND pump works cooperatively with the MFS TetA in pumping out tigecycline from the bacterial cell (Foong et al., 2020). Although RND overexpression contributes to the resistance of many antibiotics, it causes alterations in membrane composition and leads to a reduction in biofilm formation in *A. baumannii* isolates (Yoon et al., 2015).

1.5.3 Alteration of antibiotic targets

β-lactams compete with substrate for binding to the penicillin-binding protein (PBP), thereby interrupting bacterial cell wall synthesis and leading to cell lysis (Zapun et al., 2008). Conflicting results have been demonstrated in *A. baumannii* regarding the link between changes in PBP and nonsusceptibility to β-lactams. One study reported the existence of an association (Vashist et al., 2011), while another study revealed no direct effect (Cayô et al., 2011).

Acinetobacter employs posttranscriptional methylation of its 16S rRNA using 16S-RMTase as a mechanism to evade the impact of aminoglycoside antibiotics, including gentamicin, amikacin, tobramycin, and plazomicin (Doi et al., 2016). In *A. baumannii*, the predominant plasmid-borne gene encoding this enzyme is *armA* (Doi et al., 2016; Taylor et al., 2022). Additionally, the genes rmtA-E have also been implicated as responsible agents (Taylor et al., 2022).

Concurrent mutation in the gyrase (GyrA) and topoisomerase IV (ParC), specifically in the quinolone resistance determining sequence (QRDS) where the drug binds, enables *A. baumannnii* to be substantially refractory to quinolone treatment (Ardebili et al., 2015; Mohammed et al., 2021). Additionally, the alteration of dihydrofolate reductases by plasmid-encoded genes (e.g., *sul1*, *sul2*, *dfrA1*, and *dfrA5*) and the ribosome subunit by *tetM* (encoding the ribosome protection protein) causes trimethoprim and tetracycline resistance, respectively (Girija et al., 2019; Ribera et al., 2003). Furthermore, mutations in the genes (*lpxA*, *C,* and *D*) responsible for the biosynthetic pathway of lipid A, or in the two-component regulator (*pmrA and pmrB*) that controls this process, lead to resistance to colistin, which is considered the last resort of antibiotics (Beceiro et al., 2011; Moffatt et al., 2010).

1.5.4 Reduction of permeability

Defects in the outer membrane proteins (OmpA, Omp33-36, and Omp37) can inhibit drug influx. The details related to antimicrobial resistance of these proteins have been addressed in Section 1.3.1.

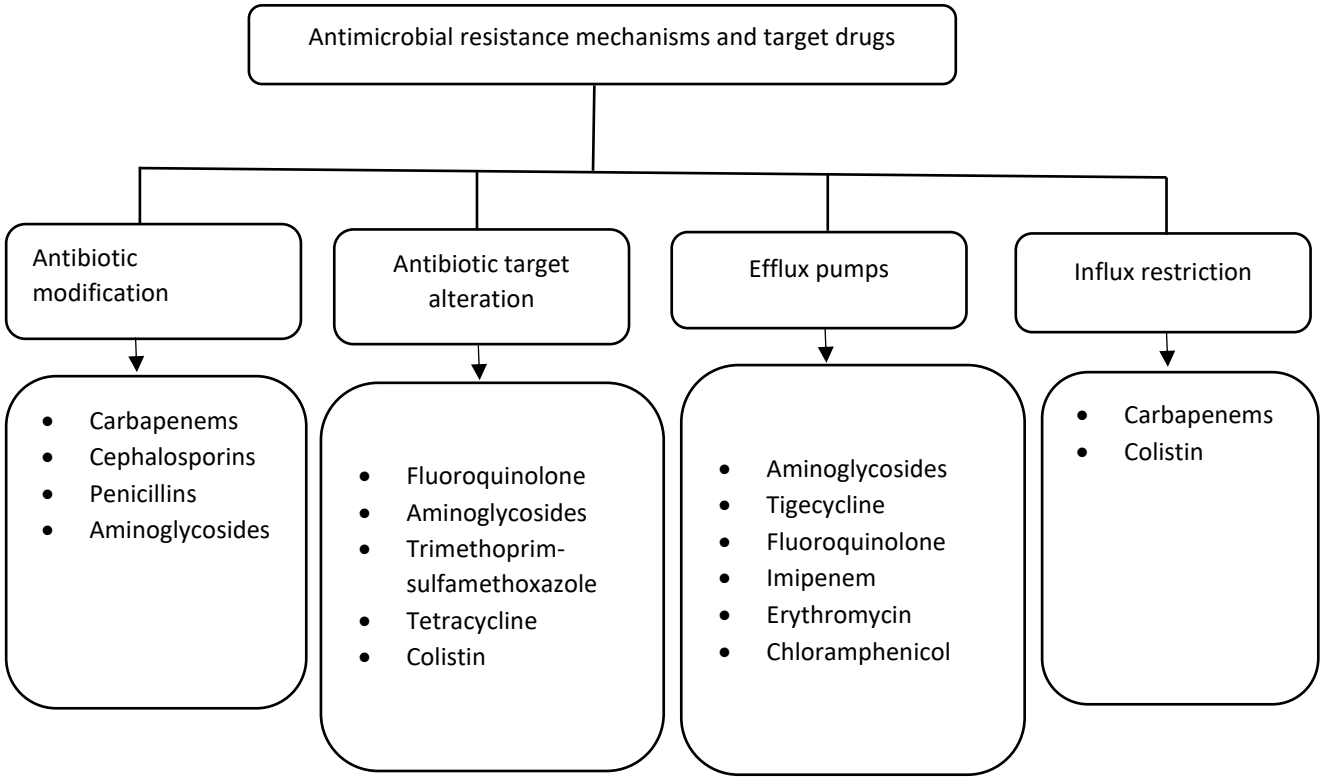

Figure 1.2 Antimicrobial resistance mechanisms toward the antibiotics or antibiotics group recommended by CLSI for Acinetobacter species susceptibility testing (Jean et al., 2017).

1.5.5 Biofilm-mediated antimicrobial resistance and tolerance

It has already been established that the sessile form of growth in bacteria confers antimicrobial resistance. The variation lies in the degree of resistance (ranging from 10 to 1000-fold) and the mechanisms of resistance, which depend on the species of bacteria and the antibiotic involved (Davies, 2003; Mah & O'Toole, 2001). In *A. baumannii*, a study showed a 2048-fold and 1024-fold increase in the concentration of antibiotics needed to inhibit and kill biofilms compared to their planktonic cell counterparts in different strain types, respectively. The highest fold change was recorded for imipenem (Shenkutie et al., 2020). He et al also reported an increased fold of minimum inhibitory concentration (MIC) in biofilm (He et al., 2015). The reasons why the biofilm develops tolerance and resistance can

be broadly classified into physical, chemical, physiological, and genetic factors (Ciofu et al., 2022; Roy et al., 2022).

The surrounding matrix of biofilm cells, primarily composed of EPS, plays a significant role in impeding the entry of antimicrobial agents at bactericidal concentrations (Cao et al., 2015, 2016). In addition to size exclusion, the polysaccharides and extracellular DNA (eDNA) present in EPS possess the ability to sequester cationic drugs, such as aminoglycosides, and hinder their diffusion (Cao et al., 2016; Montanaro et al., 2011). The matrix further serves as a reservoir of β-lactamases (Bagge et al., 2004).

In conditions where a low dose of antibiotics reaches the biofilm, limited availability of nutrients and low oxygen tension within the biofilm microenvironment initiate stress responses and the production of efflux pumps. These factors can potentially lead to the development of adaptive resistance to antibiotics (Ciofu et al., 2022; He et al., 2015). Following deprivation of the essential extrinsic factors, cells enter a slow growth phase, rendering them less susceptible to most antimicrobial agents available in the market that specifically target actively dividing cells (Roy et al., 2022). This phenomenon also applies to persister cells, which are a subpopulation within the biofilm and are characterized by an increased tolerance to antibiotics, and when the antibiotic pressure is removed, they resume growth (Alkasir et al., 2018; Shenkutie et al., 2020).

Besides the above determinants, genetic factors such as mutation and horizontal gene transfers (HGT) are significantly responsible for biofilm antimicrobial resistance. The adaptive stress response can activate mutation-prone DNA polymerase subtypes (IV and III) (Ciofu et al., 2022). Biofilms have been reported as hotspots for the acquisition of antimicrobial resistance genes (ARGs), especially in polymicrobial biofilms (Michaelis & Grohmann, 2023). Savage et al and Hausner et al demonstrated higher rates of plasmid transfer in biofilm than planktonic growth (Hausner & Wuertz, 1999; Savage et al., 2013). The close proximity of bacterial cells within the confined biofilm environment might be facilitating the transfer of resistance gene-containing genetic elements. In addition, Metzger et al. reported a reduced loss of regions crucial for conjugative plasmid transfer and persistent retention of multidrug-resistant (MDR) plasmids in biofilms, suggesting a potential increase in HGT (Metzger et al., 2022).

1.6 Regulation of virulence gene expression in *A. baumannii*

To ensure proper expression of virulence factors during pathogenesis, precise regulation and coordination are necessary. Kröger et al have summarized the major systems involved in the regulation of virulence and antibiotic resistance gene expression in *A. baumannii*. These systems include two-component systems, transcription factors, quorum sensing, and small regulatory RNAs (Kröger et al., 2017).

1.6.1 Transcription factors

Transcription factors (TFs) play a prominent role in fine-tuning the expression of virulence determinants by binding to promoter nucleotides or sensing specific signals. In the pathogenic strain *A. baumannii* AB5075, a total of 243 TFs have been identified through bioinformatics computations of databases. These TFs exhibit high conservation in other pathogenic strains, suggesting their involvement in virulence (Casella et al., 2017).

A Tet-R family TF was reported to regulate phenotypic alteration between avirulent translucent and virulent opaque variants (Chin et al., 2018). Other examples of transcription factors include AdeN (a TetR-like regulator), AdeL (a LysR-type regulator), and the ferric-uptake regulator (Fur), which control the AdeIJK and AdeFGH efflux pumps, and acinetobactin expression, respectively (Coyne et al., 2010; Daniel et al., 1999; Rosenfeld et al., 2012). Additionally, the H-NS TF has been implicated in epithelial cell adherence, colistin resistance, quorum sensing, and secretion system (Morris et al., 2019).

1.6.2 Two-component systems

Two-component systems (TCSs) are abundant in bacteria and facilitate transduction of external stimuli through a membrane-bound sensor (histidine kinase, HK) to a DNA-binding response regulator (RR) by a phosphorylation process. This signal transduction pathway enables bacteria to survive in diverse environments (Kröger et al., 2017; Morris et al., 2019). Although 14 two-component systems (TCSs) have been identified in *A. baumannii* (Casella et al., 2017), only half of them have been studied, and their respective functions are illustrated in Table 1.1.

Table 1.1 Roles of two-component systems in *A. baumannii.*

Gene name	Related functions	References
AdeRS	Modulate AdeABC efflux pumps and biofilm formation.	(Richmond et al., 2016)
BaeSR	Controls both the AdeABC and AdeIJK efflux pumps. Deletion leads to tigecycline and tannic acid susceptibility.	(M. F. Lin et al., 2014; M. F. Lin, Lin, et al., 2015)
bfmRS	Mediate csuA/BABCDE-dependent and independent adhesion, biofilm formation, capsule production, antibiotic susceptibility, siderophore metabolism, and type IV pili synthesis.	(Palethorpe et al., 2022; Tomaras et al., 2008)
gacSA	Regulate pili synthesis, motility, biofilms, and phenylalanine metabolism. Deletion resulted in virulence attenuation in septicaemic animal model.	(Bhuiyan et al., 2016; Cerqueira et al., 2014)
pmrAB	Mutation of *pmrB* gene confers resistance to polymyxin B through lipid A modification. *pmrAB* is also implicated in colistin heteroresistance.	(Arroyo et al., 2011; Beceiro et al., 2011; Charretier et al., 2018)
ompR-envZ	Regulate switch from opaque to translucent colony and motility. Mutation in both Both *ompR* and *envZ* led to reduced virulence.	(Tipton & Rather, 2017)
AmsSR	Involves in membrane polarity and cytoplasm acidification.	(Casella et al., 2023)

1.6.3 Quorum sensing (QS)

Quorum sensing has emerged as a sensing and responding system alongside the well-known two-component system. This process is mediated through the production of signaling molecules (auto-inducers). The auto-inducer at a certain concentration triggers the expression of genes that enable maintenance of the cell population through cell-to-cell communication (Whitehead et al., 2001). In addition to controlling cell density, this system is also implicated in biofilm formation and surface motility. In gram-negative bacteria, the quorum sensing is primarily based on the release of N-acyl homoserine lactone (AHL). The overall signal transduction cascade includes AHL synthases, AHL auto-inducers, signal receptors, and target genes (Lade et al., 2014).

AHL-dependent QS is among the key virulence determinants in *A. baumannii* and comprises AbaI and AbaR as the inducer and signal receptor, respectively (Saipriya et al., 2020). The inducer gene *AbaI* promotes the release of N-acyl-homoserine lactone (AHL) by encoding the AbaI auto-inducer synthase, which is analogous to LuxI family members found in other gram-negative bacteria (Niu et al., 2008). When the released AHL reaches a certain threshold, it binds to AbaR, which subsequently activates a cascade that positively modulates the expression of *abaI* by acting on the promoter lux box (Man Hwan Oh, 2020; Saipriya et al., 2020). Recently, a T26 transposon mutagenesis study identified another gene named *AbaM*. This gene is located between AbaI and AbaR and functions as a negative regulator of AHL and QS targets in *A. baumannii* (López-Martín et al., 2021).

Lack of genes involved in the quorum-sensing (QS) system of *A. baumannii* resulted in a substantial increase in survival rates in murine and zebrafish models (Bhuiyan et al., 2016), as well as in the *Galleria mellonella* model (Fernandez-Garcia et al., 2018). Additionally, a study demonstrated that clinical isolates with detectable levels of AHL (N-acyl-homoserine lactone) by biosensor exhibited higher adherence to A549 cell lines and increased virulence to *Galleria mellonella* compared to AHL-deleted isolates (Tang et al., 2020). These findings suggest that quorum sensing (QS) could be among the candidate targets to alleviate the pathogenicity of *A. baumannii*.

1.6.4 Non-coding small RNA

Small RNAs (sRNAs) with sequences ranging from 50-500 nucleotides mediate gene expression at the post-transcription level by influencing mRNA decay and/or translation (Carrier et al., 2018). It is predicted that they have evolved through duplication from homologous sRNAs, horizontal gene transfer, and de novo origination (Dutcher & Raghavan, 2018). As a source, sRNAs are primarily transcribed from intergenic regions, but they can also originate from 3' and 5' untranslated genomic regions (Carrier et al., 2018).

Many of the sRNAs exert control over a broad range of mRNAs, either directly or indirectly (Storz et al., 2011). Based on their genomic location relative to the interactome mRNA, sRNAs can function as either trans-acting or cis-acting molecules. Trans-acting bacterial sRNAs bind to mRNA targets through limited pairing, enabling positive and negative regulation of gene expression. On the other hand, cis-acting sRNAs form strong attachments to their target RNAs due to perfect complementarity (Carrier et al., 2018). For trans sRNAs to function properly in Gram-negative bacteria, RNA chaperones such as host factors (Hfq) or ProQ are crucial. The proposed mechanism suggests that Hfq enhances annealing rates, stabilizes sRNA-mRNA pairing, or facilitates conformational changes in one of the partners by binding to A/U-rich region of sRNA (Soper et al., 2010; Storz et al., 2011).

Typically, sRNAs bind to the target mRNA at or near the Shine-Dalgarno sequences (SDS) to repress gene expression. However, in some cases, sRNAs can bind to the secondary structure of mRNA and activate gene expression (Figure 1.3A and B)(Dutta & Srivastava, 2018). Additionally, investigations have also demonstrated that sRNAs can carry out both positive and negative gene regulation by binding to coding regions, which represents an uncanonical binding site (Figure 1.3C) (Melamed et al., 2023).

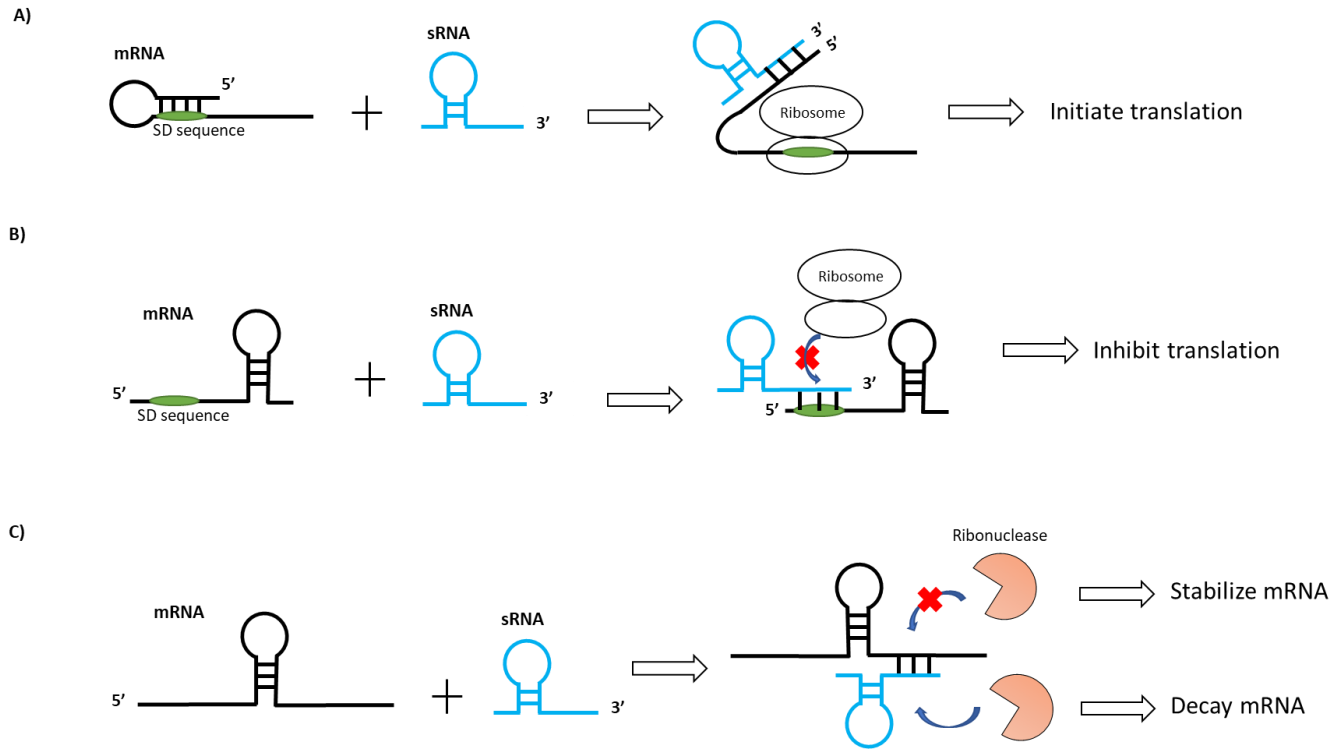

Figure 1.3 Molecular mechanism of regulatory sRNAs in bacteria.

Most of sRNA play their regulatory role through base pairing. (A) sRNA binds to the 5' UTR of the target mRNA, relieving the secondary structure to expose the Shine-Dalgarno sequence (SDS). This allows the ribosome to bind freely to the SD sequence, thereby promoting translation. (B) Some other sRNA can base pairs with the upstream region of the target mRNA, forming a duplex around SDS or start codon. The duplex prevents ribosome binding and represses the translation of the target mRNA. (C) Binding of sRNA to distinct regions of the targ gene can either prevent the action of ribonucleases, thereby stabilizing the target, or recruit ribonucleases to degrade the duplex. The figure was adapted from (Mahendran et al., 2022).

Compared to regulation by proteins that mediate transcription and translation, sRNA-mediated regulation is effective in both activating and repressing target genes. It is also quick to respond to external stresses (Guillier et al., 2006; Shimoni et al., 2007). Moreover, sRNA-mediated regulation minimizes the number of steps involved in the regulatory process, thereby reducing energy consumption (Beisel & Storz, 2010; Felden & Augagneur, 2021).

The initial detection of sRNAs relied on genetic methods, which focused on its unique features such as small size, lack of open reading frames, presence in intergenic regions, and Rho-independent termination (Hör et al., 2020). More recently, a combination of computational searches and RNA sequencing has been employed in the majority of reports to detect small RNAs. Furthermore, the enrichment of sRNA detection has been achieved through co-immunoprecipitation with Hfq, followed by high-throughput analysis of the bound RNAs (Zhang et al., 2003), as well as cross-linking studies of RNAs associated with RNAse E (Waters et al., 2017) or Hfq (Melamed et al., 2016). The Hfq-based enrichment methods have also aided in the identification of both known and novel targets (Melamed et al., 2016). In addition, interacting-protein independent methods such as MS2 affinity purification and RNA sequencing (MAP-seq) (Lalaouna et al., 2015) and global small non-coding RNA target identification by ligation and sequencing (GRIL-seq) are also part of searching base-pairing targets of sRNA in bacteria (Han et al., 2016). However, it remains challenging to differentiate between direct or indirect non-base-pairing targets.

The roles of sRNAs in bacteria have been found to be more extensive and flexible than initially anticipated. They orchestrate various functions, including but not limited to virulence, stress adaptation, host-microbe interactions, and antibiotic resistance (Felden & Augagneur, 2021). In the case of *A. baumannii*, sRNAs have been confirmed to be among the highly expressed genes (Weiss et al., 2016), and most of them are derived from intergenic regions (Kröger et al., 2018). However, only a limited number of studies have elucidated the physiological and virulence roles of the sRNAs (Table 1.2). The following subsection will discuss relevant aspects pertaining to this matter.

1.6.4.1 Role of non-coding sRNA in biofilm formation

The initiation and progression of biofilm formation are regulated biological processes in bacteria. It has been discovered that various gram-negative bacteria produce different forms of regulatory sRNA that influence the development of biofilms. Small RNA molecules often control biofilm development either by binding to regulatory proteins or mRNAs (Chambers & Sauer, 2013)**.**

In a study, several differentially expressed sRNAs were identified in *A. baumannii* 17978 when comparing sessile cells to planktonic cells. Among these sRNAs, sRNA 13573 exhibited more than 100-fold increase in expression. Interestingly, although overexpression of sRNA 13573 led to a substantial increase in biofilm production, deletion of the gene did not result in a significant difference in biofilm formation between the mutant and wild strains (Álvarez-Fraga et al., 2017). This could be due to a complex regulatory network or compensatory mechanism in the mutant strain. Conversely, in our published study, we demonstrated a significant increase in the expression of sRNA00203 in sessile cells of clinical *A. baumannii* 1894 strain. Afterward, upon deleting this gene, we observed an 85% reduction in biomass within the biofilm formed by the isogenic mutant strain (Shenkutie et al., 2023). This reduction in biofilm formation in the sRNA00203 deleted strain could be due to sRNA00203's role in the expression of biofilm-associated genes such as novel00738 (*pgaB*) and E5A72_RS03500 (*secA*) (Shenkutie et al., 2023). However, despite these findings, how this sRNA modulates the biofilm development and related genes remains elusive and demands further investigation.

1.6.4.2 Role of non-coding sRNA in antimicrobial resistance

Few studies have demonstrated the involvement of non-coding sRNAs in response to chemical stress, including antimicrobial agents, in *A. baumannii*. One of the first identified sRNAs, AbsR25, was found to be repressed during exposure to ethidium bromide, while one of its predicted target transporters (A1S_1331) was activated (R. Sharma et al., 2014). Subsequently, the putative target was confirmed to be a member of the major facilitator superfamily and named *AbaF*. This confirmed that AbsR25 negatively modulates fosfomycin susceptibility by acting on the efflux pump (A. Sharma et al., 2017).

In another study, the contribution of sRNAs to the biological adaptation of colistin was evaluated. Colistin-resistant *A. baumannii* was found to have both under-expressed (AbsRNA1, AbsRNA2, AbsRNA3, and AbsRNA4) and over-expressed (AbsRNA5) sRNAs that were predicted to target distinct mRNAs. However, no difference in colistin MIC was observed between the strains with manipulated AbsRNA1, AbsRNA3, and AbsRNA5 targets and the wild-type *A. baumannii* ATCC17978 (Cafiso et al., 2020). Based on these preliminary results, it is challenging to conclude that these sRNAs have no effect on colistin adaptation. The effect could be attributed to the possibility that these sRNAs have a distinct modulation network in the resistant strain. Therefore, deleting the sRNA in the multidrug-resistant strain may provide stronger evidence.

Recently, our study reported that sRNA00203 facilitated biofilm formation, resulting in more than 1000-fold increase in the minimum biofilm inhibitory concentration (MBIC) and minimum biofilm eradication concentration (MBEC) of carbapenem (Shenkutie et al., 2023). However, this observation did not answer the question of whether this effect is solely due to the shielding effect of the biofilm or other factors. In other gram-negative bacteria, in addition to acting on efflux pumps and biofilms, sRNA modulates antibiotic resistance by influencing outer membrane proteins and lipopolysaccharide (LPS) synthesis (Mediati et al., 2021).

1.6.4.3 Role of non-coding sRNA in adhesion and other processes

The lack of sRNA13573 in *A. baumannii* 17978 has been shown to have a significant impact on the organism's adherence to A549 alveolar epithelial cells (Álvarez-Fraga et al., 2017). The Hfq protein, sRNA partner in gram-negative pathogens, has also been reported to influence adhesion and invasion in *A. baumannii* (Kuo et al., 2017). However, the precise mechanisms by which sRNA13573 mediates adhesion remain unclear, particularly regarding its link with Hfq. The Hfq protein has also been reported to regulate outer membrane proteins and iron acquisition in *Acinetobacter baumannii* ATCC 17978, suggesting that Hfq-dependent sRNAs may be involved in these processes (Kuo et al., 2017). Initial identification of an sRNA (Aar) from non-pathogenic *Acinetobacter baylyi* under iron-limited conditions was predicted to modulate protein metabolism (Schilling et al., 2010). Later, the Aar confirmed to inhibit translation of outer membrane protein CarO type III and TonB-

dependent siderophore receptor through occluding its SD sequence region in *A. baumannii* strain (Hamrock et al., 2024).

Another sRNA derived from 5’ end of coding gene appeared to regulate virulent opaque (VIR-O) transition to an avirulent translucent (AV-T) subpopulation variant in *A. baumannii* AB5075 (Anderson et al., 2020). Similarly, the expression of three newly identified sRNAs (CsrB, CsrC, and CsrD) was found to contribute to the repression of the switch to the AV-T state by inhibiting the CsrA protein (Singh et al., 2025). Together, all of the above findings indicate that the regulatory role of sRNA and sRNA-interacting protein has not been fully unleashed, and the investigation of the network of interplay between regulator and regulon in clinical *A. baumannii* isolates is still in its infancy.

Table 1.2 Summary of function and characteristics of sRNA identified in *Acinetobacter* species.

Acinetobacter species	**No. of identified sRNA**	**sRNA that has been investigated**	**Size(bp)**	**Related function**	**References**
Acinetobacter baylyi	14	Aar	181	Amino acid metabolism	(Schilling et al., 2010)
Acinetobacter baumannii ATCC17978	31	AbsR25	93	Efflux pump	(R. Sharma et al., 2014)
Acinetobacter baumannii AB5075	78	ABUWs030, ABUWs042, ABUWs062, ABUWs074, ABUWs076 and ABUWs077	130, 115, 81, 173, 160 and 154, respectively	Not assessed their roles	(Weiss et al., 2016)
Acinetobacter baumannii ATCC 17978	183	sRNA 13573	76	Biofilm formation and adhesion	(Álvarez-Fraga et al., 2017)
Acinetobacter baumannii	5	AbsRNA1, AbsRNA2, AbsRNA3 and AbsRNA5	NR,35,75,21 and 20, respectively	Virulence*	(Cafiso et al., 2020)
Acinetobacter baumannii AB5075	1	sRNA	300	Phenotypic switching	(Anderson et al., 2020)
Acinetobacter baumannii ST1894	5	sRNA00203	53	Biofilm formation	(Shenkutie et al., 2023)
Acinetobacter baumannii AB5075	1	Aar	90	Outer membrane and iron acquisition proteins	(Hamrock et al., 2024)
Acinetobacter baumannii	3	CsrB, CsrC, and CsrD	169,120 and 130, respectively	Phenotypic switching	(Singh et al., 2025)

NR: not reported; * predicted function.

1.7 Research gap and significance of the study

Globally, more than half of *A. baumannii* clinical strains are biofilm formers (Gedefie et al., 2023). The biofilm formation increases the pathogen's ability to adhere and survive long-term on both medical equipment and health care environments, facilitating persistence and transmission (Lucidi et al., 2023). The biofilm microenvironment also contributes to chronic infections and treatment failures. Reports have demonstrated that biofilm cells tolerate several-fold higher concentrations of antimicrobial agents, including carbapenem drugs, relative to their planktonic cell counterparts (He et al., 2015; Shenkutie et al., 2020). Moreover, in patients with ventilator-associated pneumonia (VAP), biofilm-forming strains of *A. baumannii* significantly compromise the survival rate compared to non-biofilm-forming strains (Chukamnerd et al., 2024). Thus, in the 2024 updated WHO report, carbapenem-resistant *A. baumannii* continued to be among the priority pathogens that pose the highest threat to public health (WHO, 2024).

We believe that investigating the molecular mechanisms involved in the regulation of biofilm formation will contribute to the control of biofilm-related burdens. Post-transcriptional regulatory sRNAs are known for their roles in this adaptive process of a pathogen (Chambers & Sauer, 2013). However, only two studies, including ours, have demonstrated the involvement of sRNA in biofilm formation in *A. baumannii* (Álvarez-Fraga et al., 2017; Shenkutie et al., 2023). Our previous study revealed that the expression of novel sRNA00203 was strongly linked to biofilm formation, leading to biofilm-induced resistance in the antibiotic-susceptible *A. baumannii* ST1894 strain (Shenkutie et al., 2023). Although the impact of sRNA00203 on a small subset of genes associated with biofilm and antibiotic resistance was studied, the majority of influenced genes and pathways remain undeciphered. Additionally, neither study identified the primary target mRNAs of the sRNAs and the associated sRNA-binding proteins necessary to understand the regulatory circuits of the sRNAs in *A. baumannii*.

Therefore, this study investigated the regulatory networks of the sRNA00203 in the clinical *A. baumannii* ST1894 strain with strong biofilm-forming capacity. The findings provide insights into the molecular mechanisms by which the sRNA underpins biofilm formation and further strengthen candidacy of the sRNA as a viable target for devising new antibiofilm agents.

2. Aim and Objectives of the study

This project aims to investigate the underlying regulatory mechanism of biofilm formation by the non-coding small RNA00203 through combined omics studies of wild-type and sRNA00203 deletion mutant strains of *A. baumannii* and tag-based sRNA00203 interactome capture.

2.1 Objectives

Objective 1: To identify the genes and pathways influenced by non-coding sRNA00203 in *A. baumannii* ST1894.

Objective 2: To reconfirm the impact of non-coding sRNA00203 on biofilm formation and its associated genes through an overexpression study in *A. baumannii* ST1894.

Objective 3: To identify and validate the primary target mRNAs of non-coding sRNA00203 in biofilm cells of *A. baumannii* ST1894.

Objective 4: To identify proteins that potentially interact with sRNA00203 in biofilm cells of *A. baumannii* ST1894.

3. Materials and Methods

3.1 Overview of methods workflow

A comprehensive overview of the methods workflow employed to achieve the stated objectives is presented in Figure 3.1. The investigation was conducted on wild-type, sRNA00203 deletion mutant, sRNA0023 overexpressing, tagged sRNA00203 expressing, and empty plasmid-harbouring *A. baumannii* ST1894 strains.

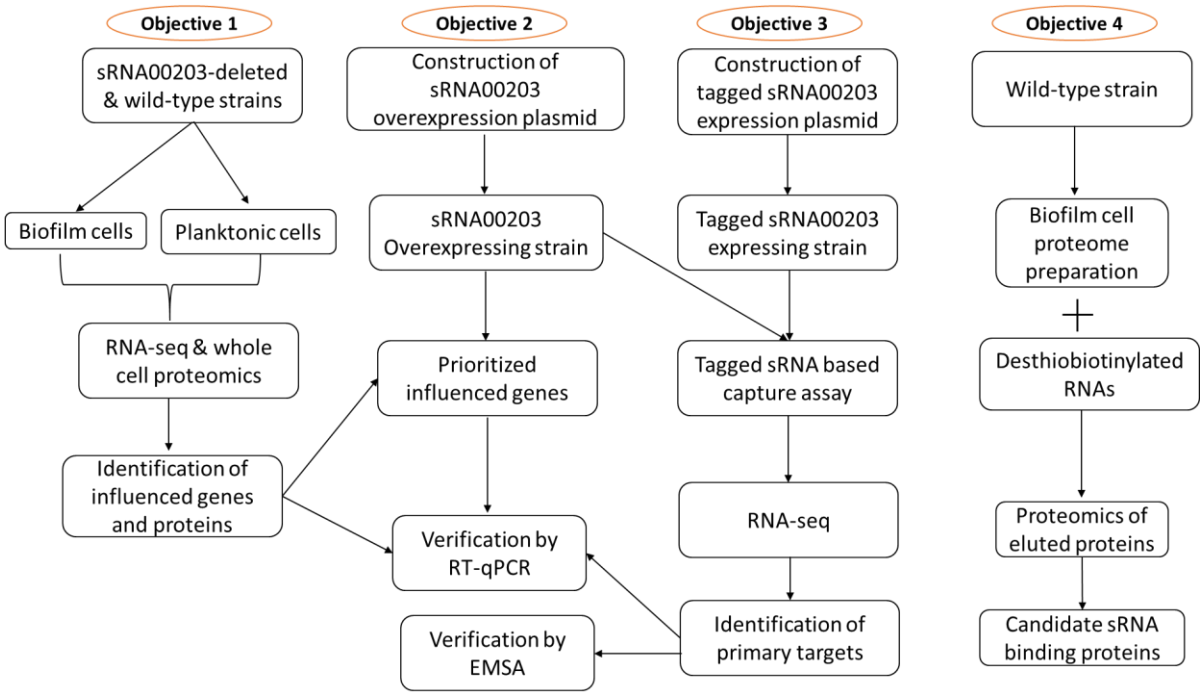

Figure 3.1 Summary of the study workflow.

The tag is a 24-nucleotide-long sequence used as bait to capture the RNA interactome. Prioritized influenced genes are differentially upregulated genes at the biofilm level, as well as influenced in the sRNA00203-deleted biofilm cells. EMSA: Electrophoretic mobility shift assay.

3.2 Bacterial strain and cultivation conditions

A. baumannii ST1894 wild-type and sRNA00203-deleted strains, stored in 20% glycerol at -80 °C and obtained from our previous study, were collected for further study. In the deletion mutant strain, the sRNA00203 coding region was substituted by a kanamycin cassette (aph (3´)-I gene) through homologous recombination using the pMo130 TelR suicide plasmid. Successful deletion of the sRNA was then confirmed by Sanger sequencing of the left and

right junctions of the aph (3´)-I that integrated into the chromosome (Shenkutie et al., 2023).

To prepare planktonic and biofilm cells, the isogenic strains were subcultured to Luria Bertani (LB) agar overnight at 37 °C. Additionally, the deletion mutant strain was also checked for growth in 50 µg/mL Kanamycin-containing LB media. A single colony from each isogenic strain was subcultured into 20 ml of LB broth for 48 hours of planktonic growth at 37 °C under shaking conditions at 110 rpm. For biofilm cell preparation, five colonies from the overnight growth were inoculated into a 1:1 ratio of LB broth and maximum recovery diluent solution (MRD) in a larger Petri dish (150mm) and incubated similarly to the planktonic cells, but under static conditions (Shenkutie et al., 2023).

3.3 Transcriptomic study of wild-type and sRNA-deleted mutant strains

3.3.1 RNA sample preparation and RNA quality assessment

Biofilm cells were scraped and collected after three rounds of washing the growth plate surface with sterile 1x phosphate-buffered saline (PBS, pH 7.4). Subsequently, both 48-hour-old planktonic and biofilm cells in three biological replicates were subjected to centrifugation at 4500 rpm (4 °C) for 15 minutes. The pellet was washed once with PBS, and total RNA was isolated using PureLink™ RNA Mini Kit (Thermo Fisher Scientific, USA) as instructed by the manufacturer. To ensure DNA-free RNA, we treated the RNA sample with DNase I for 25 minutes at 37 °C, followed by deactivation for 5 minutes using reagents from TURBO DNA-free kit (Thermo Fisher Scientific, USA).

RNA samples were collected after treatment, comprising three biological replicates each from biofilm and planktonic cells of both wild-type and sRNA-deleted mutant strains. The samples were then assessed for purity using a NanoDrop 2000 spectrophotometer (Thermo Fisher Scientific, USA) based on the 260/280 and 260/230 ratios. The OD ratios above 1.8 were regarded as pure. The Qubit ™ 4.0 Fluorometer with the Qubit™ RNA High Sensitivity Assay kit (Thermo Fisher Scientific, USA) was employed to determine the concentration. The integrity of these samples was evaluated using an Agilent Bioanalyzer 2100 system with Agilent RNA 6000 Pico Kit (Agilent Technologies, USA). The average quality and quantity assessment results of the RNA samples are depicted in Table 3.1. Additionally, Figure 3.2 presents representative electropherograms illustrating the integrity of the RNA samples.

Samples with an RNA integrity number (RIN) value of ⩾ 7.0 were considered acceptable for downstream analysis (Jahn et al., 2008).

Table 3.1 Average quality assessment results of RNA samples used in the transcriptomic study.

Sample name	**RNA Conc.(ng/µl) by Qubit Fluorimeter**	**RNA Purity, NanoDrop 2000**		**RNA integrity number (RIN)**
		260/280	**260/230**	
Wild planktonic cells	340	2.16	2.36	8.3
Wild biofilm cells	373	2.10	2.52	7.4
Mutant planktonic cells	402.7	2.13	2.46	9.1
Mutant biofilm cells	251.3	2.13	2.56	8.9

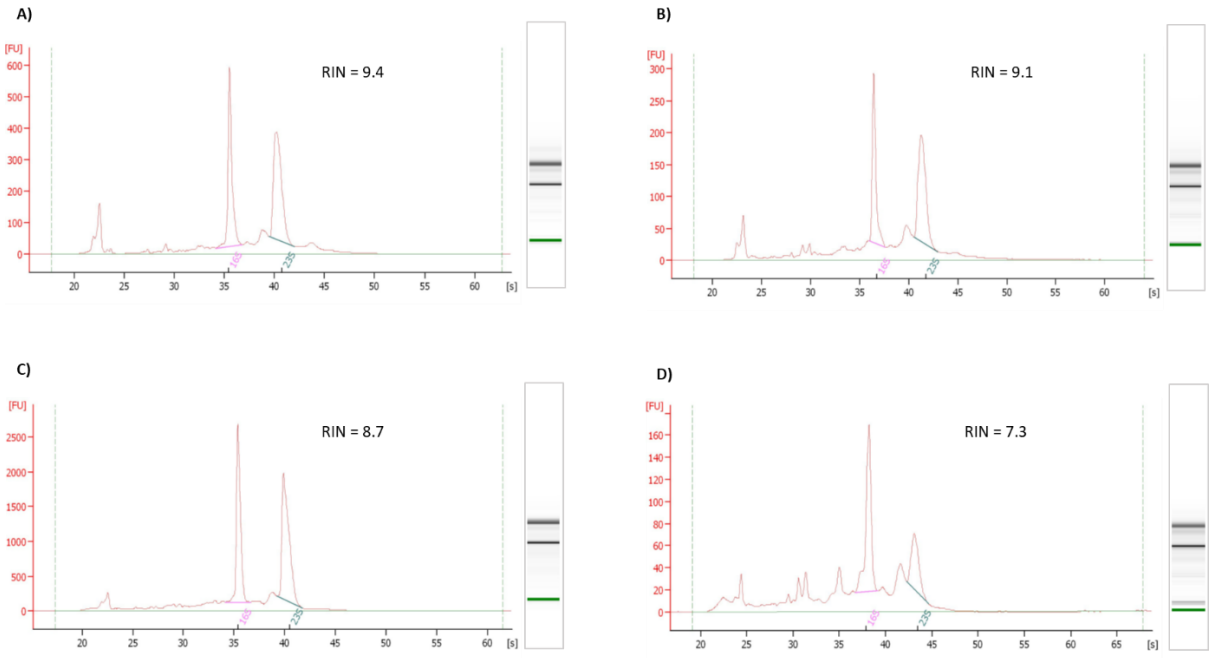

Figure 3.2 Representative electropherograms showing the integrity of the RNA samples. (A) and (B): sRNA-mutant planktonic and biofilm RNA, respectively. (C) and (D): wild-type planktonic and biofilm RNA, respectively. The peaks for 16S (pink) and 23S (green) are shown and labeled sequentially.

3.3.2 cDNA library preparation and sequencing

RNA samples that passed the quality assessment (as shown in Table 3.1) were included for library preparation after removing ribosomal RNA with Ribo-Zero rRNA Removal Kit (Illumina, USA). Briefly, the RNAs were fragmented, and complementary DNA (cDNA) was synthesized using random hexamer primers and reverse transcriptase enzyme. The cDNA was then subjected to consecutive steps, including end repair, A-tailing, P5 and P7 adapter ligation, size selection, USER (Uracil-Specific Excision Reagent) enzyme digestion, PCR amplification, and purification, to generate directional cDNA libraries using Illumina TruSeq Stranded Total RNA Library Prep Kit (Illumina, USA). The concentration and size distribution were analyzed using the Qubit Fluorometer and Agilent 2100, respectively. Finally, the libraries for all the RNA samples underwent prokaryotic paired-end RNA-seq independently using Illumina NovaSeq 6000 with a 150 bp read length.

3.3.3 RNA sequencing data filtering and analysis

The RNA sequencing produced approximately 2 Gbp per sample, resulting in a total of 24 Gbps. The raw sequencing data in FASTQ format were subjected to quality checks using fastp. After trimming reads containing adapters, poly-N sequences (more than 10%), and reads with low quality using Trimmomatic (v0.36), the clean reads were used for downstream analysis. Bowtie2 (v2.3.4.3) was employed to align the clean reads to the reference genome *A. baumannii* ATCC 17978 (GenBank assembly accession: GCA_004797155.2).

The identification of novel genes was performed using Rockhopper (v2.0.3), a tool specifically designed for efficient and accurate analysis of bacterial RNA-seq data (McClure et al., 2013). Then, FeatureCounts (v1.5.0-p3) was employed to enumerate the aligned novel and annotated genes. The count was further normalized by converting it into the expected number of fragments per kilobase of transcript sequence per million base pairs sequenced (FPKM) value, which considers both gene length and sequencing depth. The FPKM is a widely applied technique for estimating gene expression levels (Trapnell et al., 2011).

The estimated transcripts of the sRNA00203 deleted and wild-type *A. baumannii* ST1894 in planktonic and biofilm growth forms were compared to identify the differentially expressed genes (DEGs). This comparison was performed using DESeq2 (v1.20.0), utilizing a negative

binomial distribution model. Genes that showed an absolute fold change value of ≥ 2 and adjusted p-value < 0.05 were classified as significantly transcribed genes.

3.3.4 GO term and KEGG enrichment investigation of DEGs

The clusterProfiler of R software package was utilized to investigate Gene Ontology (GO) enrichment analysis of DEGs, incorporating gene length bias correction. The same R package was used to test the statistical enrichment of DEGs in Kyoto Encyclopedia of Genes and Genomes (KEGG) pathways. These functional annotation data were utilized in the enrichment analysis to facilitate a comprehensive understanding of the biological functions and pathways associated with the DEGs. GO terms and KEGG pathways with adjusted P-value < 0.05 were considered significantly enriched. All the bioinformatics tools used for the transcriptomic data analysis is summarized in Figure 3.3.

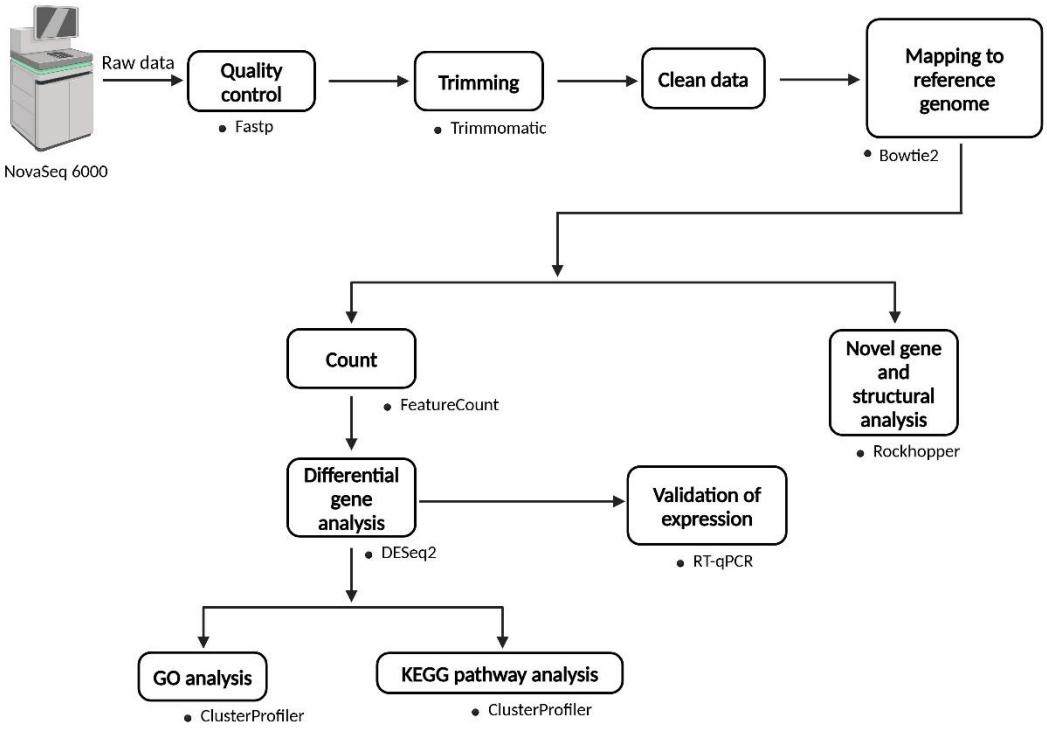

Figure 3.3 Bioinformatics pipeline workflow used for comparative bacterial transcriptomic data analysis.

3.3.5 Quantitative RT-PCR

Reverse transcription-quantitative polymerase chain reaction (RT-qPCR) analyses were conducted on 16 differentially expressed genes to validate the findings from RNA-seq. The RT-qPCR was performed using newly synthesized complementary DNA (cDNA) derived from the same RNA samples used in the RNA sequencing process. For reverse transcription, 600 ng of RNA from each of the three independent biological replicates was converted to cDNA using LunaScript RT Supermix (New England Biolabs, UK), following the manufacturer's instructions in a 20 µl reaction volume. The cDNA was further diluted 1:100 in nuclease-free water. Then, quantitative PCR was carried out using the SYBR Green method with Luna Universal qPCR Master Mix (New England Biolabs, UK) on a ViiA 7 Real-Time PCR system (Thermo Fisher Scientific, USA). The cycling conditions were as stated: an initial denaturation step at 95°C for 1 minute, followed by 40 cycles of denaturation at 95°C for 15 seconds and extension at 60°C for 30 seconds. To affirm the specificity of PCR products, final step involved raising the temperature from 60°C to 95°C to generate the dissociation curve.

Oligonucleotides used in this study were designed based on the RNA-seq annotation and are described in Table 3.2. To ensure the absence of DNA remnants after DNase treatment and reagent contamination, non-reverse transcriptase-containing samples and non-template control reaction tubes were included as quality controls. Additionally, we also performed three technical replicates for each biological replicate. Lastly, transcript levels were normalized using the internal fragments of housekeeping gene *gyrB*, and fold changes between comparison groups were calculated using $2^{-\Delta\Delta Ct}$ (Livak method) (Livak & Schmittgen, 2001).

Table 3.2 Oligonucleotides used for RT-qPCR.

Gene ID	Description	Primer label	Sequence (5'- 3')	Product length (bP)
E5A72_RS09705	3-isopropylmalate dehydratase large subunit	IPMD1_F	TGCTTGATCCCATTGTTCGC	136
		IPMD1_R	GCCATGATTGTTCCGGGTTC	
E5A72_RS16120	Class I SAM-dependent methyltransferase	SAM1_F	TAGAAGTGATTCGAGACCCTAGT	142
		SAM1_R	ATGCGCTGTACCCAACTATC	
E5A72_RS04580	50S ribosomal protein L16	rpIP1_F	GCACATCGTGGTAGTACAGTATC	96
		rpIP1_R	ACGACGTGCAGCTTCAAT	
E5A72_RS04585	30S ribosomal protein S3	30srRNA_F	GCTTCATAGCACGACGGAAC	146
		30srRNA_R	ACAGCGCGAACTTACCAACA	
Novel00134		Novel00134_F	TCATTGCCAAGCACATTGAG	117
		Novel00134_R	TTGTTCCGGGTTCTGGTTTA	
E5A72_RS05200	Pilus assembly protein PilM	PlM_F	GCTATGCTTTGATGCCTTTACC	94
		PlM_R	TTCATCGCCCGTTCCAAA	
E5A72_RS11885	Type IV pilus twitching motility protein PilT	PlT_F	GCTGAGTACATTTGCGCGAC	189
		PilT_R	TGACGTATTCCCTGCCGAAG	
E5A72_RS05115	Bacterioferritin-associated ferredoxin	Bac_F	GTCGTGGCATTACCGATCA	118
		Bac_F	CAGCGTCCACAGCAAGTA	
E5A72_RS05990	TonB-dependent siderophore receptor	Ton_F	AATGAAGGCACAACTTACGG	94
		Ton_R	CGAAGTAATCGTAGCGGAGT	
E5A72_RS06620	MFS transporter	Mfs_F	CCCATGACTTCCACACAAGG	120
		Mfs_R	TAAATCGGCTGCAACGCTA	
E5A72_RS14385	Phenylacetate-CoA oxygenase subunit PaaC	Phe_F	GTGCGAAACAAGGATTGCATAC	88
		Phe_R	CAGGTCATTCCCGGATAAGTTC	
E5A72_RS01455	LysR family transcriptional regulator	Lys_F	ATTCGTTTGGGCAGTATGGA	116
		Lys_R	TATCCTGTCGGGTGAGTTTG	
E5A72_RS11050	DUF1852 domain-containing protein	DUF1852_F	AGCAGACAATACGCGTATTACA	128
		DUF1852_R	GGTTGTCCCAATGAGCTAAGG	
E5A72_RS12660	Cation diffusion facilitator family transporter	CDF_F	CGTTTCACCTGAACCGATGG	189
		CDF_R	GTTCCAAACACGCCTACAGC	
E5A72_RS05715	AzlC family ABC transporter permease	AzlCfamily_F	GCACAGCCTGATTTCGACAC	118

		AzlCfamily_R	GGTCTGGAATAGCACTCCCA	
sRNA00056		sRNA00056_F	CTTCATTGTTCAAGCCCAATCC	87
		sRNA00056_R	GTCGTGTTCAAACTCTTGCTAAC	
E5A72_RS09035	Preprotein translocase subunit SecE	secE_F	GGCTTCGTTCGTTTGCTGAA	95
		secE_R	AGAACCTGCCACGATGTTGT	
E5A72_RS17700	UDP-3-O-(3-hydroxymyristoyl) glucosamine N-acyltransferase	LpxD_F	GGAGTGGCAGGACACCTTTC	105
		LpxD_R	TCCGGTTCCCGAAGAGTAAG	
E5A72_RS07575	DNA topoisomerase subunit B	gyrB_F	ACGATTTACCGTGCTGGTC	93
		gyrB_R	GGTATTATCCGTTTCACCAATC	

3.4 Proteomic study of wild-type and deletion mutant strains

3.4.1 Whole-cell protein extraction and peptide preparation

Similar to the RNA samples prepared for RNA sequencing, the culture growth conditions for whole cell protein extraction from the isogenic strains were as described in Section 3.2. The bacterial pellets from twelve independent samples of the comparison groups were washed twice with PBS. Following washing, each pellet was mixed with 220 µL of lysis buffer sourced from EasyPep™ Mini MS Sample Prep Kit (Thermo Fisher Scientific, USA) and incubated at room temperature for five minutes. The lysis buffer was modified by incorporating lysozyme (10 mg/mL). The protein concentration of the lysate was measured using Qubit™ 4 Fluorometer with reagents from Qubit Protein Assay Kit (Thermo Fisher Scientific, USA) to ensure proper digestion. The working solution was prepared at a 1:200 dilution. The sample to buffer ratio and the standard to buffer ratio were 1:200 and 1:20 dilutions, respectively.

Approximately 100 µg of the protein-containing bacterial lysate was further processed into peptides. The process of preparing peptides using the aforementioned kit included reduction/alkylation, digestion, and clean-up. For reduction and alkylation of proteins, 50 µL each of the reduction solution and alkylation solution was added consecutively to the lysate and incubated at 95°C using a heat block for 10 minutes. Then, fifty microliters of reconstituted Trypsin/Lys-C Protease Mix were added to the reduced, alkylated, and cooled protein samples, and the mixture was incubated with shaking at 37°C for 3 hours to facilitate digestion. The reaction was stopped by adding 50 µl of Digestion stop solution. The

peptides were then cleaned to remove hydrophilic and hydrophobic contaminants using a peptide clean-up column provided by the kit manufacturer. Finally, the peptides were then collected in 300 µl elution buffer.

3.4.2 Peptide concentration measurement

The eluted peptides were transferred to a CentriVap vacuum concentrator (Labconco, USA) and incubated for eight hours to dry. Freshly prepared 100 µL of 0.1% formic acid was used to reconstitute the peptides. Pierce Quantitative Colorimetric Peptide Assay (Thermo Fisher Scientific, USA) was then used for peptide measurement. The assay was performed in a 96-well microplate with a sample and standard volume of 5 µl and a total assay volume of 200 µl, and it was incubated for 15 minutes at 37°C. After obtaining the absorbance, the peptide concentration was calculated based on the standard curve using the formula $x = \frac{y-0.0412}{0.0012}$, where x represents the sample peptide concentration and y represents the absorbance of the sample at 480 nm. The correlation score (~0.99) indicated reliable determination of the peptide concentration (Figure 3.4). The average calculated values of peptides in each group of samples per millilitre are depicted in Table 3.3.

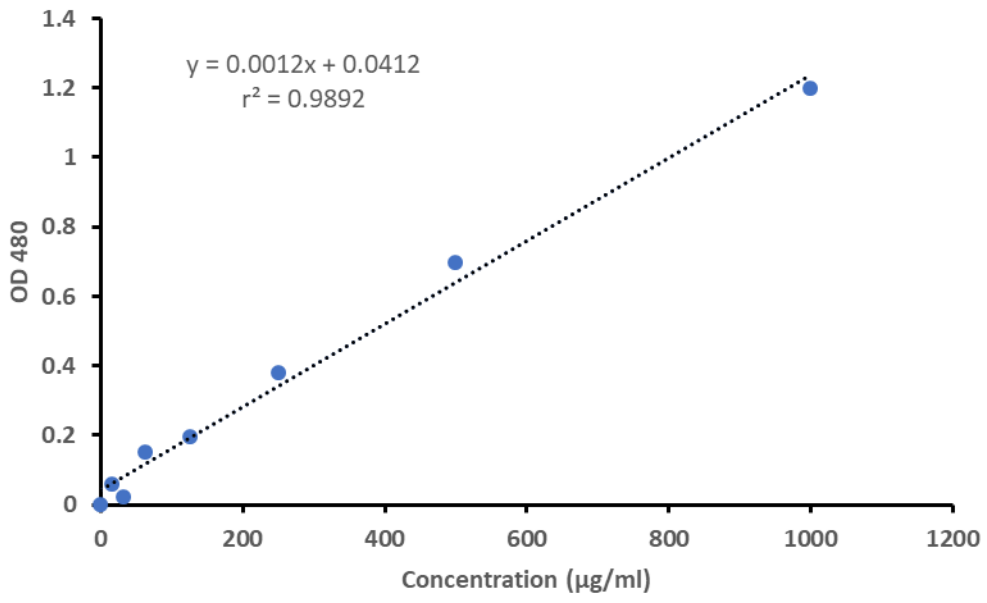

Figure 3.4 Standard curve used for whole-cell peptide determination.

Table 3.3 Average peptide concentration of the samples for whole-cell proteome analysis.

Sample type	Concentration (μg/mL)
sRNA00203-deleted planktonic cells	1445
sRNA00203-deleted biofilm cells	1353.5
Wild-type planktonic cells	1557.5
Wild-type biofilm cells	1101

3.4.3 Liquid chromatography-Mass spectrometry data acquisition

The peptide concentration was normalized to approximately to the lowest measured value (~1000 μg/mL) of the sample using 0.1% formic acid. After gentle spin down, 10 μL was transferred to LC vials and 1 μL was injected onto a nanoscale C18 reverse-phase chromatography system (RPLCnano). Based on hydrophobic interactions, the peptides were separated using a flow rate of 0.3 μL /min, with a gradient ranging from 2% to 40% acetonitrile in 0.1% formic acid (Solvent B) over 90 minutes. The gradient time also included column re-equilibration and organic-wash steps.

The separated peptides were introduced into an Orbitrap Fusion™ Lumos™ mass spectrometer (Thermo Fisher Scientific, USA), and the built-in nanoelectrospray ionization (nano ESI) converted the peptides into charged ions for analysis. The mass spectrometer was set to data-independent acquisition (DIA) mode for both full-scan (MS) and tandem MS (MS/MS) acquisition at an orbital resolution of 60,000. Precursor ions within the scan range of m/z 400-1500 were selected for fragmentation, and higher-energy collisional dissociation (HCD) with a normalized collision energy of 30% was utilized for fragmentation. The fragments were resolved with an Orbitrap resolution of 7,500. All data acquisition, setting parameters, and real-time monitoring of instrument performance throughout the process were accomplished using Thermo Xcalibur software.

3.4.3 Proteome data analysis

Raw DIA MS/MS spectral data from four groups of samples, each with three biological replicates, were collected using the mass spectrometry and imported into Spectronaut version 19 for analysis. We set up a directDIA analysis to produce a spectral library from the runs, and peptide identification was performed by matching the reconstructed MS2 spectra (pseudo-MS2 spectra) with the *A. baumannii* ATCC 17978 FASTA protein sequence obtained

from the UniProt database (uniprotkb_proteome_UP000072389_2024_07_04.fasta downloaded 04 July 2024). In the pulsar search against the database, the parameters were set to a trypsin digest, with minimum and maximum peptide lengths of 2 and 7, respectively, and a tolerance of 2 missed cleavages. Additionally, a 1% false discovery rate (FDR) was employed for precursor ion and protein identification.

The abundance of peptides in each sample was determined from the extracted ion chromatograms (XICs) and normalized by the total ion current (TIC) to account for biases introduced due to instrument or sample preparation process. Then, the IDPicker and MaxLFQ tools within Spectronaut were used for protein inference and label-free quantification (LFQ), respectively, to compare protein expression across conditions. Finally, an unpaired t-test was performed, and proteins with an absolute fold change ≥ 2 and q-value <0.05 were considered as differentially expressed proteins (DEPs). We also included proteins that were uniquely identified in at least two biological replicates within a single condition and were completely absent in the corresponding condition.

3.5 Transmission electron microscopy (TEM)

Biofilms of each isogenic strain (wild-type and sRNA-deleted) were prepared according to the procedures described in Section 3.2. Formed biofilm cells were scraped and collected using 6% glutaraldehyde. To preserve the morphology, the collected biofilm cells were immediately incubated for 1 hour at 4°C. Ten microliters of each preserved biofilm culture was then dropped onto a glow-discharged, carbon-coated 200 mesh grid and allowed to be absorbed for 10 minutes. The excess sample was blotted using filter paper, and the grid was washed twice with ultrapure water. About 10 µL of X solution (formulated from phosphotungstic acid (PTA) and ytterbium chloride ($YbCl_3$)) (Moscardini et al., 2020) was added to the blotted grid and incubated for 15 seconds. The stain was blotted using filter paper and incubated for 1 hour to dry. Finally, the grid was inserted through the holder, and images were captured using a Gatan Orius camera fixed on the ThermoFisher Talos TEM operating at 120 kV (Thermo Fisher Scientific, USA).

3.6 Oxidative stress response assay

Growth response of the sRNA-deleted and wild-type strains to oxidative stress induced by hydrogen peroxide was analyzed. Overnight cultures of the strains grown in LB broth were adjusted to an OD600 of 0.1. The adjusted culture was further grown on fresh 10 mL LB broth for 3 hours. The culture was then diluted to an OD600 of 0.05, with and without hydrogen peroxide (2 mM), in a 96-well microtiter plate, with each well containing 150 µL. The microtiter plate was incubated inside BMG SpectroStar Nano Microplate Reader (BMG LABTECH, Germany) set to 37 °C. Continuous optical density measurements of the plate at 600 nm were conducted for 24 hours after gentle shaking. The experiment was performed using three biological replicas.

3.7 Genomic DNA extraction

Extraction of genomic DNA of *A. baumannii* ST1894 used for various downstream applications was performed using QIAamp BiOstic Bacteremia DNA Kit (QIAGEN, Germany). Briefly, an overnight 20 mL culture was centrifuged at 13,000 xg for 2 minutes, and the supernatant was discarded. The pellet was resuspended in 450 µL lysis solution and transferred to a 2 mL PowerBead tube garnet. The sample was then incubated at a 70 °C heat block for 15 minutes. The lysed sample was vortexed and centrifuged at 10,000 xg for 1 minute. The supernatant was transferred to a new tube and mixed with 100 µL inhibitor removal solution (IRS). After 5 minutes of incubation, binding of the DNA to the column was carried out by adding 1 mL of binding buffer (BB). Subsequently, the bound genomic DNA was eluted in 50 µL of elution buffer (EB) and stored at -20 °C until further use.

3.8 Construction of overexpression strain

3.8.1 sRNA00203 insert preparation

To construct sRNA0203 overexpressing *A. baumannii* strain, Gibson assembly-based NEBuilder HiFi DNA assembly cloning technique was employed. First, the sRNA sequence was amplified by PCR from the genomic DNA of *A. baumannii* using cloning primers In203AhdI-F and In203AhdI-R (Table 3.5). The primers were incorporated restriction sites and homologous nucleotides. For amplification, we used Q5 High-fidelity 2x Master Mix (New England Biolabs, UK). The PCR conditions were as follows: initial denaturation at 98°C

for 30 seconds; 30 cycles of 98°C for 8 seconds, 61°C for 20 seconds, and 72°C for 20 seconds; followed by a final extension at 72°C for 2 minutes. The PCR products were separated on 2.4 % (w/v) agarose gel premixed with 5% (v/v) RedSafe nucleic acid staining solution (iNtRON Biotechnology, Korea) and visualized using a Gel Doc Method XR (Bio-Rad, USA). The correct band size was then extracted from the gel using Monarch DNA Gel Extraction Kit (New England Biolabs, UK) for cloning into an expression plasmid.

3.8.2 Recombinant plasmid preparation

After preparing the insert, the expression plasmid constructed from pWH1266 and pUC57 vector backbone, named pSGAb-km (a generous gift from Quanjiang Ji, Addgene plasmid #121999), was used for recombinant plasmid construction. The plasmid harbours a kanamycin resistance marker and a 35-nucleotide-long SpeI constitutive promoter. *E. coli* harbouring the plasmid was subcultured on LB agar containing 50 µg/mL kanamycin and incubated overnight at 37°C. A single colony was further subcultured into 5 mL of LB broth containing kanamycin and incubated for 24 hours. The LB broth culture was pelleted and subjected to plasmid extraction using a FavorPrep Plasmid DNA extraction Mini kit (FAVORGEN BIOTECH CORP., China) as per the manufacturer's instructions. Then, two µg of plasmid DNA was digested with AhdI (Eam105I) (New England Biolabs, UK) for 4 hours in a 37°C incubator. The digested plasmid was analysed on a 1% agarose gel and purified using GeneJet PCR Purification Kit (Thermo Fisher Scientific, USA).

Once the insert and linearized plasmid were prepared, the assembly reaction was conducted using the NEBuilder HiFi DNA Assembly Master Mix (New England Biolabs, UK). The assembly process shares the principles of Gibson assembly, but unlike Gibson assembly, it is capable of 3' and 5' end mismatch removal. In the Gibson assembly, three enzymes were used in combination for cloning. DNA fragments were digested from the 5' ends by an exonuclease to generate single-stranded overhangs for annealing. Gaps were then filled in by DNA polymerase after annealing, and nicks were covalently sealed by DNA ligase to produce a continuous double-stranded plasmid.

In the assembly reaction, the insert-to-plasmid ratio was 5:1, calculated based on the formula provided on the webpage (https://nebuildercalculator.neb.com/). The detailed volumes of the insert, plasmid fragment, and master mix used for HiFi assembly are

summarized in Table 3.4. The mixture was then incubated in a thermocycler at 50°C for 30 minutes and stored at -20°C for the subsequent transformation.

3.8.3 Competent cell preparation and transformation

The chilled assembly reaction was used to transform competent cells of *A. baumannii* ST1894. The electrocompetent cells were prepared according to previous protocol (Y. Wang et al., 2020). The main reagent in the preparation of the competent cells was ice-cold 10% glycerol. It was used to repeatedly wash cells in the mid-logarithmic phase to make their cell membranes permeable to DNA. Fifty microlitres of competent cells were mixed with 2 µL of HIFI assembly reaction and incubated on ice for 10 minutes. We then transferred the cell-DNA mixture into a prechilled 2 cm wide electroporation cuvette (Thermo Fisher Scientific, USA) and subjected it to a 1.5-kV electric pulse using a GenePulser Xcell (Bio-Rad, USA) set to 25 µF capacitance and 200 ohms external resistance. The pulse was applied for 4.8 ms, indicating that it was of sufficient duration. For recovery of the cells, 1 mL of pre-warmed LB broth was immediately added to the pulsed cells, and the mixture was incubated at 37°C with agitation at 250 rpm for 1 hour. Finally, the liquid culture was pelleted, and 20 µL of the suspension was streaked onto LB agar containing 50 µg/mL kanamycin for overnight incubation at 37°C.

Table 3.4 Content and volume of components in HIFI assembly reaction.

Component	**Volume**	**NEBuilder positive control**	**Negative control**
Insert (n = 1)	1 µL	0.5 µL	-
Linearized vector	3 µL	2 µL	2 µL
NEBuilder HiFi DNA Assembly Master Mix	10 µL	10 µL	10 µL
Deionized H2O	6 µL	7.5	8 µL
Total volume	20 µL	20 µL	20 µL

3.8.4 Screening and validation of transformants

Several colonies from the overnight culture of recovered cells were picked for PCR. Primer pairs were designed to hold the flanking region of the insert. The picked colonies were resuspended in 10 µL of sterile, nuclease-free water in PCR tubes. The PCR was performed using 2x Taq Quick-Load Master Mix (New England Biolabs, UK). Two microliters of the colony suspension were transferred to the 23 µL amplification reaction mixture. During the PCR, the initial denaturation step was extended to 10 minutes to lyse the cells. As controls, we included both negative and positive control reactions. The positive control reaction contained 1 µL of the assembly reaction. Subsequently, all amplification reactions were visualized using a 2.4 % agarose gel premixed with RedSafe nucleic acid stain.

The colonies that harbour DNA of the expected size were candidates for further validation by Sanger sequencing. The candidate colonies were subcultured in LB broth containing 50 µg/mL kanamycin. After overnight incubation, plasmids were extracted using the FavorPrep Plasmid DNA extraction Mini kit (FAVORGEN BIOTECH CORP., China) and checked for the presence of the insert. The plasmids with the correct insert size were subjected to Sanger sequencing using forward and reverse primers using Applied Biosystems 3730xl DNA Analyzer (Thermo Fisher Scientific, USA). The primers used for PCR and Sanger sequencing are described in Table 3.5.

3.9 Growth curve analysis

The wild-type, sRNA00203-overexpressing, and empty vector-containing *A. baumannii* strains were cultured in biological triplicates, subcultured into 20 ml of fresh LB broth, and incubated overnight at 37°C. The LB broth cultures were diluted until the optical density at 600 nm (OD600) has reached a value of 0.05. Subsequently, 150 µL of the diluted cultures were dispensed into a 96-well microtiter plate and incubated in a BMG SpectroStar Nano Microplate Reader (BMG LABTECH, Germany) set to 37°C. Bacterial cell density was measured at OD600 at 1-hour intervals for 24 hours.

3.10 Quantitative biofilm mass determination

Crystal violet staining method was used to determine the biofilm masses formed on the Calgary Biofilm Device (CBD), which is a 96-well microtiter plate with pegs on the lid (Innovotech, Canada). A total volume of 180 microliters, consisting of a 1:1 ratio of LB broth and 1.5 × 10^8 CFU/mL of either the sRNA000203 overexpressing strain or the strain harboring an empty plasmid in MRD, was incubated for 48 hours at 37°C. The planktonic cells were removed, and the wells and pegs were washed thrice with PBS. Each dried well of the microtiter plate was then filled with 200 µL of 0.1% aqueous crystal violet stain, covered with the lid, and incubated for 15 minutes. To detach the crystal violet bound to the biofilm, 200 µL of 33% (v/v) acetic acid was added to each well of the dried CBD. The detached stain absorbance was measured at 570 nm using a microplate spectrophotometer (Bio-Rad, USA) (Shenkutie et al., 2020). For reliable comparison of biofilm mass between the isogenic strains, the experiment was performed three times using independent cultures.

3.11 Phylogenetic analysis

FASTA files of the sRNA00203 sequence from the NCBI database for the *Acinetobacter* species (E-value ≤ 1e-04) were used to construct a phylogenetic tree using MEGA 11. In the software, alignment was performed with MUSCLE, and the phylogenetic tree was constructed using the neighbour-joining method (Tamura et al., 2021).

3.12 Detection of sRNA00203 from clinical isolates

A total of 42 *A. baumannii* strains identified from blood (n = 20), CSF (n = 5), urine (n = 7), aspirate (n = 3), and other clinical samples (n = 4) were used for PCR detection of the sRNA00203 sequence. Additionally, three isolates from hospital environment were included. The kit 2x Taq Quick-Load Master Mix (New England Biolabs, UK) was used for the PCR amplification of the sRNA from genomic DNA. The PCR conditions and gel detection were the same as described in section 3.8.1.

3.13 Tag-based RNA-RNA interactome capture

Tag-based RNA capture experiment design is derived from MS2-affinity purification coupled with RNA sequencing (MAPS) protocol developed by Lalaouna et al.(Lalaouna et al., 2015) with major modifications. It consists of the construction of a 24-nucleotide-tagged

sRNA00203 expression strain, RNA hybridization, bead-based RNA capture, and RNA purification. The simplified design is illustrated in Figure 3.5.

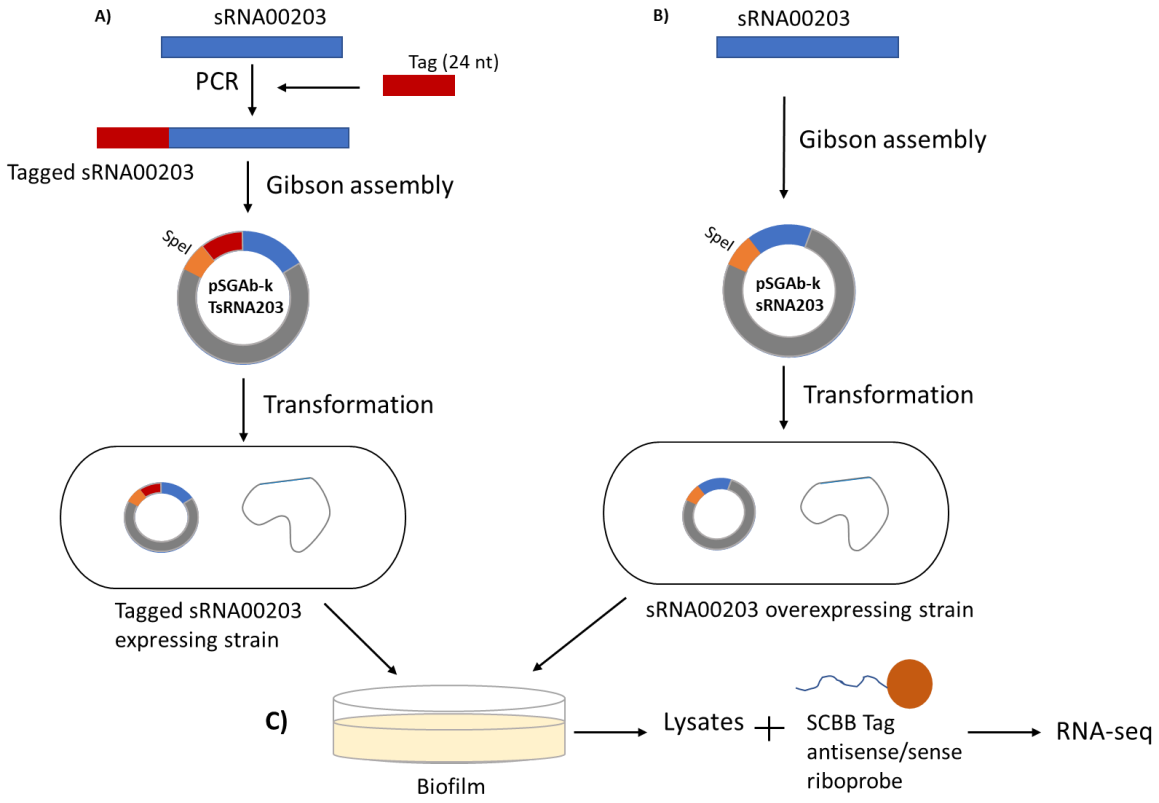

Figure 3.5 Schematic of RNA-RNA interactome capture in *A. baumannii* biofilm cells. Construction of tagged sRNA00203 expressing (A) and sRNA00203 overexpressing *A. bauamnnii* strain (B) was done using Gibson assembly. (C) Biofilm cell lysates of the strain transformed with the tagged sRNA00203 or untagged sRNA00203 plasmid were incubated with bead-bound biotin-labelled antisense/sense riboprobe to capture target RNAs. The captured RNAs from the experimental (A) and control reaction (B) were subjected to RNA sequencing. SCBB: Streptavidin-coated bead bound.

3.13.1 Construction of tagged sRNA00203 expression strain

3.13.1.1 Tagged sRNA00203 DNA preparation

To enable sRNA00203 to bind to target mRNA with full capacity, we considered tagging as a valuable tool. A 24-nucleotide-long tag (CAGTCTCCGAATCTGTCGGTAGTG) was added to the sRNA00203 DNA sequence using PCR. The forward primer at the 5' end, which comprises the tag, a few additional nucleotides, and sRNA00203-specific sequences, was designed for the preparation of tagged sRNA00203 template. Then, the 86-nucleotide (nt) long product

was served as a template to generate a 129-nt long tagged sRNA00203 insert through the use of primer pairs designed using NEBuilder (https://nebuilder.neb.com/) (Table 3.5). The forward primer contains left homologous regions (16nt) and reverse primer contains right homologous regions (15nt) of plasmid DNA. In all the PCR processes, we used Q5 High-fidelity 2x Master Mix (New England Biolabs, UK) as described in Section 3.8.1.

3.12.1.2 Tagged sRNA00203 expression plasmid preparation

Similar to the overexpression study, we used the pSGAb-k plasmid to construct a tagged sRNA expression plasmid. Two micrograms of the pSGAb-k plasmid were digested for 4 hours in a 50 µL reaction at 37°C using AhdI restriction enzyme (New England Biolabs, UK). The prepared tagged sRNA insert and digested expression plasmid were checked to ensure correct size and proper digestion, respectively, by agarose gel electrophoresis. The correct bands were excised from the gel and purified using Monarch DNA Gel Extraction Kit (New England Biolabs, UK). Concentration and purity of the purified insert and plasmid were assessed by measuring OD260/280 and OD260/230 ratios using a NanoDrop 1000 spectrophotometer (Thermo Fisher Scientific, USA).

For assembly, the purified tagged sRNA and pSGAb-k plasmid were mixed in a 10:1 molar ratio in the presence of NEBuilder HiFi DNA Assembly Master Mix (New England Biolabs, UK) and incubated at 50°C for 1 hour. Two microliters of the ligated product were used to transform *A. baumannii* competent cells prepared with 10% glycerol. Immediately, 1 mL of prewarmed LB broth was added to the electroporated cells and incubated at 37°C for 1 hour in a shaking incubator at 200 rpm. Then, the recovered cell pellet was plated on LB agar containing 50 µg/mL kanamycin and incubated overnight at 37°C. The grown colonies were screened using colony PCR to ensure the presence of the insert. Plasmids from positive clones were checked for the fusion of the insert near the SpeI promoter and for sequence accuracy using Sanger sequencing. The oligonucleotides used for colony PCR and Sanger sequencing are listed in Table 3.5.

3.13.2 Cell lysate preparation and hybridization

Biofilm cell pellets from tagged sRNA00203-expressing and sRNA00203-overexpressing *A. baumannii* strains were washed twice with PBS. The washed pellet was then resuspended in 100 µl of lysozyme (10 mg/mL) and mixed with one µl of 10% sodium dodecyl sulphate

(SDS). After 5 minutes of incubation, lysis buffer from PureLink™ RNA Mini Kit (Thermo Fisher Scientific, USA) was added to the resuspended pellet and centrifuged for 5 minutes at 12,000 g. The cleared supernatant lysates were equally transferred into 2 mL Lobind microcentrifuge tubes. Two times volume of hybridization buffer (750 mM NaCl, 1% SDS, 1 mM EDTA, 50 mM Tris-HCl, pH 7.0,15% Formamide) was added to each lysate and mixed by vortexing. A 3' Biotin-TEG labelled sense probe (0.5 pmole) and antisense probe (0.5 pmole) of the tag sequence were then added separately to the tubes containing tagged lysate. Only the 3' Biotin-TEG labeled antisense probe (0.5 pmole) was added to the tube containing the sRNA00203-overexpressing cell lysate. To prevent degradation of the RNAs, SUPERase·In™ RNase Inhibitor (0.25 U) (Thermo Fisher Scientific, USA) was incorporated into the reaction. Finally, the hybridization reactions were incubated at room temperature with rotation at 25 rpm for 5 hours. The lysate from the tagged sRNA-expressing strain mixed with the sense probe and the lysate from the sRNA-overexpressing strain mixed with the antisense probe served as controls to rule out non-specifically bound RNAs.

3.13.3 Streptavidin-coated bead-assisted RNA capture

Streptavidin-coated beads, specifically Dynabeads™ M-270 Streptavidin (Thermo Fisher Scientific, USA), were utilized to isolate the bound RNAs formed during the hybridization process. A hundred microliters of beads were withdrawn into a 2 mL Lobind microfuge tube for each sample and placed on a magnetic rack. The supernatant was removed, and the beads were then washed and blocked to minimize RNase contamination and non-specific binding, respectively. Freshly prepared washing buffer (5 mM Tris-HCl, pH 7.5; 0.5 mM EDTA; 1 M NaCl) was used to wash the beads three times for 2 minutes each, followed by a wash with RNase-inactivating solution (0.1 M NaOH, 0.05 M NaCl) for 2 minutes each, repeated twice. Subsequently, the beads were resuspended in 0.1 M NaCl and transferred to a magnetic rack to collect RNase-free beads.

The prepared beads were resuspended in a blocking buffer that contained yeast tRNA (2 µg/µL) and bovine serum albumin (1 µg/µL) (Thermo Fisher Scientific, USA) for 10 hours at 4°C with rotation (20 rpm). After two washes with the wash buffer, the blocked beads were mixed with the bound RNA in the presence of freshly prepared binding buffer (10 mM Tris-HCl, pH 7.5; 1 mM EDTA; 2 M NaCl). To protect the streptavidin that coats the bead, Halt™

Protease Inhibitor Cocktail (2.5X) (Thermo Fisher Scientific, USA) was also part of the reaction. The mixture was then incubated overnight at 4°C with rotation (20 rpm) to facilitate the capture of the biotin-labelled probe bound to the target RNA by the streptavidin-coated beads.

3.13.4 Bound RNAs purification and DNase treatment

The incubated mixture was transferred to the magnetic rack for 2 minutes to retain the beads bound to RNAs. Non-specifically bound RNAs and other molecules were washed away using a wash buffer composed of 0.5% sodium dodecyl sulphate (SDS) and saline-sodium citrate (2X SSC). In each round, 1 mL of wash buffer was used for five washes with rotation for 5 minutes. The washed beads coupled to molecules were resuspended in 190 µL of proteinase K buffer (100 mM NaCl, 1 mM EDTA, 10 mM Tris-HCl, pH 7.0, and 0.5% SDS) and 10 µL of proteinase-K enzyme (10 mg/mL) to elute the RNA interactome. It was then transferred to a 50 °C heat block for 50 minutes, followed by heating at 95°C for 10 minutes. For subsequent RNA purification, we used Monarch® Spin RNA Cleanup Kit (New England Biolabs, UK). The supernatant detached from the beads was collected in a new Eppendorf tube. Buffer BX and absolute ethanol were added to the tube at volumes twice and three times that of the supernatant, respectively. Subsequently, it was transferred to a purification column and centrifuged at 16,000 g for 1 minute. The flow-through was discarded, and washing was performed twice with wash buffer. The purified RNA was then eluted in 16 µL of nuclease-free water. Lastly, residual DNA was removed by treating the captured RNA sample pools with TURBO DNase I (Thermo Fisher Scientific, USA) for 25 minutes at 37°C.

Table 3.5 Oligonucleotides used for tag-based primary sRNA target identification and validation.

Name	**Sequence**	**Purpose**
sRNA203AhdI_F	GGTATAATACTAGTCGAgaccattggtcCCGATATCAAGGAAGAGATCA	Insert preparation for overexpression
sRNA203AhdI_R	TAGCTCTAAAACTGAgaccaatggtcCCTCTTGAAACTGTTCTTACTC	
sRNA203Tem_F	CTCATATGCAGTCTCCGAATCTGTCGGTAGTGCCGATATCAAGGAAGAGATCA	Tagged sRNA00203 template preparation
sRNA203Tem_R	GCTCATATGCCTCTTGAAACTGTTCTTACTC	
sRNA203TAh_F	GGTATAATACTAGTCGAgaccattggtcCAGTCTCCGAATCTGTCGGTAGT	Tagged sRNA00203 insert preparation
sRNA203TAh_R	TAGCTCTAAAACTGAgaccaatggtcCCTCTTGAAACTGTTCTTACTCAAGTTCCT	
sRNA203LFI_F	GTTGCATGGGCATAAAGTTGC	Colony PCR
sRNA203RFI_R	ACTCGGTGCCACTTTTTCAAG	
sRNA203LPla_F	TTAGGTCTTGCCTGCTTTATC	Sanger sequencing
sRNA203LPla_R	ACTCGGTGCCACTTTTTCAAG	
Tag antisense RNA probe	CACUACCGACAGAUUCGGAGACUG	Tag-based RNA capture assay
Tag sense RNA probe	CAGUCUCCGAAUCUGUCGGUAGUG	Control for Tag-based RNA capture assay
sRNA00203_RT_F	GTTTTTTTTAATACGACTCACTATAGGCCGATATCAAGGAAGAGATCA	In vitro transcription of sRNA00203
sRNA00203_RT_R	CCGATATCAAGGAAGAGATCA	
secE_RT_F	GTTTTTTTTAATACGACTCACTATAGGGTCCCTCCTGACCTGCCATA	In vitro transcription of *secE* region
secE_RT_R	TCTTTGAGGAATTGGCGCGT	
lpxO_RT_F	GTTTTTTTTAATACGACTCACTATAGGGTGACCAAACAGGGGGCTTA	In vitro transcription of *lpxO* region
lpxO_RT_R	TTAAAACACGTATGGTCGAAC	
SAM_RT_F	GTTTTTTTTAATACGACTCACTATAGGGTGGTGGCCATGTAGCTTAT	In vitro transcription of 3-isopropylmalate dehydratase large subunit region
SAM_RT_R	TCGAGCATTGGCAGCTTT	

Lower case: restriction site of AhdI; Underlined: homologous regions.

3.13.5 RNA sequencing of captured RNA and data analysis

Captured RNA sample pools from biological triplicate of the tagged sRNA expressing cell lysate (experimental) and sRNA overexpressing cell lysate (control) were considered for RNA sequencing separately. The average concentration and quality score assessment of the RNA samples are shown in Table 3.6. For the preparation of a directional cDNA library, the procedures were identical to those described in Section 3.3.2, ranging from the removal of randomly bound ribosomal RNA to library quality control. The libraries of experimental RNA and control RNA samples underwent prokaryotic paired-end RNA-seq independently using Illumina NovaSeq X Plus with a 150-bp read length. The RNA sequencing produced approximately 1.3 Gbp of raw data per sample. The data analysis process, which includes data cleaning through to ontological analysis, utilized the same software as stated in Sections 3.3.3 and 3.3.4. Differentially enriched genes were identified using edgeR. Genes with a p-value <0.05, a fold change ≥ 2, and an FKPM value ≥ 50 were taken as candidate primary base pairing targets.

Table 3.6 Description of capture RNA samples considered for RNA-seq.

Sample name	**RNA Conc.(ng/µl) by Qubit Fluorimeter**	**RNA Purity, NanoDrop 2000**	
		260/280	**260/230**
Experimental	14.1	2.31	1.67
Control	7.42	2.10	1.02

3.13.6 Quantitative RT-PCR

Reverse transcription-quantitative polymerase chain reaction (RT-qPCR) analyses of the top-enriched genes in the tag-based capture RNA-seq analysis were similar to those described in Section 3.3.5, except for two points. First, cDNA synthesis was performed using a total of 50 ng of RNA and was then diluted tenfold for RT-qPCR. Second, during the analysis, we compared the cycle threshold (Ct) values of gene expression in biological triplicate samples across comparison groups without normalizing with a housekeeping gene.

3.14 In silico binding analyses of sRNA–RNA interactions

IntaRNA and copraRNA software were used for prediction of binding sites of sRNA00203 on potential primary targets identified by tag-based capture assay. The copraRNA analysis was used to predict binding regions around the starting codon of the target mRNA by extracting 200 nt upstream and 100 nt downstream sequences from *A. baumannii* ATCC 17978 genome (GenBank assembly accession: NZ_CP039025). We used the IntaRNA to predict binding sites on the target coding region, considering a minimum seed region of seven nucleotides. Most of the parameters of the prediction tools were set to their default values.

3.15 In vitro transcription

Template DNA required for in vitro transcription was prepared by designing a forward primer that contains the T7 promoter motif at the 5' end (TAATACGACTCACTATAG) and a reverse primer containing only gene-specific sequences. The amplification was carried out by Q5® High-Fidelity DNA Polymerase (New England Biolabs, UK). The PCR conditions were as described in Section 3.8.1. The PCR product was checked in a 2.5 % agarose gel for correct size and purified by GeneJET PCR Purification Kit (Thermo Fisher Scientific, USA).

The T7 promoter containing purified DNA template was then transcribed using HiScribe T7 Quick High Yield RNA Synthesis Kit (New England Biolabs, UK). Based on the instructions for template < 300 bp, nuclease-free water, NTP Buffer Mix, template DNA (20ng), and T7 RNA Polymerase were mixed in a 30 µL reaction volume and incubated at 37°C for 6 hours for transcription. The untranscribed template DNA was eliminated by adding DNase I and incubating the mixture at 37°C for 15 minutes. Then, the transcription product was checked for size by running it on a 10% urea PAGE gel (Beyotime, China) in 1X TBE running buffer and comparing it to RiboRuler™ Low Range RNA Ladder (Thermo Fisher Scientific, USA). The synthesized RNA was then purified using the Monarch® Spin RNA Clean-up Kit (New England Biolabs, UK) and stored at -80°C for downstream experiments.

3.16 RNA-to-RNA interaction shift assay

To verify the interaction between sRNA00203 and potential primary targets, we performed an electrophoretic mobility shift assay (EMSA) according to a previous study (Jia et al., 2021). In vitro transcribed and purified sRNA, target RNAs, and positive control RNAs, which were prepared as stated in Section 3.13, were used for the assay. The sRNA (1 pmol) was

mixed with increasing target mRNA concentrations (2, 4, and 6 pmol) in the presence of a binding buffer containing 200 mM KCl, 24 mM MgCl2, 100 mM HEPES (pH 7.3), and 24 mM DTT. The positive control reaction included sRNA (Aar) (2 pmol) and its confirmed target, CarO type III (4 pmol), as identified in *A. baumannii* (Hamrock et al., 2024). The mixture was then incubated at 85°C for 2 minutes, followed by 40 minutes at 37°C. After incubation, each reaction was loaded onto a 5% native polyacrylamide gel and run for 30 minutes at 120 V. The gel was stained with SYBR™ Gold Nucleic Acid Gel Stain (1x) (Thermo Fisher Scientific, USA) for 10 minutes and visualized using a Gel Doc Method XR (Bio-Rad, USA). Densitometric analysis of the formed complexes was performed using ImageJ software.

3.17 RNA-Protein pulldown

3.17.1 Desthiobiotinylation of RNAs

Pierce RNA 3' End Desthiobiotinylation Kit (Thermo Fisher Scientific, USA) was used for the desthiobiotinylation of both the in-house prepared sRNA00203 and supplier-provided control RNA. The 43-nucleotide-long control RNA (5´-CCUGGUUUUUAAGGAGUGUCGCCAGAGUGCCGCGAAUGAAAAA-3´) originates from a eukaryotic cell and has no sequence similarity to the *A. baumannii* genome. The RNAs were heated at 85°C for 5 minutes to relieve secondary structures before being transferred to the RNA ligation reaction. The thirty-microliter ligation reaction containing nuclease-free water, 10X RNA ligase reaction buffer (1X), RNase inhibitor (40U), the heated control RNA or sRNA00203, T4 RNA Ligase (U), and 30% PEG (15%) was incubated at 16°C for 16 hours to achieve efficient labelling. During the reaction, biotinylated cytidine bisphosphate was incorporated into the 3’ of the RNAs by T4 RNA Ligase. Once biotinylated, 70 µL of nuclease-free water was added to each reaction, followed by RNA purification using the Monarch® Spin RNA Clean-up Kit according to the manufacturer’s instructions (New England Biolabs, UK).

3.17.2 Binding of proteins to labelled RNA

For capture of sRNA00203 binding proteins, we utilized Pierce™ Magnetic RNA-Protein Pull-Down Kit (Thermo Fisher Scientific, USA). For binding the RNAs to streptavidin magnetic beads, 70 picomoles of either the biotinylated sRNA00203 or control RNA were added to the pre-treated 50 µL beads (according to section 3.11.3) in the presence of an equal volume of

1X RNA capture buffer. The mixture was incubated for 40 minutes with agitation to facilitate the binding of labelled RNA to the magnetic beads. The tube was placed into a magnetic stand to collect the beads against the side of the tube and washed twice with an equal volume of 20mM Tris (pH 7.5) to remove unbound RNAs. The beads were then mixed well with 100 µL of 1X Protein-RNA binding buffer and incubated until the RNA-protein binding master mix was prepared.

On average, 100 mg/mL of protein extracted from the wild-type biofilm cells of *A. baumannii* ST1894 was included in each 100 µL binding master mix. The protein was extracted based on the procedures explained in Section 3.4.1. Additionally, the binding mix consisted of 10X Protein-RNA binding buffer (1X), 50% glycerol (15 %), 0.5 M sodium chloride (50 mM), and nuclease-free water. The sRNA00203 or control RNA-bound beads mixed with the binding buffer were then incubated for 90 minutes at 4°C with agitation to capture proteins. After incubation, the tube was placed into a magnetic stand to collect the beads against the side of the tube, and the supernatant was discarded. The collected bead was washed three times with 1X wash buffer (100 µL each time). The bound proteins were then eluted by incubating the beads in 50 µL of elution buffer for 30 minutes at 37°C with shaking at 500 rpm. The experiment was performed three times for downstream analysis.

3.17.3 Protein measurement and LC-Mass spectrometry

Eluted proteins from the three replicas of both comparison groups were subjected to reduction, alkylation, digestion, and purification procedures, the same as described in Section 3.4.1. The cleaned and eluted peptides were dried for 8 hours using the CentriVap vacuum concentrator (Labconco, USA) and reconstituted in 50 µL of 0.1% formic acid. Reconstituted peptides were measured using Pierce Quantitative Colorimetric Peptide Assay (Thermo Fisher Scientific, USA), and calculated values based on the standard curve (Figure 3.6) are described in Table 3.7. Considering the low peptide concentration, ten microlitres from each sample was injected onto a nanoscale C18 reverse-phase chromatography system (RPLCnano). The remaining process, including mass spectrometry data acquisition and analysis, was also the same as stated in Section 3.5, except that the quantity correction factor was considered here during data analysis. The highest peptide value (63.43 µg/mL) obtained from the sample (sRNA00203_3) was taken as reference for the adjustment.

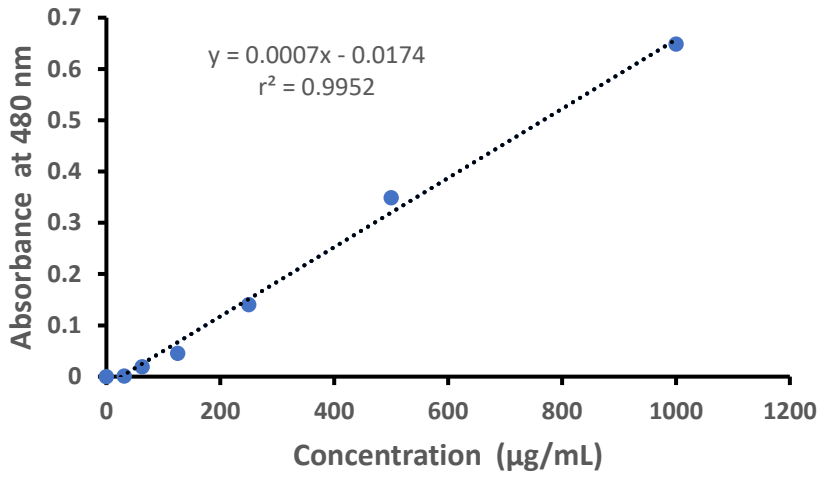

Figure 3.6 Standard curve used to calculate the concentration of pulled peptides.

Table 3.7 Description of sample peptide values obtained from RNA-Protein pull-down assay.

Sample name	Concentration (µg/mL)	Quantity correction factor
sRNA00203_1	54.14	1.17
sRNA00203_2	32.71	1.94
sRNA00203_3	63.43	1
Control RNA_1	24.86	2.55
Control RNA_2	50.57	1.25
Control RNA_3	48.43	1.32

3.18 Data presentation and statistics

GraphPad Prism V.8 was employed to generate volcano plots, heat maps, and bar graphs using data obtained from the differential transcription and functional enrichment analysis. Mean, independent t-test, correlation, and z-score to present proteomics and RT-qPCR data were also computed using the same tool.

4. Results

4.1 Transcriptomic profiles of *A. baumannii* isogenic strains

4.1.1 RNA sequencing data description

In our previous study, we reported the impact of non-coding sRNA00203 on biofilm formation and biofilm-related antibiotic resistance in *A. baumannii* ST1894. When the sRNA was deleted, biofilm formation was substantially reduced, which rendered the deletion mutant strain more susceptible to imipenem and ciprofloxacin. Selected few biofilm and antibiotic-attributable genes were also affected (Shenkutie et al., 2023). To gain further genome-wide insights, we performed RNA sequencing of both the wild-type strain and the sRNA00203-deleted strain at biofilm and planktonic growth forms in biological triplicates. The sequencing generated an average cleaned read count of 17.1 million for wild-type planktonic cells, 15.35 million for wild biofilm cells, 15.95 million for deletion mutant planktonic cells, and 19.33 million for deletion mutant biofilm cells. The minimum base call quality of 30 achieved 90.43% coverage in the wild-type biofilm cells, confirming that we obtained high-quality reads suitable for downstream analysis (Table 4.1).

Table 4.1 Average read count, quality score, and mapping description of four types of samples with biological triplicates.

Sample name	Raw reads	Cleaned reads	Error rate (%)	Q20(%)	Q30(%)	Mapped reads		
						Total mapped (%)	Single mapped (%)	Multiple mapped (%)
Wild-type planktonic	17265238	17097040	0.03	97.98	94.07	15166320 (88.71)	13180523 (77.09)	1985797 (11.61)
Wild-type biofilm	15656782	15348786	0.03	95.59	90.43	11814401 (76.97)	8509913 (72.03)	3304488 (4.94)
Deletion mutant planktonic	16306768	15946062	0.03	97.66	93.69	14669754 (92)	12302400 (77.15)	2367354 (14.85)
Deletion mutant biofilm	19447614	19328644	0.03	98.02	94.09	17937839 (92.80)	17036670 (88.14)	901169 (4.66)

Q20: bases with 20 Phred value (base call accuracy of 99%); Q30: bases with 30 Phred value (base call accuracy of 99.9%).

4.1.2 Differentially regulated genes in biofilm cells

The transcriptomic influence of non-coding sRNA00203 on 3765 genes was evaluated by cultivating the isogenic strains under biofilm conditions. Of these genes, 816 (21.7%) genes were significantly dysregulated (Padj < 0.05), with 406 (10.8%) genes upregulated and 410 (10.9%) genes downregulated by at least 2-fold in the sRNA00203-deleted strain compared to the wild-type strain. Among the genes that exhibited altered expression, EamA-like transporter family encoding gene (E5A72_RS15275) displayed the highest upregulation, with a fold change of 13. On the other hand, the gene E5A72_RS09705, which encodes a small subunit of 3-isopropylmalate dehydratase, demonstrated the most significant downregulation, with a fold change of -21 (Figure 4.1A).

Genes associated with membrane proteins, MFS efflux pump, type IV pili, and iron acquisition systems were repressed. In contrast, genes related to ribosomal proteins, Ade IJK efflux pumps, Csu pili, and porins were induced (Table 4.2). The expression patterns of genes included in these functional categories were consistent in the three biological replicate samples of each comparison group, as illustrated in the heatmap (Figure 4.1B).

Numerous genes involved in ribosome synthesis were upregulated. About twenty-three large subunit and nineteen small subunit ribosomal protein-encoding genes were induced (Figure 4.4). Of these, the top three genes with their expression level are presented in Table 3.2. The other affected structure was type IV pili (T4P). Genes responsible for assembly (E5A72_RS09280 and E5A72_RS05200) and biogenesis (E5A72_RS05190) of T4P and twitching motility (E5A72_RS11885) were among the negatively influenced (Table 3.2). The relative expression levels of the genes encoding 50S ribosomal protein L16, 30S ribosomal protein S3, pilus assembly protein PilM, and Type IV pilus twitching motility protein PilT were validated by RT-qPCR (Figure 4.10).

Quorum sensing in *A. baumannii* has been reported to be related to biofilm formation (Xiong et al., 2022). The *AbaI* that encodes the signalling molecule (AHL) was downregulated in the mutant biofilm cells by 4-fold. Additionally, class I SAM-dependent methyltransferase (E5A72_RS16120), which is known for macromolecule methylation and suspected to have a role in the quorum-sensing system, was repressed by 104-fold.

Amino acid metabolism was also among the positively influenced processes, particularly leucine biosynthesis due to the downregulation of both large and small isopropylmalate dehydratase coding genes (Table 4.2). The above findings together highlight the involvement of the sRNA in both negative and positive regulation of diverse biological processes.

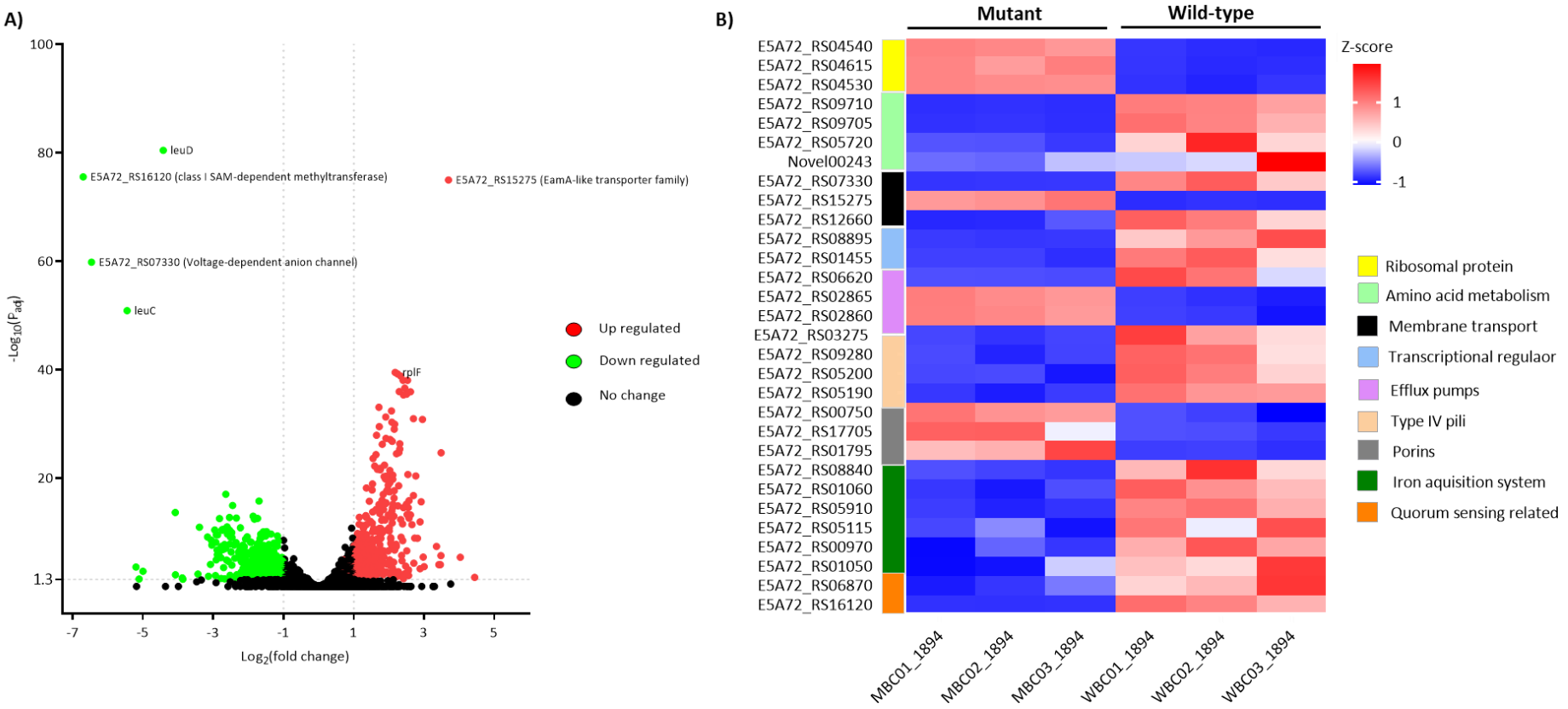

Figure 4.1 Gene expression status in biofilm cells of *A. baumannii* ST1894 isogenic strains. (A) Volcano plot showing differentially expressed transcripts in sRNA00203-deleted biofilm cells compared to the wild-type biofilm cells. Genes with an absolute log2 fold change ≥1 and Padj < 0.05 were considered significantly altered and are illustrated in green and red colors. (B) Heat map showing the prioritized 30 influenced genes' expression pattern in the biological triplicate samples of each sRNA00203 mutant and wild-type biofilm cells. Rows indicate a gene, and columns correspond to biological replicate samples. Fragments per kilobase of transcript per million mapped reads (FPKM) values of genes were used for Z-score determination. MBC: Deletion mutant biofilm cells; WBC: Wild-type biofilm cells.

Table 4.2 DEGs in key functional groups in the sRNA00203-deleted versus wild-type biofilm cells of *A. baumannii* ST1894 strain.

Functional annotation	Product	$Log_2(FC^{\#})$	Padj.
Amino acid metabolism			
E5A72_RS09710(*leuD*)	3-isopropylmalate dehydratase small subunit	-4.42	1.23E-77
E5A72_RS09705(*leuC*)	3-isopropylmalate dehydratase large subunit	-5.46	9.20E-49
E5A72_RS05720	Branched-chain amino acid transport protein (AzlD)	-2.10	2.43E-05
Novel00243	Amino acid permease	-2.53	0.0292
Membrane transporter			
E5A72_RS07330	TDT family transporter (Voltage-dependent anion channel)	-6.47	1.27E-57
E5A72_RS12660	Cation diffusion facilitator family transporter	-3.16	1.49E-08
E5A72_RS15275	EamA-like transporter family	3.70	1.24E-72
Transcriptional regulator			
E5A72_RS08895	TetR/AcrR family transcriptional regulator	-2.64	5.54E-16
E5A72_RS01455	LysR family transcriptional regulator	-2.34	7.72E-12
Efflux pumps			
E5A72_RS06620	MFS transporter	-4.09	8.47E-13
E5A72_RS02865(*adeK*)	Multidrug efflux RND: subunit AdeK	1.93	3.19E-19
E5A72_RS02860(*adeJ*)	Multidrug efflux RND: subunit AdeJ	2.10	1.28E-13
Porins			
E5A72_RS00750	OmpW family protein	1.74	3.22E-07
E5A72_RS17705	OmpH family outer membrane protein	2.16	2.43E-06
E5A72_RS01795	Ornithine uptake porin CarO type 4	2.70	9.18E-16
Ribosomal proteins			
E5A72_RS04540(*rplF*)	50S ribosomal protein L6	2.18	1.91E-37
E5A72_RS04615(*rplC*)	50S ribosomal protein L3	2.25	2.90E-37
E5A72_RS04530(*rpsE*)	30S ribosomal protein S5	2.33	6.53E-37
Type IV pili subunits			
E5A72_RS03275 (*pilG*)	Twitching motility response regulator PilG	-2.60	4.79E-09
E5A72_RS09280(*pilB*)	Type IV-A pilus assembly ATPase PilB	-2.47	2.54E-09
E5A72_RS05200	Pilus assembly protein PilM	-2.08	3.19E-08
E5A72_RS05190	Type 4a pilus biogenesis protein PilO	-2.18	2.93E-06
CSU pili			
E5A72_RS19205(*csuAB*)	Csu fimbrial major subunit CsuAB	2.14	0.0071

E5A72_RS19190 (*csuC*)	Csu fimbrial biogenesis chaperone CsuC	1.54	0.0331
Iron acquisition systems			
E5A72_RS08840	FeoA family protein	-2.57	8.13E-10
E5A72_RS01060(*bauF*)	Acinetobactin utilization protein	-2.46	1.91E-08
E5A72_RS05910	TonB-dependent siderophore receptor	-1.74	9.17E-12
E5A72_RS05115	Bacterioferritin-associated ferredoxin	-1.96	0.0020
E5A72_RS00970(*basJ*)	Acinetobactin biosynthesis isochorismate synthase	-1.90	1.74E-05
E5A72_RS01050(*basB*)	Acinetobactin non-ribosomal peptide synthetase subunit	-1.84	0.0138
Quorum sensing and related			
E5A72_RS06870(*AbaI*)	Acyl-homoserine-lactone synthase	-1.86	0.0015
E5A72_RS16120	Class I SAM-dependent methyltransferase	-6.71	4.77E-73
Non-coding			
sRNA00056	-	-4.38	5.52E-07

[#] - FC: Fold change.

4.1.3 Functional annotation of DEGs in biofilm cells

The gene ontology (GO) enrichment analysis of the DEGs between sRNA00203 mutant and wild-type *A. baumannii* ST1894 biofilm cells revealed 77 upregulated and 49 downregulated Gene Ontology (GO) terms. These GO terms were associated with three physiological processes: biological process (n = 92), cellular component (n = 14), and molecular function (n = 20) (Figure 4.2A).

Among the upregulated functional categories, the primary influences were observed in biological processes such as translation and metabolic processes in general. Within the cellular component category, the ribosome was the most prominent organelle. Regarding molecular function, processes related to structural constituents of the ribosome and purine nucleotide binding were among the significantly affected (Figure 4.2B).

Among the significantly altered GO terms of the downregulated genes, nearly all observed functional classes within the biological process category were related to transcriptional regulation. Molecular function-related GO terms included DNA binding and transcription regulator activity. In terms of cellular components, the membrane was the only component that exhibited substantial influence (Figure 4.3A).

Furthermore, the Kyoto Encyclopedia of Genes and Genomes (KEGG) pathway enrichment analysis of the upregulated genes in the mutant biofilm cells revealed a significant enhancement in two pathways: ribosome and oxidative phosphorylation. About 86% and 67% of differentially regulated genes annotated in the ribosome and oxidative phosphorylation pathways, respectively, demonstrated upregulation (Figure 4.3B). As illustrated in Figure 4.5, gene set enrichment analysis also demonstrated that the ribosome pathway exhibited the highest normalized enrichment score (NES = 1.8, FDR = 0.04).

Although no pathway met the cutoff value for significant downregulation (Padj < 0.05), genes involved in the two-component system (p = 0.004), such as *pilG*, E5A72_RS01325 (substrate-binding domain-containing protein), and E5A72_RS03265 (chemotaxis protein CheW), were found to be downregulated in the sRNA00203 mutant strain.

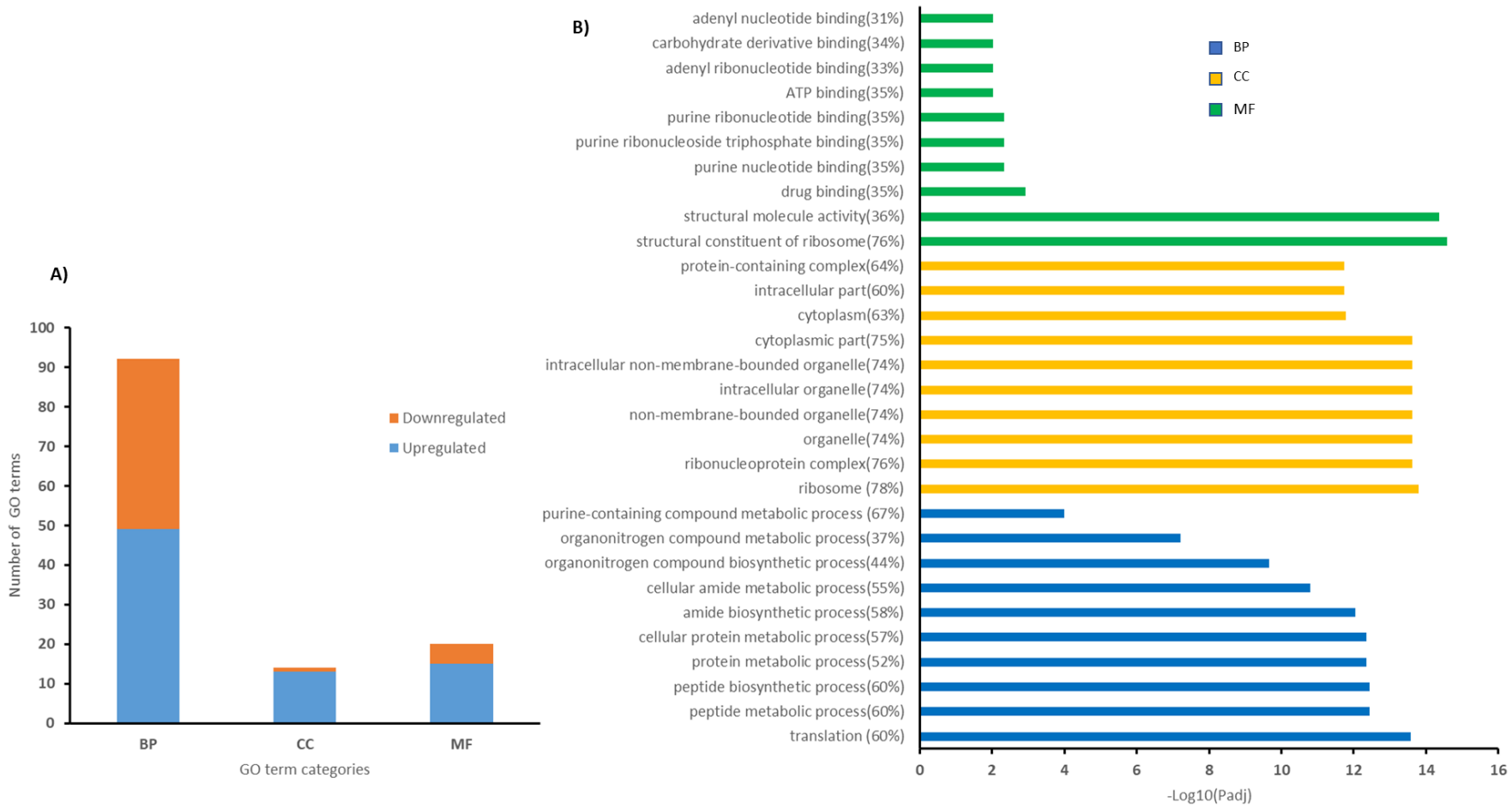

Figure 4.2 Functional categories based on GO analysis of differentially regulated genes in biofilm cells of the sRNA00203-deleted *A. baumannii* ST1894 strain. (A) Distribution of all significantly enriched GO terms across GO term categories. (B) Top ten significantly upregulated GO terms from each GO term classification. The percentage on the y-axis reflects the ratio of upregulated or downregulated genes to the total number of DEGs annotated for each GO term. BP: biological process; CC: Cellular component; MF: molecular function.

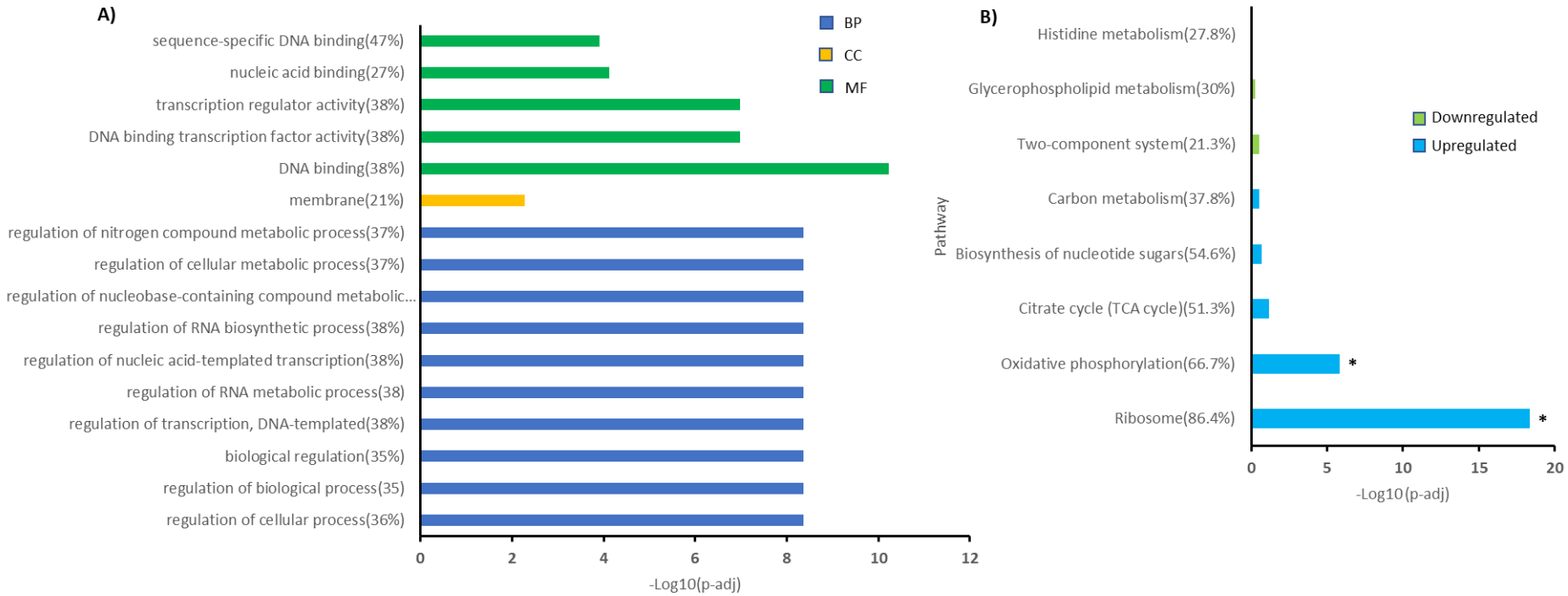

Figure 4.3 Functional categories of differentially regulated genes in biofilm cells of sRNA00203-deleted *A. baumannii* ST1894 strain. (A) Bar graph shows significantly down-regulated GO terms. (B) KEGG pathway enrichment for both down and upregulated genes. The percentage in the y-axis shows the ratio of upregulated/downregulated genes to the total number of DEGs in each GO term annotated (A) or KEGG pathway annotated (B). BP: biological process; CC: Cellular component; MF: molecular function. * indicates a significantly altered pathway.

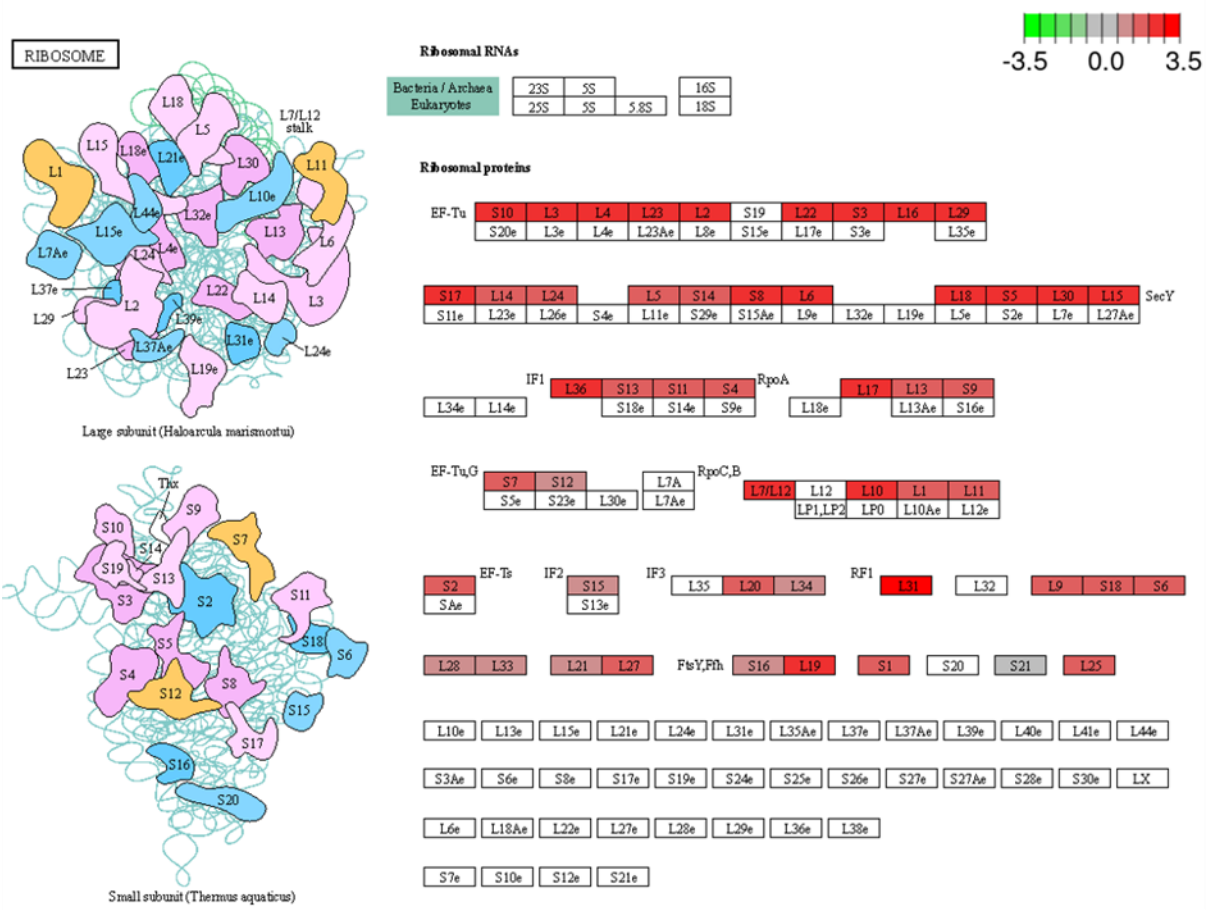

Figure 4.4 Dysregulated genes involved in the ribosome synthesis pathway of sRNA00203-deleted biofilm cells. Red boxes show upregulated genes.

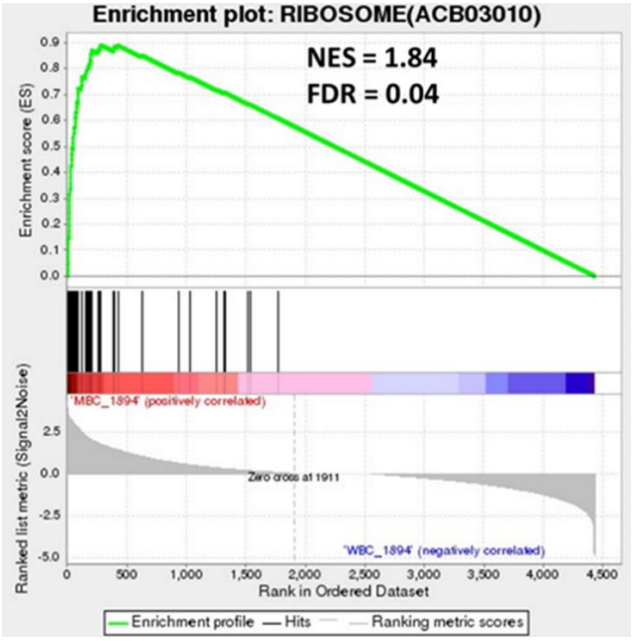

Figure 4.5 Ribosome gene set enrichment analysis in the sRNA00203-deleted biofilm cells. NES: Normalized enrichment score.

4.1.4 Differentially regulated genes and their functional annotation in planktonic cells

Deletion of sRNA00203 also impacted gene expression of 48-hour-old planktonic cells. Of the 3638 genes identified in the RNA-seq data, a total of 181(5%) genes exhibited significantly altered expression in the deletion mutant compared to wild-type planktonic cells, encompassing 122 upregulated genes and 59 downregulated genes (Figure 4.6A).

Hypothetical proteins were dominantly upregulated in the sRNA00203-deleted planktonic cells. Whereas the phenylacetic acid catabolic proteins, encoded by the *paa* operon, were negatively impacted in the planktonic growth form. Genes within this operon, such as *paaA*, *paaB*, and *paaC*, appeared at the top of the list of downregulated genes (Table 4.3). The impairment of the paa operon in *A. baumannii* could enhance host survival by bolstering innate immune defence (Bhuiyan et al., 2016).

Similar to the biofilm cells, genes such as *leuC*, the MFS transporter (E5A72_RS06620), and the pilus assembly protein PilM (E5A72_RS05200) were repressed, while the OmpW family protein (E5A72_RS00750) was induced in deletion mutant planktonic cells. However, the level of impact on these genes was lower under planktonic conditions compared to the biofilm condition (Table 4.4).

The differentially regulated genes did not enrich any GO terms (Figure 4.6B). In contrast, as illustrated in Figure 4.7, four pathways were found to be significantly enriched by the DEGs in the planktonic cells of the deletion mutant. Among these pathways, phenylalanine metabolism (Figures 4.8 and 4.9), microbial metabolism in diverse environments, and benzoate degradation were enriched under the group of repressed genes. On the other hand, the sulfur relay system pathway was enriched among the group of induced genes.

Table 4.3 Top ten upregulated and downregulated genes in sRNA00203-deleted planktonic cells of *A. baumannii* ST1894.

Gene status	Product	$Log_2(FC^{\#})$	P-value
Upregulated			
E5A72_RS07405	hypothetical protein	3.58	3.15E-08
E5A72_RS04925	hypothetical protein	3.98	7.37E-07
E5A72_RS04720	ABC transporter substrate-binding protein	3.60	9.41E-07
E5A72_RS12295	hypothetical protein	3.33	2.40E-06
E5A72_RS04870	hypothetical protein	3.39	6.18E-06
E5A72_RS05510	hypothetical protein	3.53	6.77E-06
E5A72_RS18890	hypothetical protein	3.67	8.06E-06
E5A72_RS02820 (*lolA*)	outer membrane lipoprotein chaperone LolA	3.27	8.86E-06
E5A72_RS00385	hypothetical protein	3.01	2.10E-05
E5A72_RS12075	hypothetical protein	2.87	2.15E-05
Downregulated			
E5A72_RS14375 (*PaaA*)	phenylacetyl-CoA epoxidase subunit A	-4.43	4.62E-07
E5A72_RS14380 (*PaaB*)	phenylacetyl-CoA epoxidase subunit B	-4.17	3.38E-06
E5A72_RS14385 (*PaaC*)	phenylacetate-CoA oxygenase subunit PaaC	-4.67	2.14E-05
E5A72_RS00590	tRNA 5-hydroxyuridine modification protein YegQ	-3.14	0.0001
E5A72_RS14390	phenylacetate-CoA oxygenase subunit PaaJ	-3.82	0.0008
E5A72_RS14370	phenylacetic acid degradation bifunctional protein PaaZ	-3.22	0.0009
E5A72_RS13785	hypothetical protein	-3.44	0.0013

E5A72_RS03030	fatty acid desaturase family protein	-2.57	0.0014
E5A72_RS01345	aldehyde dehydrogenase family protein	-2.19	0.0016
E5A72_RS14395 (*PaaK*)	phenylacetate-CoA oxygenase/reductase subunit PaaK	-2.97	0.0038

[#] - FC: Fold change.

Table 4.4 Differentially regulated genes at both biofilm and planktonic conditions.

Gene ID	**Product**	**MBC and WBC**		**MPC and WPC**	
		$Log_2(FC^{\#})$	**P-value**	**$Log_2(FC^{\#})$**	**P-value**
E5A72_RS09705	3-isopropylmalate dehydratase large subunit	-5.46	1.37E-51	-1.6195	0.021509
E5A72_RS06620	MFS transporter	-4.09	2.23E-14	-2.17818	0.032413
E5A72_RS05200	pilus assembly protein PilM	-2.08	1.72E-09	-1.49403	0.027585
E5A72_RS00750	OmpW family protein	1.74	2.07E-08	1.802368	0.007526
E5A72_RS07405	hypothetical protein	3.489094	2.22E-25	3.58	3.15E-08
E5A72_RS04925	hypothetical protein	1.760909	0.000129	3.98	7.37E-07
E5A72_RS04720	ABC transporter substrate-binding protein	2.092334	1.9E-12	3.6	9.41E-07
E5A72_RS12295	hypothetical protein	1.726	3.38E-30	3.33	2.40E-06
E5A72_RS04870	hypothetical protein	2.083915	2.47E-13	3.39	6.18E-06
E5A72_RS05510	hypothetical protein	2.957192	1.61E-31	3.53	6.77E-06
E5A72_RS18890	hypothetical protein	1.798785	8.44E-05	3.67	8.06E-06
E5A72_RS00385	hypothetical protein	2.068967	1.3E-08	3.01	2.10E-05
E5A72_RS12075	hypothetical protein	2.162212	1.16E-30	2.87	2.15E-05

MBC: Deletion mutant biofilm cells; WBC: Wild-type biofilm cells; MPC: Deletion mutant planktonic cells**;** WPC: Wild-type planktonic cells; [#] - FC: Fold change.

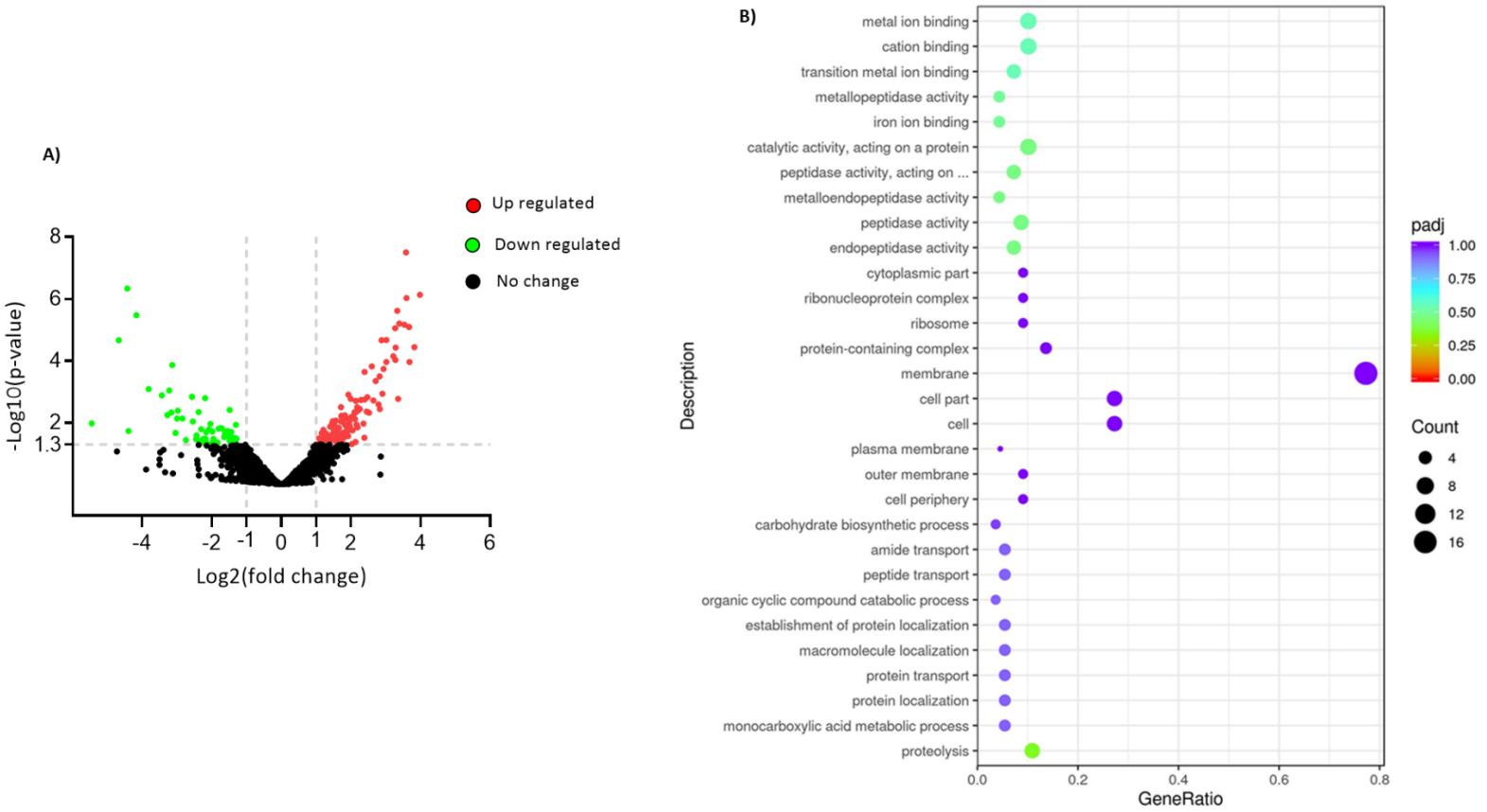

Figure 4.6 DEGs and their functional annotation in sRNA00203-deleted compared to wild-type *A. baumannii* ST1894 planktonic cells. (A) Volcano plot showing differentially expressed transcripts. Genes with an absolute log_2(fold changes) value ≥1 and a p-value of < 0.05 were considered significantly altered and are illustrated in green (n=59) and red colors (n=122). A black-colored dot indicates genes that are not significantly changed (n=3457). (B) Dot plot showing all GO terms enriched by the DEGs. GeneRatio represents the ratio of DEGs to all genes associated with the specified GO terms. Go term with Adj. p-value of < 0.05 was taken as significantly altered.

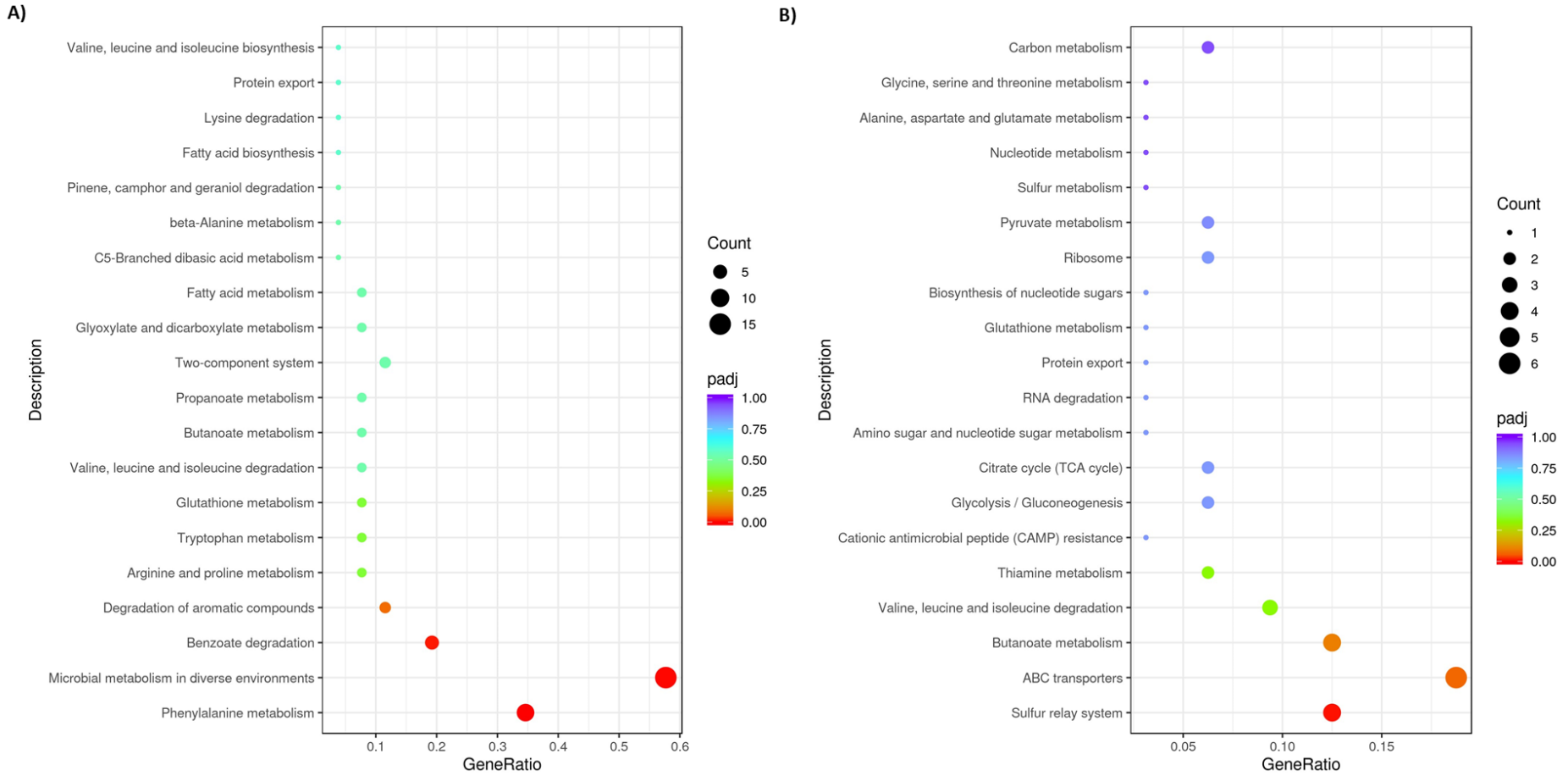

Figure 4.7 Dot blot showing KEGG pathway enrichment for both down (A) and upregulated (B) genes in sRNA00203-deleted compared to wild-type planktonic cells of *A. baumannii* ST1894.

GeneRatio represents the ratio of DEGs to all genes associated with the specified pathway. KEGG pathway with Padj < 0.05 was taken as significantly altered.

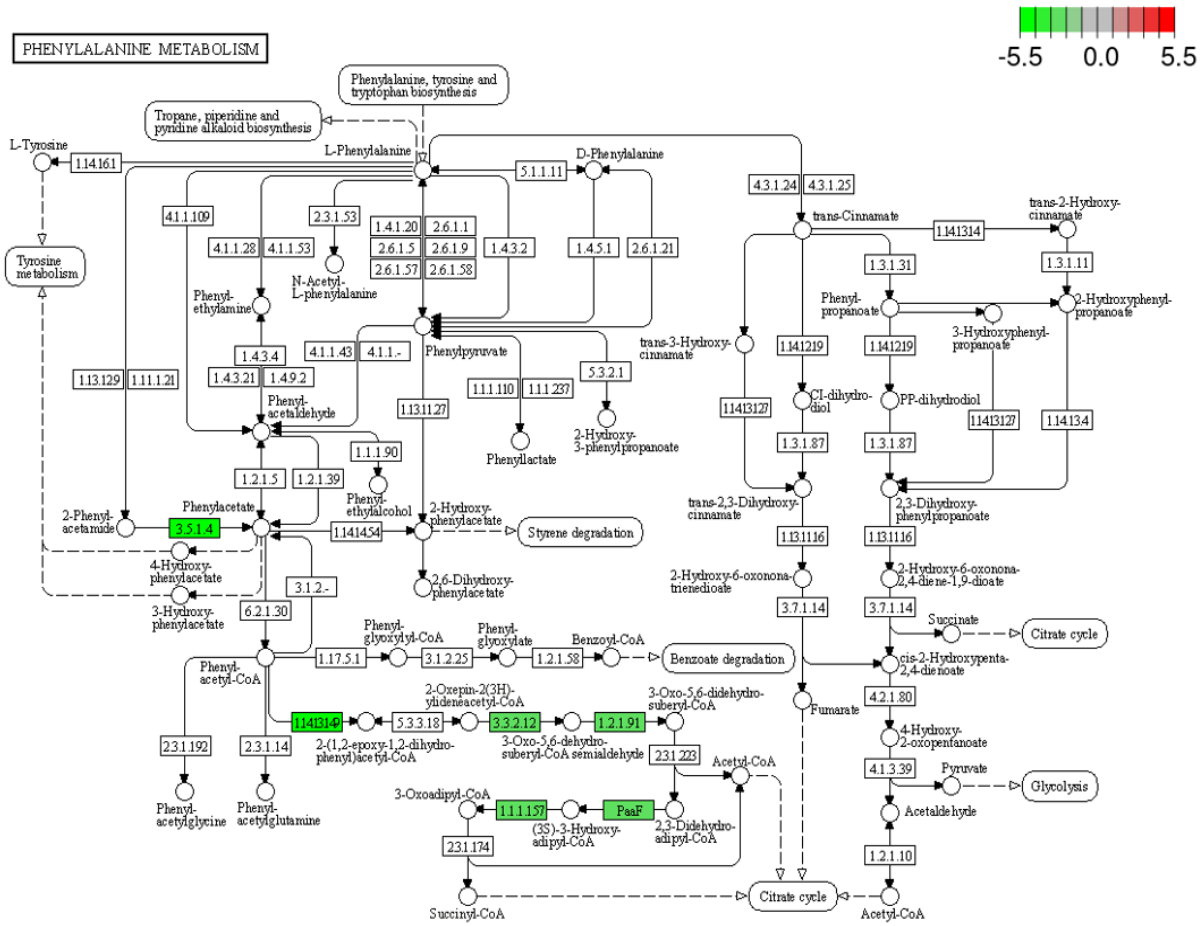

Figure 4.8 Differentially regulated genes involved in the phenylalanine metabolism pathway of sRNA00203 deleted planktonic cells. Green boxes show downregulated genes.

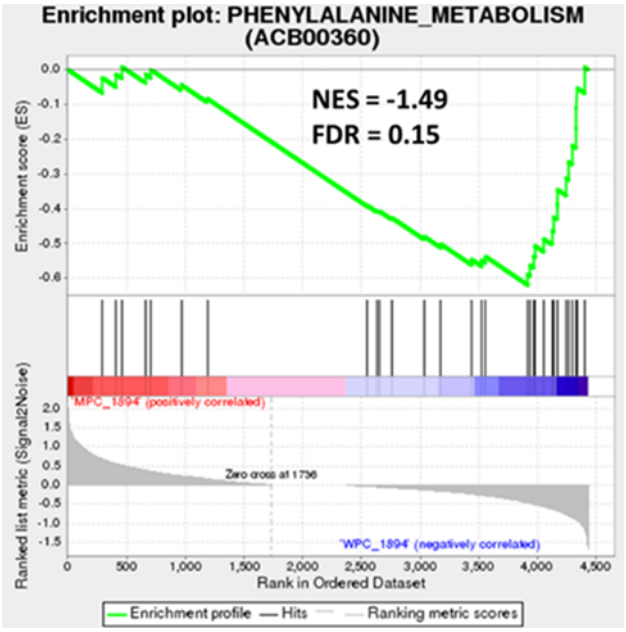

Figure 4.9 Phenylalanine metabolism gene set analysis of sRNA00203-deleted planktonic cells.

NES: Normalized enrichment score.

4.1.5 Verification of DEGs

RT-qPCR was performed to verify the RNA-seq findings for 16 selected differentially expressed genes (DEGs), including both downregulated and upregulated genes. These genes were related to iron acquisition, type IV pili, amino acid metabolism, phenylalanine metabolism, non-coding sRNA, or quorum sensing. As illustrated in Figure 4.10, the $\log_2$ (fold change) in RT-qPCR expression shows a strong correlation with the RNA-seq findings (r^2 = 0.951). These results provide evidence for the successful identification of differentially influenced genes and affirm the reliability of the RNA-seq data for further analysis.

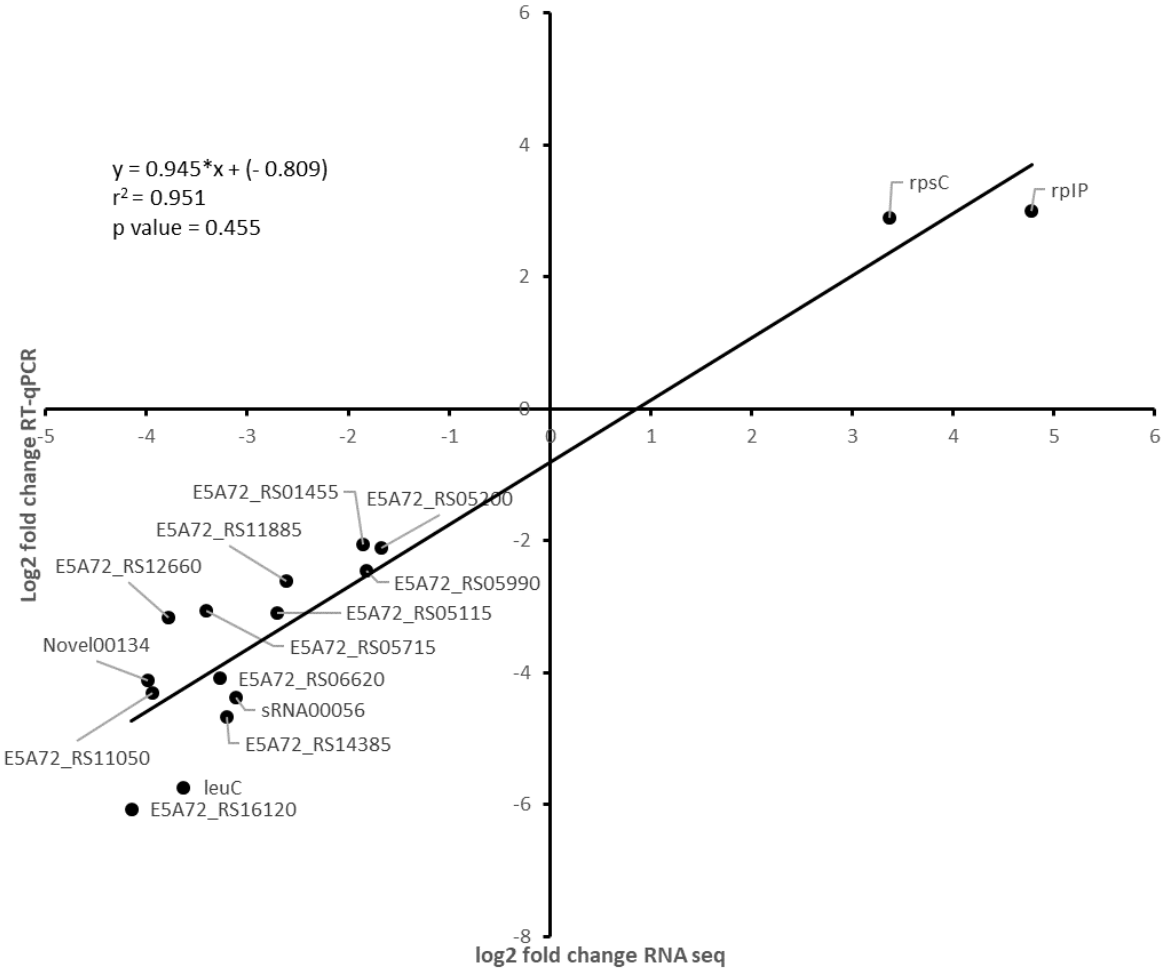

Figure 4.10 Correlation between RNA-seq and quantitative RT-PCR data for selected genes. Data are depicted as the mean of the $\log_2$(fold change) value of three biological replicates. Pearson correlation analysis was performed, and the coefficient of determination (r^2) was calculated.

4.2 Influence of sRNA00203 on protein expression of *A. baumannii*

Bacterial small RNAs regulate gene expression post-transcriptionally by acting on mRNA stability and/or translation (Carrier et al., 2018). The comparative transcriptome study of the sRNA00203-deleted and wild-type strains demonstrated the impact of sRNA00203 on mRNA stability, but could not address effects on translation initiation or termination. To unravel the effects on both mRNA stability and translation, we conducted a comparative proteome study. Protein samples for label-free quantitative proteomics were extracted from bacteria cultured under the same conditions as those used for RNA sequencing. Samples, comprising biological triplicates of the two isogenic strains in both biofilm and planktonic growth forms, were included for whole-cell proteome data acquisition.

Approximately one µg/mL of trypsin-digested peptides from each sample was injected into an Orbitrap Fusion™ Lumos™ mass spectrometer coupled with a Dionex UltiMate 3000 RSLCnano system. The peptide detection by the liquid chromatography-mass spectrometry (LC-MS) was performed over a 90-minute gradient. The fragmentation efficiency of peptides in all samples was greater than 85%, which was satisfactory and enabled improved peptide identification. Additional sample characteristics as determined by LC-MS are presented in detail in Table 4.5. After directDIA analysis using Spectronaut, a total of 21,207 precursors and 18,269 peptides were identified across all the samples. The peptides were mapped to 2,095 proteins at a 1% FDR, representing 53.7 % of the entire *A. baumannii* proteome. However, not all proteins were detected in every sample, and their numbers varied across conditions (Table 4.5).

Table 4.5 LC-MS data characteristics of the four categories of samples

Parameters	**Sample categories**			
	Wild-type biofilm cell	**Deletion mutant biofilm cell**	**Wild-type planktonic cell**	**Deletion mutant planktonic cell**
Median XIC width (min)	1.7	1.8	1.8	1.9
Missed cleavage (%)	15.07	15.67	13.65	14.85
Data completeness (%)	88.6	77.6	89.9	92.2
Fragmentation efficiency (%)	87.57	88.13	86.75	88.1
Recovery (%)	94	95.7	93.6	94.5
Precursors	18649	15400	16643	17072
Peptides	16346	13610	14854	14914
Protein	2031	1819	1939	1897

XIC: extracted ion chromatogram

4.2.1 Differential regulation of proteins in biofilm cells

The label-free proteomic analysis identified a total of 2,031 proteins in the wild-type biofilm cells and 1,819 proteins in the sRNA00203-deleted biofilm cells. Of the 2,061 proteins detected across the two groups of samples, 1,798 proteins were quantified in both strains. This number of proteins represents approximately 46.1% of the proteins predicted from the entire *A. baumannii* genome. Principal component analysis (PCA) of the expression patterns of the quantified proteins clearly differentiated the two isogenic strains and demonstrated close clustering of their biological replicates (Figure 4.11A). Correlogram also demonstrated consistency within the biological replicates (Figure 4.11B). Proteins uniquely absent or detected in the deleted strain were also identified. Ninety-eight proteins were not detected in any of the sRNA deletion strain samples but were uniquely present in at least two replicates of the wild-type strain (Figure 4.12A).

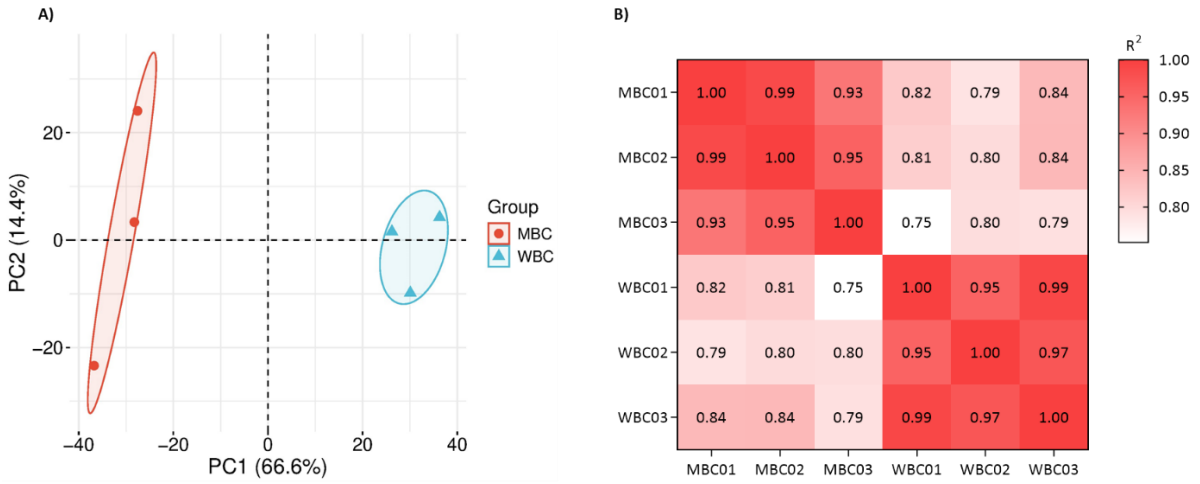

Figure 4.11 Clustering of sRNA00203-deleted and wild-type strain based on protein expression values.

(A) PCA plot illustrating the expression patterns of 1,798 proteins. (B) Correlogram showing correlation among biological replicates. Each value indicates the Pearson correlation score (R^2). MBC: Deletion mutant biofilm cells; WBC: Wild-type biofilm cells.

Next, the quantitative analysis using Spectronaut revealed that, in the biofilm cells of the sRNA00203 deletion mutant, 600 proteins (33.4% of the quantified) were differentially expressed at a significant level (absolute log_2(fold change) value ≥1 and a q-value of < 0.05). Of these, 355 (59.2%) proteins were upregulated and 245 (40.8%) proteins were downregulated (Figure 4.12B). The influenced proteins were functionally annotated to pili, ribosomal components, envelope components, efflux pumps, secretion system, or metabolism (Table 4.6).

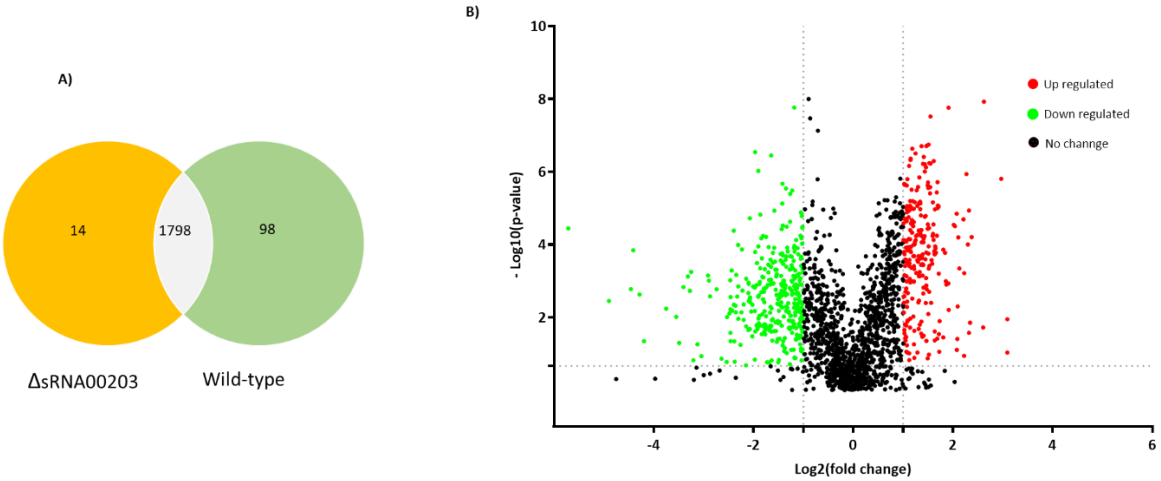

Figure 4.12 Expression status of proteins detected in the deletion mutant (ΔsRNA00203) and wild-type *A. baumannii* biofilm cells.

(A) Venn diagram showing uniquely identified proteins. (B) Volcano plot displaying the proteins considered for differential analysis. Proteins with an absolute log_2(fold change) value ≥ 1 and a q-value of < 0.05 were considered significantly altered (DEPs) and are illustrated in green (n = 245) and red (n = 355) colors. A black dot indicates proteins that are not significantly changed (n = 1198). The dotted line intercepting the y-axis corresponds to a q-value of 0.05.

4.2.2 Pili-related proteins

Several type IV pili subunit-coding genes of *A. baumannii* were among the genes influenced by sRNA00203, as demonstrated by the RNA-seq study. Similarly, the whole-cell proteome analysis revealed that the subunit transcriptional regulatory proteins encoded by *PilH* and *PilG* showed decreased translation in the sRNA00203-deleted strain (Table 4.2). In addition, Type IV-A pilus assembly ATPase PilB, PilT/PilU family type 4a pilus ATPase, and PilN domain-containing protein were uniquely identified in the wild type.

Another type of pili, such as Type I chaperone-usher pilus system (Csu), was differentially influenced. The chaperone-usher pilus system is recognized for its role in adhesion to abiotic surfaces, which leads to biofilm formation (Ahmad et al., 2023). The proteomic analysis revealed that the abundance of protein CsuC and the Csu fimbrial major subunit CsuAB was decreased by 2.6-fold and 2.3-fold, respectively, in the mutant strain. Similarly, the two-component system BfmS (histidine kinase) protein, which is reported to regulate both types of pili (Palethorpe et al., 2022; Tomaras et al., 2008), showed significant downregulation (Table 4.6). In contrast, the transcriptome analysis revealed that the corresponding genes (*csuAB* and *csuC*) were upregulated (Table 4.2).

4.2.3 Ribosomal proteins

RNA-seq analysis revealed upregulation of several ribosomal protein-coding genes, resulting in an overrepresentation of the translation pathway in the deletion mutant strain. In addition, this expression pattern was also confirmed by RT-qPCR (Figure 4.10). On the contrary, the proteome study revealed that the expression of many large ribosomal subunit proteins and a few small ribosomal subunit proteins was repressed (Table 4.6). We also observed that the Gene Ontology (GO) annotation of DEPs resulted in underrepresentation of translation (biological process), ribosome (cellular component), and structural constituent of ribosome (molecular function) (Figure 4.13). The discrepancy between transcriptomic and proteomic data suggests that most of the transcribed ribosomal protein-encoding genes in the knockout strain may not be translated into proteins to a similar extent. This explanation can be further corroborated by the growth retardation observed after 12 hours of incubation in the deletion mutant strain (Figure 4.16A).

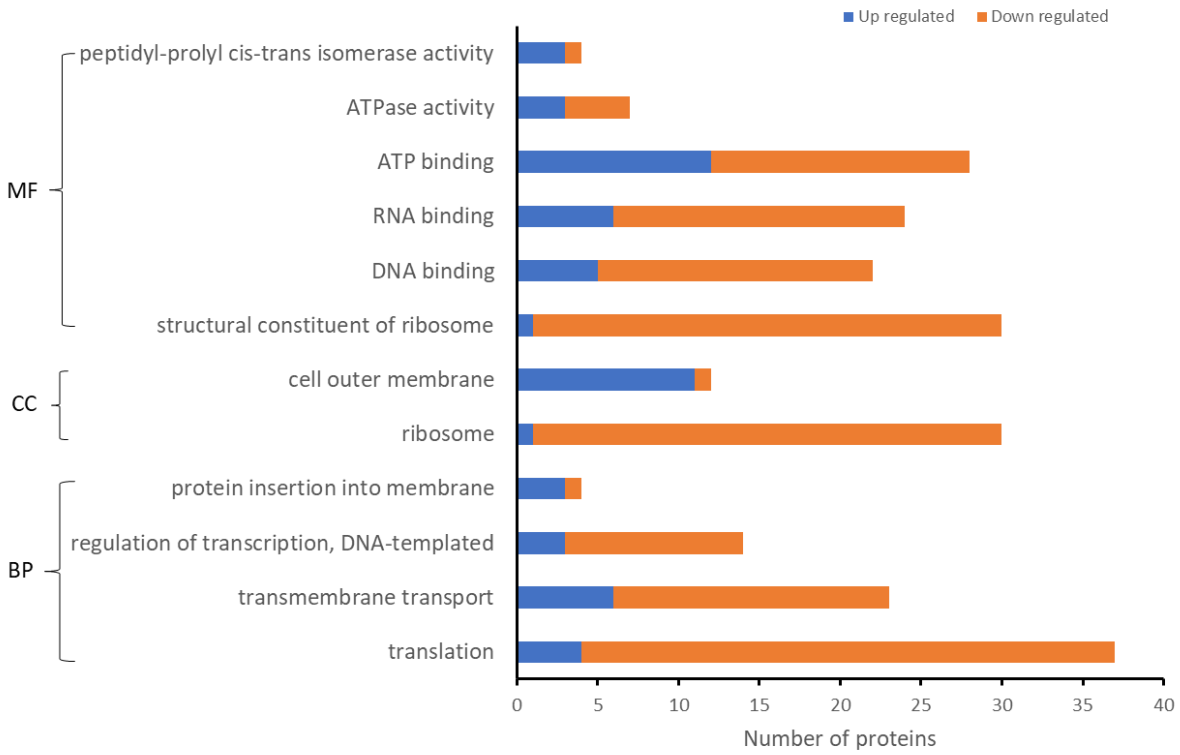

Figure 4.13 GO annotation of DEPs in sRNA00203-deleted compared to wild-*type A. baumannii* biofilm cells.

The X-axis denotes the number of DEPs included in the GO annotation. The Y-axis displayed all the significantly enriched GO terms (P-value < 0.05).MF: Molecular function; CC: Cellular function; BP: Biological process.

4.2.4 Membrane-associated proteins

The expression of several membrane-associated proteins was influenced by sRNA00203. Among these, efflux pump components, including the resistance-nodulation-division (RND) efflux pump protein AdeK (UniProt ID: Q24LT6) and a major facilitator superfamily (MFS) transporter (UniProt ID: V5VHF5), were significantly upregulated and downregulated, respectively, in the biofilm cells of the deletion mutant strain. Moreover, an outer membrane protein of the OmpW family (UniProt ID: A0A0D5YGT9) and Ornithine uptake porin CarO type 4 (UniProt ID: A0A1E3M6B5) showed increased abundance. These findings were consistent with the transcriptomic data, which demonstrated elevated mRNA levels for *adeK*, E5A72_RS18475, and E5A72_RS01795 and reduced mRNA levels for E5A72_RS06620 (Table 4.2).

As shown in Table 4.6, the proteomic profile also revealed that divergent regulation of cell wall biogenesis proteins. Enzymes necessary for lipopolysaccharide (LPS) biosynthesis, such as UDP-3-O-acylglucosamine N-acyltransferase (LpxD; UniProt ID: V5VDY4) and lipid-A-disaccharide synthase (LpxB; UniProt ID: A0A059ZK65), were significantly repressed. Conversely, UDP-3-O-acyl-N-acetylglucosamine deacetylase (LpxC; UniProt ID: A0A1E3MCP2) was significantly induced in the mutant strain, which could be attributed to a compensatory mechanism within the LPS biosynthesis pathway. Other proteins related to secretion system located in bacterial envelope were also affected. Specifically, translocase subunit SecE (UniProt ID: A0A059ZGU8) and protein-export protein SecB (UniProt ID: V5VIB6) were significantly repressed. However, the transcriptomic analysis did not show significant changes in the mRNA levels encoding these secretory proteins and LPS components.

4.2.5 Metabolism-related proteins

Metabolic rewiring can play a crucial role in supporting the energy and biosynthetic demands of *A. baumannii* transition from planktonic to biofilm lifestyle. Comparative proteomic profiling showed that deletion of the sRNA00203 led to a marked repression of proteins integral to amino acid biosynthesis and tricarboxylic acid (TCA) cycle (Table 4.6). The 2-isopropylmalate synthase (LeuA), an enzyme that catalyzes leucine synthesis, was suppressed (Fold change: -3.73; P <0.001). Additionally, enzymes related to TCA cycle, such as ATP synthase subunit B (AtpF) and fumarylacetoacetase, were significantly downregulated. A consistent result was found for the transcription of gene encoding fumarylacetoacetase.

Furthermore, a component of the iron acquisition system was influenced. A significant reduction in the abundance of ferric anguibactin-binding protein (BauB) (Fold change: -2.95; P <0.001) was observed. In line with this, transcription of the gene encoding the Acinetobactin utilization protein (*bauF*), a component of the acinetobactin-mediated iron uptake pathway, was repressed (Table 4.2).

Table 4.6 Selected DEPs at the biofilm state of the sRNA-deleted and wild-type strains

UniProt ID	Protein name	Fold change	Q-value
Pili-related proteins			
V5V9M9	Phosphate regulon transcriptional regulatory protein PhoB (*pilH*)	-2.26	6.989E-06
V5VA30	Phosphate regulon transcriptional regulatory protein PhoB (*pilG*)	-11.44	0.003
A0A1E3M404	Protein CsuC	-2.59	7.73E-06
V5VB91	Csu fimbrial major subunit CsuAB	-2.29	5.65E-05
Q2VSW5	Histidine kinase (*bfmS*)	-2.83	0.003
Ribosomal proteins			
V5V9M5	Large ribosomal subunit protein uL4 (*rplD*)	-2.27	8.57E-06
V5VH86	Large ribosomal subunit protein uL1 (*rplA*)	-2.13	9.07E-06
V5VIV0	Large ribosomal subunit protein uL10 (*rplJ*)	-2.77	1.16E-05
V5V9J2	Large ribosomal subunit protein uL30 (rpmD)	2.05	0.001
Envelope-associated proteins			
A0A0D5YGT9	OmpW family protein	3.43	0.006
A0A1E3M6B5	Ornithine uptake porin CarO type 4	1.79	0.008
Q24LT6	Adenosine deaminase (a*deK*)	3.29	0.006
V5VHF5	MFS transporter	-4.08	0.0002
A0A1E3MCP2	UDP-3-O-acyl-N-acetylglucosamine deacetylase (*lpxC*)	2.43	0.0001
V5VDY4	UDP-3-O-acylglucosamine N-acyltransferase (*lpxD*)	-3.10	0.0001
A0A059ZK65	Lipid-A-disaccharide synthase (*lpxB*)	-2.10	0.010
A0A059ZGU8	Protein translocase subunit SecE	-2.46	8.96E-05
V5VIB6	Protein-export protein SecB	-2.64	8.96E-05
Metabolism-related proteins			
A0A1E3MAD1	Fumarylacetoacetase	-2.61	1.44E-06
V5VHG5	ATP synthase subunit b (*atpF*)	-2.5	3.79E-05
A0A1E3M653	Ferric anguibactin-binding protein (*bauB*)	-2.95	0.0002
A0A059ZLY6	2-isopropylmalate synthase (*leuA*)	-3.73	0.0008

4.3 Comparison of the transcriptome and proteome data

The comparison between transcriptomic and proteomic data was restricted to genes with identified corresponding proteins, and vice versa. Assessment of the LC-MS/MS data identified corresponding proteins for 495 (62.7%) of the 790 coding DEGs (CDEGs). Of these proteins, 58 and 2 proteins were uniquely expressed in the wild-type and deletion mutant, respectively. Regarding DEPS, only the two proteins (UniProt ID: V5VHH2; UniProt ID: A0A1E3M1P0) did not exhibit corresponding identified genes. Excluding these encoding genes, 192 (9.15%) genes were significantly influenced at both transcriptome and proteome levels in the sRNA00203 deletion mutant compared to wild-type biofilm cells (Figure 4.14A). This number represented 32.1% (192/598) of the DEPS and 38.8% (192/495) of the CDEGs. Of the 192 overlapping protein-coding genes, only 94 were consistently upregulated or downregulated (Figure 4.14B). The transcriptomic status of some of these genes is presented in Table 4.2, and their proteomic status is provided in Table 4.6. Analysis revealed a good correlation between these mRNA levels and protein abundances ($r^2 = 0.8$) (Figure 4.14C).

The majority (27.6%, 27/98) of the genes with inconsistently influenced expression (opposite regulation) were those encoding ribosomal proteins, as described in Section 4.2.3. Similarly, Csu pili-related proteins showed contrasting expression at transcript and protein levels. Furthermore, we also observed that, likely, sRNA00203-dependent changes in abundance of certain other proteins occurred without corresponding significant changes at the transcript level. The expression levels of representative proteins from this group, such as translocase subunit SecE and UDP-3-O-acylglucosamine N-acyltransferase, are presented in Table 4.6. These findings highlight a low degree of concordance between transcript and protein levels, suggesting sRNA00203-mediated post-transcriptional regulation. Additionally, because the half-lives of proteins and transcripts are not similar, this may lead to discordant results (Haider & Pal, 2013).

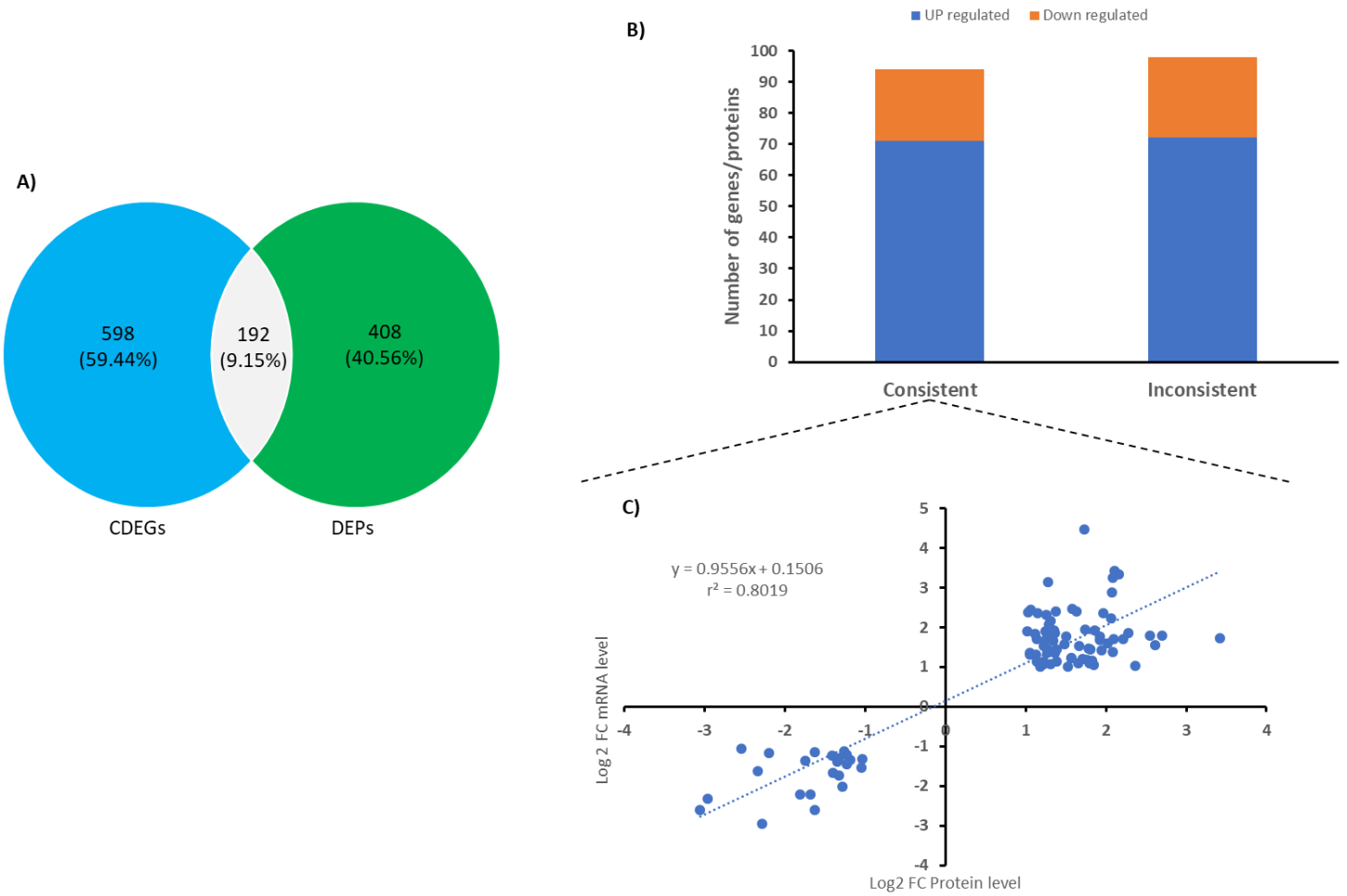

Figure 4.14 Combined analysis of differentially expressed genes and proteins following sRNA00203 deletion in biofilm state. (A) Venn diagram showing the overlap between CDEGs and DEPs. (B) Status of the 192 overlapped genes that significantly influenced in both mRNA and protein levels. (C) Scatter plot of fold changes (FC) of mRNA versus protein levels for the consistently influenced genes. CDEGs: coding DEGs.

4.4 Phenotypic influences of sRNA00203 on *A. baumannii*

4.4.1 Impact of sRNA00203 deletion on pili formation

Deletion of sRNA00203 caused downregulation of several genes encoding type IV pilus (T4P) subunits, as well as their corresponding proteins, in biofilm cells, as demonstrated by RNA-seq (Table 4.2 and Figure 4.1) and LC–mass spectrometry data (Table 4.6). These findings initiated us to examine the morphology of the isogenic strains under transmission electron microscopy (TEM). We prepared 48-hour-old mature biofilm cells in the same manner as those used for the combined omics studies. The biofilm was collected and stored in glutaraldehyde for preservation of the pili. For TEM analysis, biofilm cells were stained with X-solution. The morphology of numerous stained cells in each comparison group was examined. We found that most cells of the deletion mutant strain exhibited significantly reduced pili, as illustrated in Figure 4.15A and B. In contrast, the wild-type *A. baumannii* strain was predominantly pilated (Figure 4.15C and D).

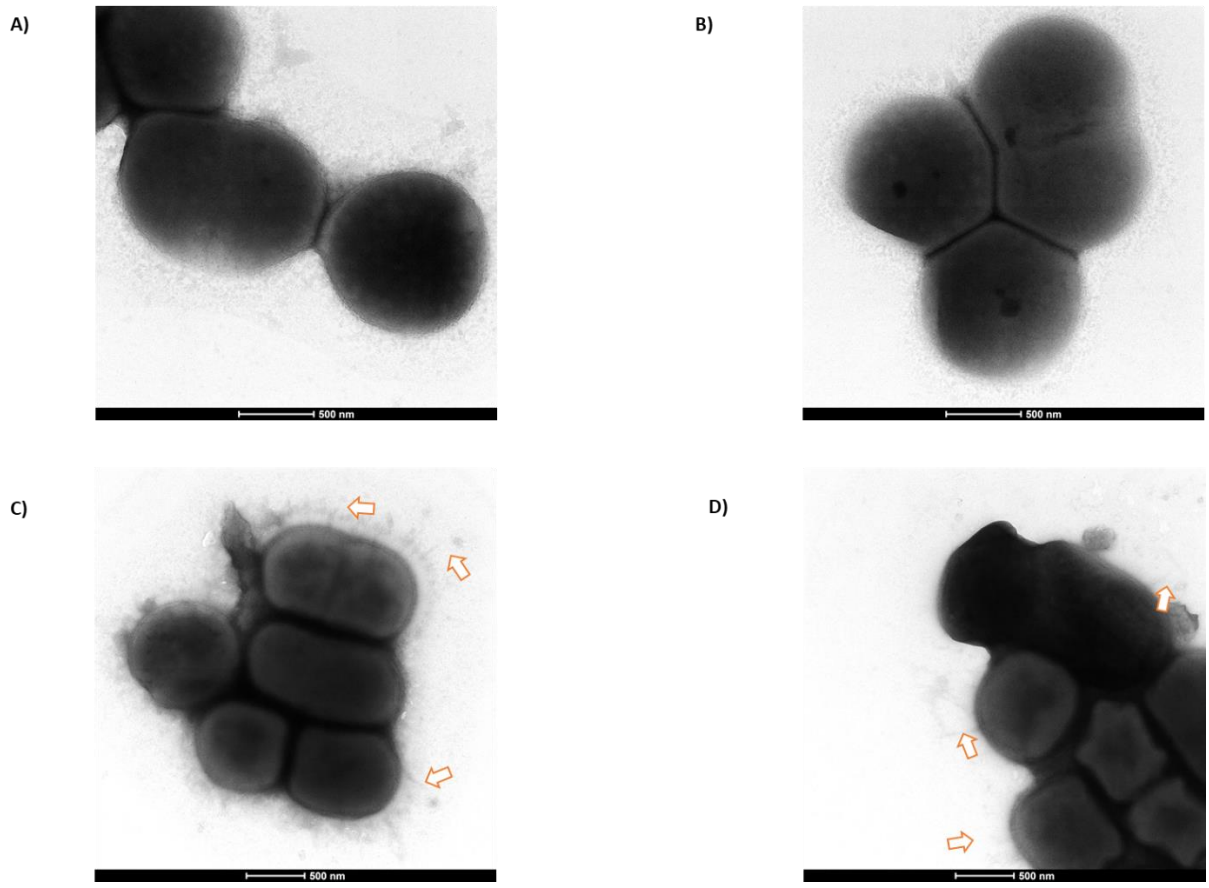

Figure 4.15 Transmission electron microscope (TEM) observation of biofilm cells.

The figures labelled A and B show representative sRNA deletion mutant biofilm cells, whereas C and D show representative wild-type biofilm cells. Arrows indicate pili. Scale: 500 nm.

4.4.2 Growth response of isogenic strains to oxidative stress

In *A. baumannii*, disruption of the phenylacetic acid catabolic pathway, a component of phenylalanine metabolism, significantly impairs the bacterium's ability to tolerate oxidative stress (Hooppaw et al., 2022). The mRNA levels of the paa operon genes (paaABC) were predominantly downregulated in the planktonic cells of the ΔsRNA00203 strain (Table 4.3). KEGG pathway analysis revealed that the phenylalanine metabolism pathway was also significantly enriched by the repressed genes (Figure 4.7). Thus, we hypothesized that exogenous hydrogen peroxide exposure could impair growth of the ΔsRNA00203 strain relative to the wild-type strain. To test this hypothesis, LB broth culture of the wild-type and ΔsRNA00203 strains was adjusted to an OD600 of 0.05 and incubated in a 96-well microtiter plate with or without two mM hydrogen peroxide in a microplate reader. The growth was continuously monitored for 24 hours. As shown in Figure 4.16A, exposure to 2 mM hydrogen peroxide extended the lag phase of the isogenic strains. For comparison between the strains, we calculated the OD600 ratio of treated to untreated samples to account for growth differences. Accordingly, the ΔsRNA00203 strain exhibited a significant growth defect at 8, 12, and 16 hours of incubation ($p < 0.05$) (Figure 4.16B). These findings indicate that the ΔsRNA00203 strain is more susceptible to oxidative stress induced by hydroperoxide exposure at the exponential phase of growth.

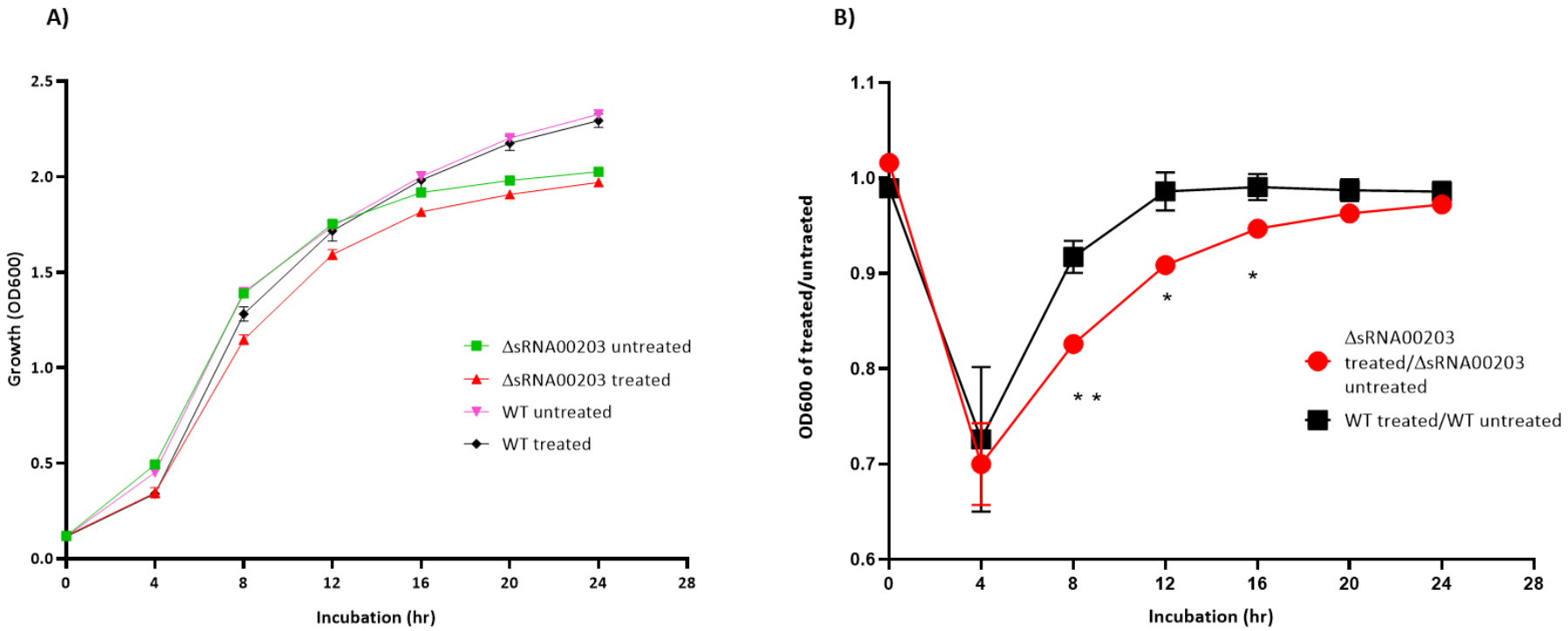

Figure 4.16 Effect of sRNA00203 deletion on *A. baumannii* growth under hydrogen peroxide stress.

(A) Growth curves over 24 hours for untreated and 2mM hydrogen peroxide-treated ΔsRNA00203 and wild-type (WT) strains. (B) Ratio of OD600 values of treated with 2 mM hydrogen peroxide to untreated isogenic strains. Error bars represent the standard deviation (SD) of biological triplicates of the isogenic strain. An independent t-test was used to determine statistical differences among comparison groups. * $p < 0.05$; ** $p < 0.01$.

4.5 Construction of sRNA00203 overexpressing *A. baumannii* strain

To complement the sRNA00203 deletion study findings, we constructed an ectopic sRNA-expressing strain using pSGAb-k plasmid. A 106-nucleotide-long fragment was amplified using PCR from genomic DNA of *A. baumannii* ST1894 (Figure 4.16A). The fragment included the coding region of sRNA00203 and homologous regions, which were incorporated for the purpose of Gibson assembly. The purified fragment was cloned downstream of the SpeI promoter to construct p-sRNA00203 vector. The constructed overexpression vector was electroporated into competent *A. baumannii* cells. Of the twenty colonies picked from kanamycin-containing LB agar and screened by colony PCR, eighteen were successful transformants, exhibiting a band size of 338 base pairs (Figure 4.17B). Sanger sequencing of extracted plasmid from the positive clones verified a correct orientation and sequence of the promoter and sRNA (Figure 4.18).

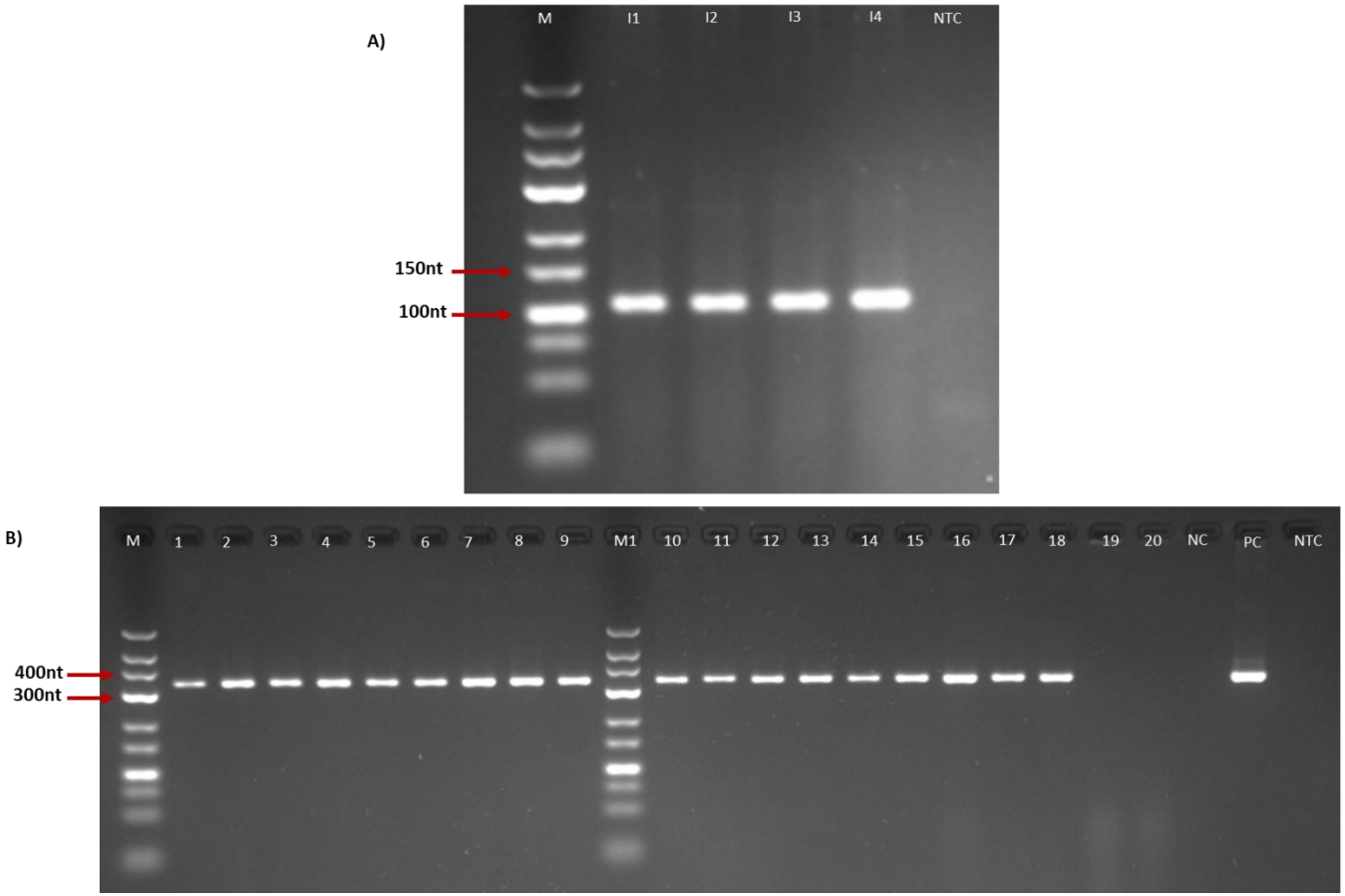

Figure 4.17 PCR results during the construction of ectopic sRNA00203 expression.

(A) Showing four insert bands with 106 nucleotide-long sizes labelled as I1 to I4. (B) Showing colony PCR results. Lane labelled 1-20 indicates colonies screened. Controls were included for reference. Negative control (NC) represents a colony transformed by a negative assembly reaction, and positive controls (PC) represent the positive assembly reaction. M: Low-range DNA ladder (Thermo Fisher Scientific, USA); NTC: No template control.

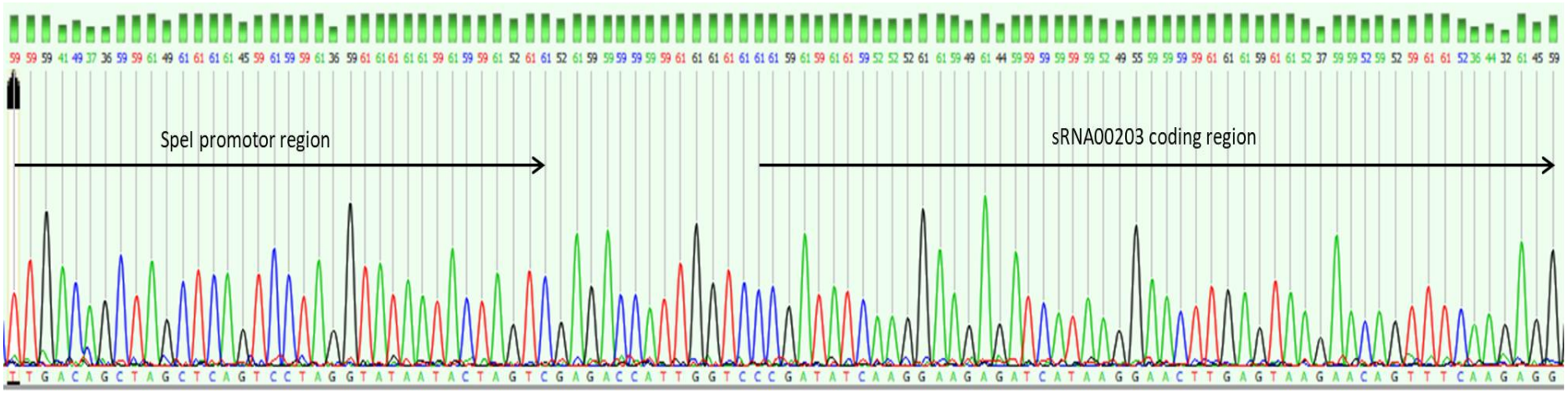

Figure 4.18 Verification sequence and orientation of sRNA00203 in the constructed p-sRNA00203 vector.

Successful integration of the coding region of the sRNA near the vector promoter was verified by Sanger sequencing using a forward primer. The values above the chromatogram indicate the quality score of each nucleotide. The minimum value was 32, which indicates a reliable enumeration of the nucleotides.

4.6 Verification of sRNA00203 ectopic expression

Before assessing the relative expression levels of genes and their phenotypic influences, we verified the impact of the high-copy plasmid on bacterial growth. Continuous optical density (OD600) assessment that could reflect growth was conducted for a 24-hour period. The results showed that the strains with and without the empty plasmid exhibited almost identical growth rates in LB broth. This implies that the plasmid did not exert a metabolic burden. However, sRNA00203 ectopic expression exerted a subtle effect on growth ($p > 0.05$) (Figure 4.19A).

To investigate the expression level of the sRNA, RT-qPCR was performed using RNA samples extracted from biofilms. As illustrated in Figure 4.19B, the biofilm cells of overexpressing strain exhibited more than a 350-fold increase in mRNA level of sRNA00203 relative to strain harbouring the empty plasmid (control). This finding confirmed successful sRNA00203 overexpression from the constitutive promoter (SpeI).

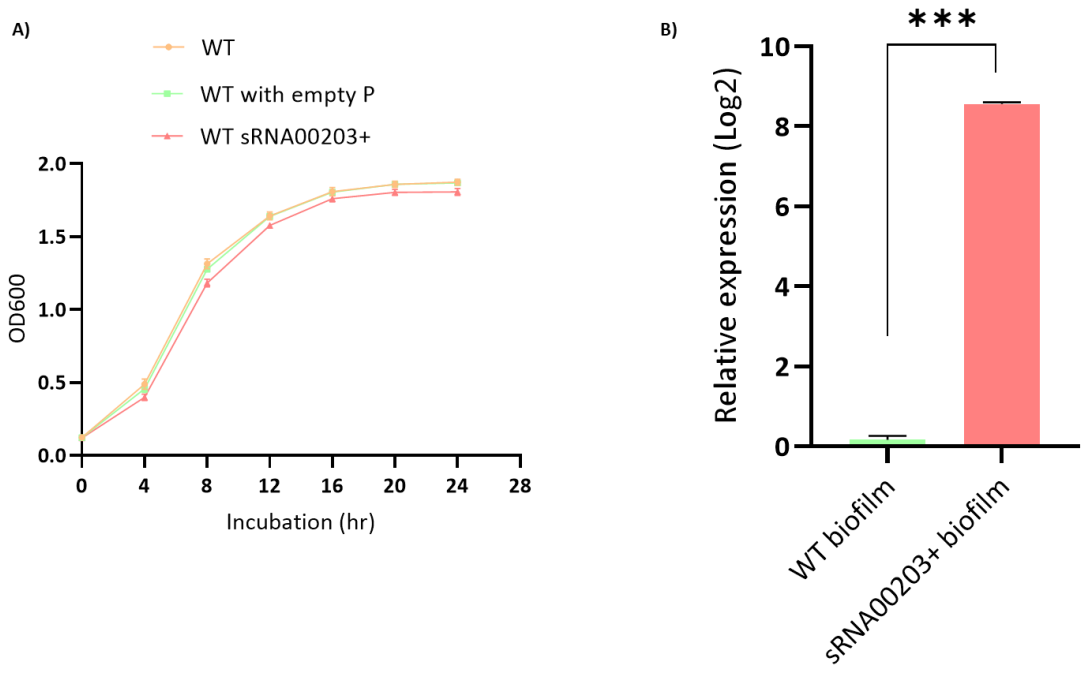

Figure 4.19 Growth curve and relative expression of sRNA00203.

(A) 24-hour growth curve of wild-type (WT), WT containing empty vector, and overexpressing *A. baumannii* ST1894 (WT sRNA00203+). (B) Relative sRN00203 mRNA levels in biofilm cells of the overexpressing strain (sRNA00203+ biofilm) compared to the empty vector control strain (WT biofilm). The error bar was plotted using the SD values of three independent cultures of strains. ***, $p < 0.001$.

4.7 Impact of sRNA00203 overexpression on biofilm

After validation of sRNA00203 overexpression, we also assessed the abundance of the sRNA in biofilm compared to planktonic cultures in both the genetically manipulated and wild-type strains. As expected, in both strains, the relative mRNA level of sRN00203 was significantly higher in biofilm cells (Figure 4.20A and B).

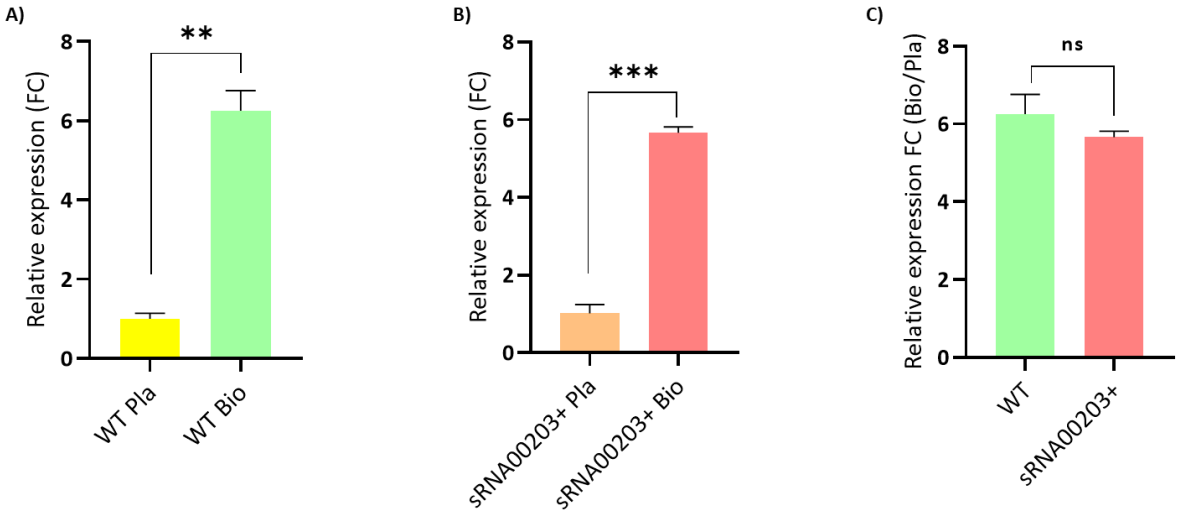

Figure 4.20 Relative sRN00203 expression on biofilm cells compared to planktonic cells. RT-qPCR analysis of the sRNA expression in Wild-type (A) and sRNA00203 overexpression (B) biofilm cells relative to planktonic cells. (C) Ratio of biofilm to planktonic sRNA expression fold change of Wild-type (A) and sRNA00203 overexpression strains. An independent t-test was employed to determine the differences between the conditions. **, $P < 0.01$. ***, $P < 0.001$. ns, non-significant.

Next, to examine the effect of the sRNA00203 overexpression on biofilm, we evaluated quantitative biofilm mass of the isogenic strains using crystal violet method. The overexpressing strain showed an average of 20.7% (95% CI: 9% to 32.5%) increase in biofilm formation compared to the control strain ($p = 0.0082$) (Figure 4.21). These results reconfirmed that the sRNA upregulation dictates biofilm nature, as previously reported by our group (Shenkutie et al., 2023).

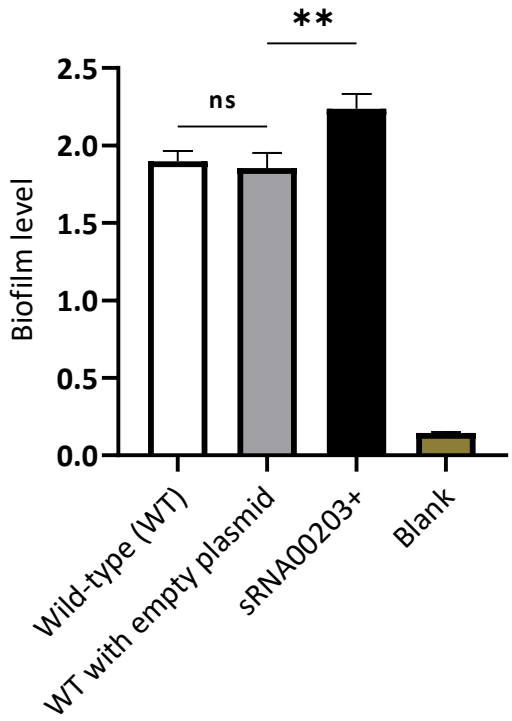

Figure 4.21 Effect of sRNA00203 overexpression on biofilm formation capability of wild-type, wild-type with empty plasmid, and sRNA00203 overexpressing *A. baumannii* strains. Quantitative crystal violet method was used to compare the biofilm levels of the strains. Three biological replicates and nine technical replicates were performed for each strain. Error bars represent the standard deviation (SD) of the replicates. An independent t-test was employed to determine the differences between the strains. **, $P < 0.01$.

4.8 Impact of sRNA00203 overexpression on biofilm-associated genes

Genes associated with biofilm formation were screened from both the transcriptome and proteome analysis of the wild-type *A. baumannii* strain. The description of upregulated genes and their corresponding proteins in the biofilm cells compared to planktonic cells is presented in Table 4.7. Of these DEGs, six genes, such as class I SAM-dependent methyltransferase (E5A72_RS16120), 3-isopropylmalate dehydratase large subunit (*leuC*), MFS transporter (E5A72_RS06620), 50S ribosomal protein L16 (*rplP*), Novel00134, and sRNA00056, expression were assessed using RT-qPCR in the sRNA00203 overexpressing strain. These genes were also identified as top differentially regulated by sRNA00203 in the combined omics studies. As illustrated in Figure 4.22, all the genes were significantly upregulated by the sRNA00203 overexpression. These findings were consistent with the results of the loss-of-function study, with the exception of the ribosomal protein gene (*rplP*).

Table 4.7 Selected biofilm-associated genes from the combined omics studies

Gene name	Description	RNA-seq		LC-mass spectrometry	
		FC	q-value	FC[#]	q-value
leuC	3-isopropylmalate dehydratase large subunit	17.57	7.59E-10	–	–
leuA	2-isopropylmalate synthase	–	–	1.67	0.018
E5A72_RS06620	MFS transporter	4.76	1.18E-06	2.81	0.004
E5A72_RS16120	Class I SAM-dependent methyltransferase	13.93	1.31E-06	–	–
Novel00134	Aconitase C-terminal domain	15.56	7.65E-16	–	–
rplP	50S ribosomal protein L16	4.56	1.99E-06	–	–
sRNA00056	Non-coding	77.7	3.33E-13	–	–
E5A72_RS00560	Type II secretion system protein E	–	–	8.6	0.007
secB	Preprotein translocase subunit SecB	12.99	3.91E-14	–	–
secE	Preprotein translocase subunit SecE	11.63	2.90E-13	–	–
fahA	Fumarylacetoacetase	2.96	< 0.001	2.15	< 0.001
pilG	Twitching motility response regulator PilG	4.29	1.37E-05	–	–
E5A72_RS01455	LysR family transcriptional regulator	7.94	2.12E-10	2.46	0.025
E5A72_RS12660	Cation diffusion facilitator family transporter	2.73	0.002	–	–
E5A72_RS05790	Cation acetate symporter	–	–	2.33	0.017
lpxO	Lipid A hydroxylase LpxO	5.35	2.79E-07	–	–
murB	UDP-N-acetylenolpyruvoylglucosamine reductase	–	–	2.97	0.006

[#]-FC: Fold change; –: Not detected or non-significant change

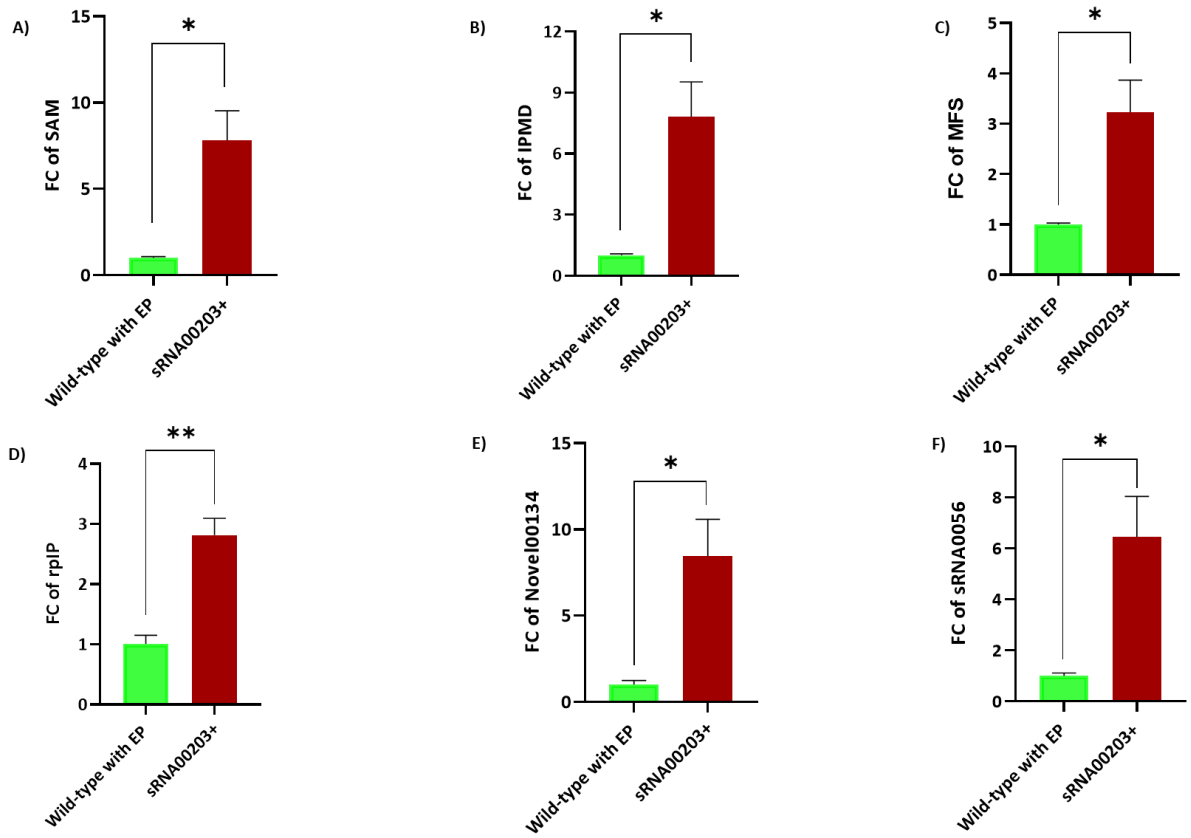

Figure 4.22 Effect of sRNA00203 overexpression on biofilm-associated genes.

RT-qPCR was used to assess the expression level of biofilm-associated genes in biofilm cells of *A. baumannii* ST1894. An independent t-test was employed to compare expression difference between strains. *, $p < 0.05$. **, $p < 0.01$. SAM: Class I SAM-dependent methyltransferase; IPMD: 3-isopropylmalate dehydratase large subunit (*leuC*); *rplP*: 50S ribosomal protein L16; EP: Empty plasmid; sRNA00203+: sRNA00203 overexpressing biofilm cells.

4.9 Conservation of sRNA00203 in *Acinetobacter* species

The sRNA was identified and verified for its impact in *A. baumannii* ST1894. To determine the conservation of the sRNA00203 sequence across other strains and the genus *Acinetobacter*, we used sequence data retrieved from the NCBI database. Blastn hits 1628 sequences in the genus, comprising 1244 *A. baumannii*, with the remaining sequences belonging to other species (Table 4.8). The sRNA sequence was entirely conserved across all the *A. baumannii* strains. Additionally, we detected the sRNA by PCR in 42 *A. baumannii* strains collected from various clinical samples and hospital environment (n = 3). The clinical isolates were from blood (n = 20), CSF (n = 5), urine (n = 7), aspirate (n = 3), and other samples (n = 4). Regarding their biofilm-forming capability, 40(95%) of the isolates were biofilm formers.

For the 19 species in the genus with E-value ≤ 1e-04, we constructed a phylogenetic tree. The medically important species (*A. baumannii, A. pittii, A. nosocomialis*, *A. seifertii,* and A. dijkshoorniae/*A. lactucae*) were found to be closely clustered (Figure 4.23). All the five species showed ≥ 96 % sequence coverage; *A. pittii* and *A. lactucae* had the highest sequence similarity (98% coverage) with *A. baumannii* (Table 4.8). Almost all the nucleotides of the sRNA were conserved, except for the two nucleotides at the 5' end, which also led to stem-loop structural conservation of the sRNA. The finding implies the sRNA is essential, and its role could also be shared at the genus-wide level.

Table 4.8 Description of the conservation level of sRNA00203 in *Acinetobacter* species.

Species	**Number of sequences**	**Alignment length**	**Sequence coverage (%)**	**E-value**
A. baumannii	1244	53	100	1e-16
A. pittii	84	52	98	4e-16
Other *A. pittii*	2	51	96	1e-15
A. lactucae	5	52	98	4e-16
A. nosocomialis	23	51	96	1e-15
A. seifertii	44	51	96	1e-15

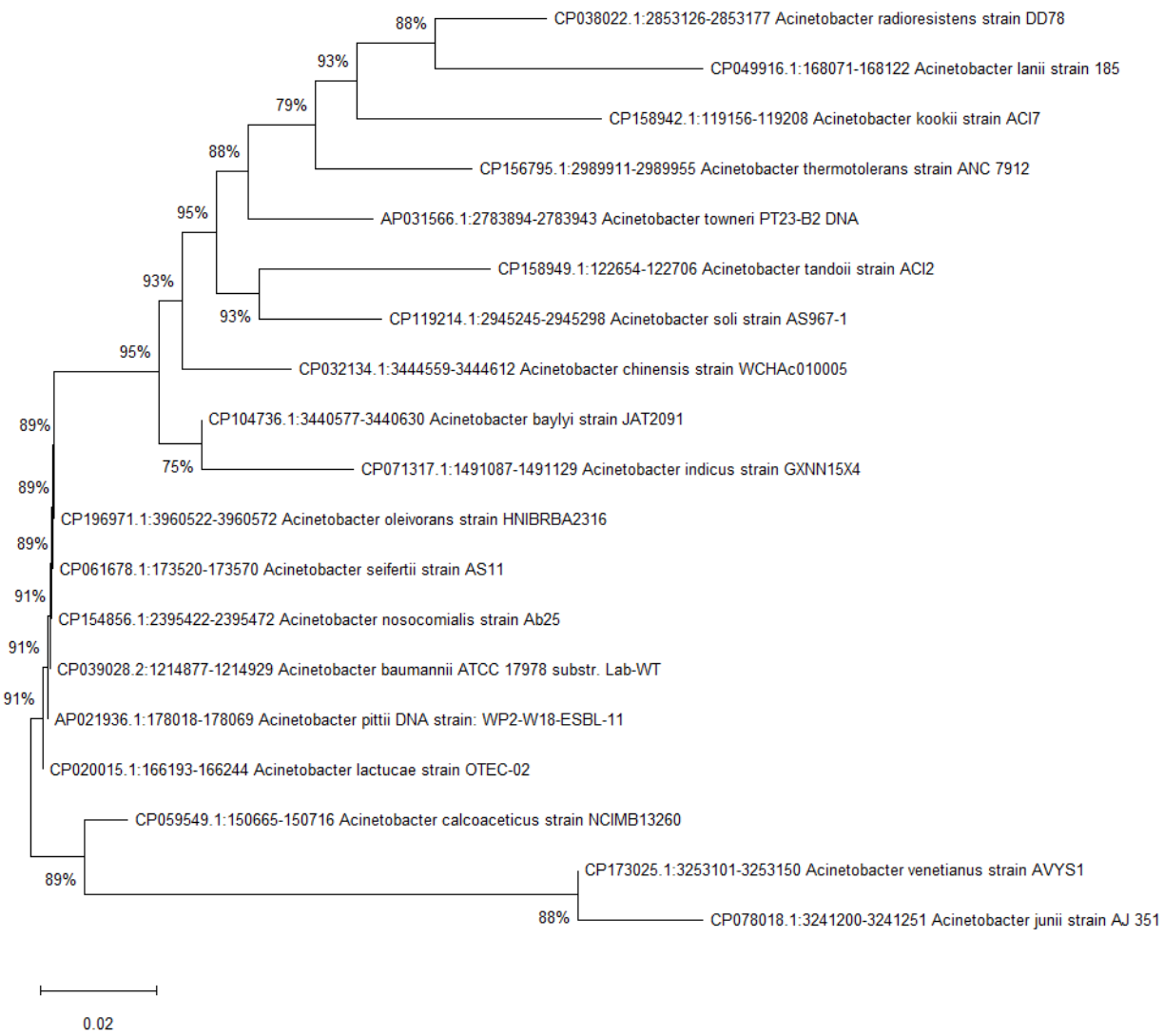

Figure 4.23 Relationships of the sRNA00203 sequence among *Acinetobacter* species.

The neighbour-joining method was used to construct the phylogenetic tree in MEGA 11 software. FASTA files (matched for the sRNA00203 sequence) from each of the *Acinetobacter* species (E-value ≤ 1e-04) retrieved from the NCBI database were included for the analysis. The percentage adjacent to the branches represents the site coverage. Accession numbers, species and strain names are indicated for each sequence.

4.10 Identification of base pairing primary targets of sRNA00203

Bacterial trans-encoded sRNAs primarily function through base pairing with target mRNAs (Felden & Augagneur, 2021). Based on this fact, we hypothesized that a subset of the genes identified in our combined omics studies are influenced by sRNA00203 due to sequence complementarity. To identify these primary base-pairing targets, we employed an orthogonal approach by tagging the sRNA, similar to the MS2 tagging used in MAP-seq in a previous study (Lalaouna et al., 2015). The tag was 24 nucleotides long and have no sequence similarity in the *A. baumannii* genome.

4.10.1 Construction of tagged sRNA00203 expressing strain

We used the pSGAb-k plasmid to construct a tagged sRNA00203-expressing strain, which was employed to identify base-pairing targets. The 24-nucleotide-long tag was fused to sRNA00203 by PCR. Initially, a template of 86 nucleotides in length was produced using a forward primer containing the tag at its 5' end. Using this template, we prepared a tagged sRNA insert with a 129-nucleotide-long sequence (Figure 4.24). The assembled plasmid was transformed into competent *A. baumannii* cells. As shown in Figure 4.25A and B, out of 37 colonies screened by colony PCR, 36 colonies harboured the insert (254 nt). Plasmids from positive clones were subjected to Sanger sequencing. The sequencing results confirmed the correct sequence and orientation of the tagged sRNA00203 (Figure 4.26).

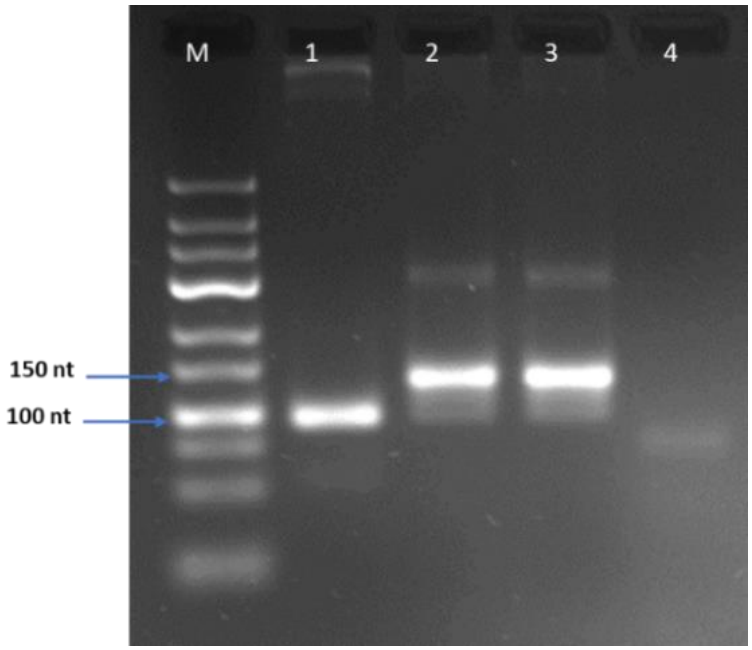

Figure 4.24 Tagged sRNA00203 preparation using PCR.

Agarose gel electrophoresis was used to verify the size of the template and the tagged sRNA00203 insert. Inserts of the correct size were excised and purified. M: low range DNA ladder (Thermo Fisher Scientific, USA); 1: Template; 2 & 3: 129 nt long tagged sRNA0023 insert; 4: No template control.

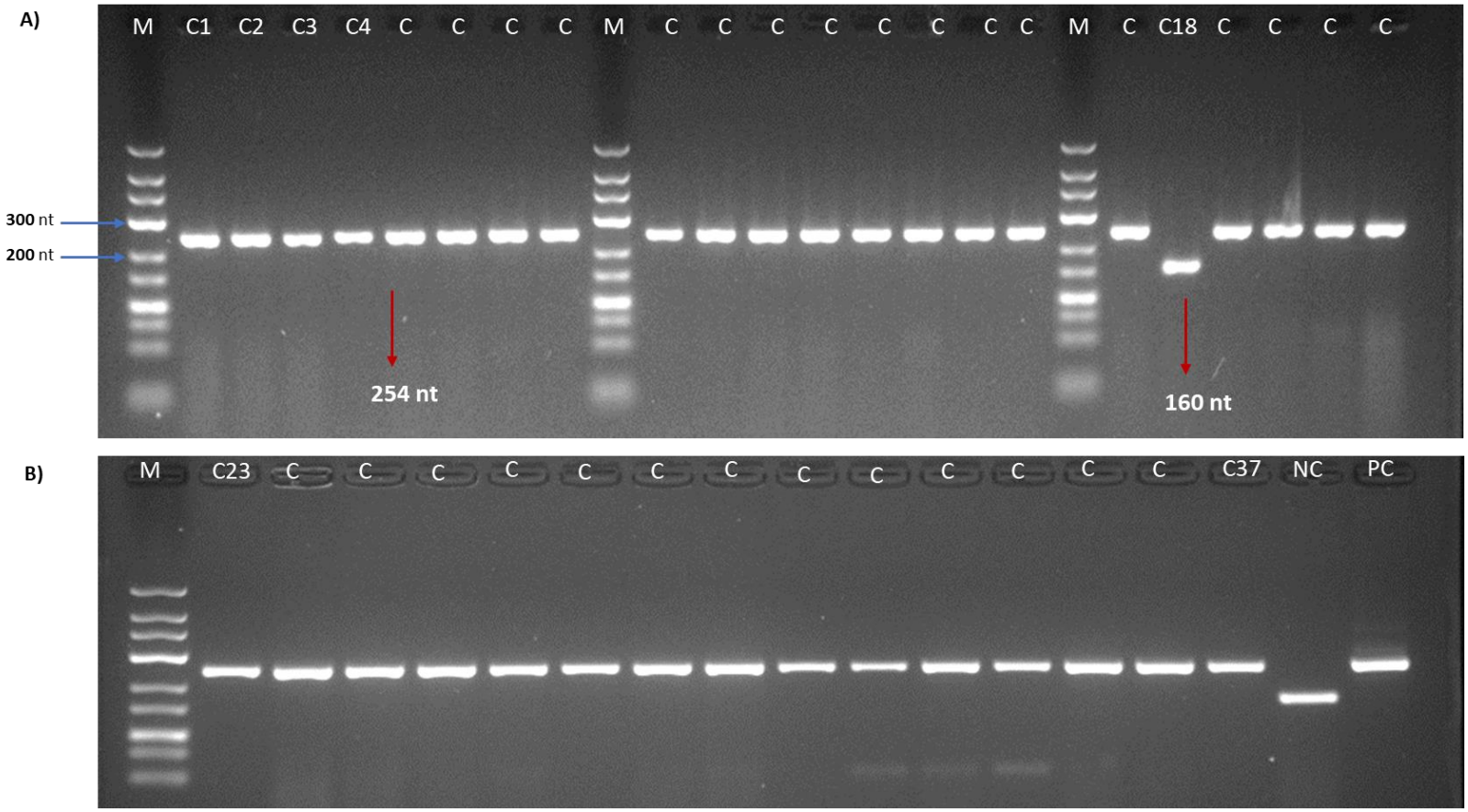

Figure 4.25 Colony PCR results of colonies screened during preparation of tagged sRNA00203 expressing strain.

Both figures (A) and (B) show colony PCR results. Lane labelled C1-C37 indicates colonies screened. Controls were included for reference. Negative control (NC) represents colonies transformed by the negative assembly reaction, and positive controls (PC) represent the positive assembly reaction. M: Low-range DNA ladder (Thermo Fisher Scientific, USA); NTC: No template control.

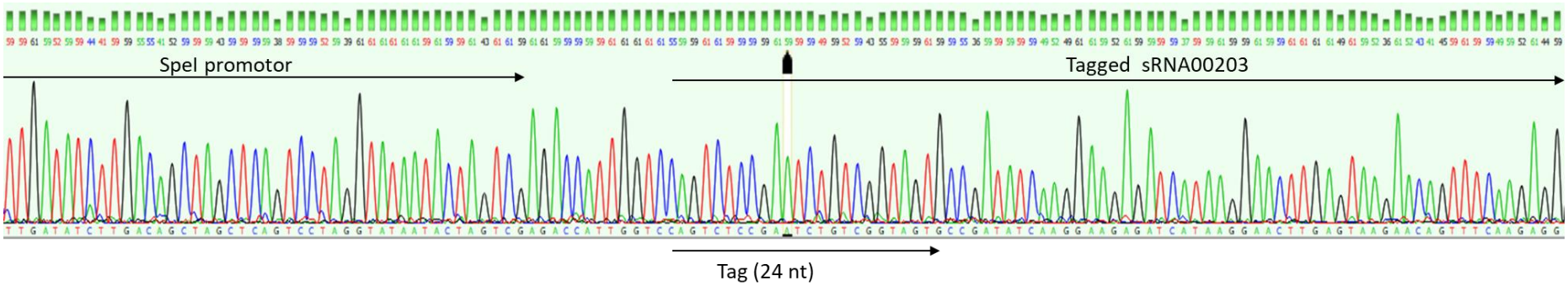

Figure 4.26 Verification of the sequence and orientation of tagged sRNA00203 in the recombinant plasmid.

Successful integration of the tagged sRNA00203 near the vector promoter was verified by Sanger sequencing using a forward primer. The values above the chromatogram indicate the quality score of each nucleotide. The minimum value was 36, which indicates a reliable enumeration of the nucleotides.

4.10.2 Validation of tagged sRNA00203 expression

To validate the expression of the tagged sRNA00203 from the recombinant plasmid in *A. baumannii* cells, RT-qPCR was performed. Total RNA was extracted from biofilm cells of the tagged sRNA00203-expressing strain and strain with an empty vector as a control. The results revealed that sufficient tagged sRNA mRNA levels (average CT value of 17 at 100-fold cDNA dilution) were found in the recombinant strain, confirming successful transcription driven by the constitutive SpeI promoter. The expression level of tagged sRNA in the control was negligible, with an average CT value of 34. Subsequently, the secondary structure of the transcribed RNA was predicted using RNAfold. The tagged sRNA (Figure 4.27B) was predicted to exhibit a secondary structure without major distortion compared to sRNA00203 (Figure 4.27A). This may highlight that the expressed tagged sRNA possesses similar base-pairing capabilities.

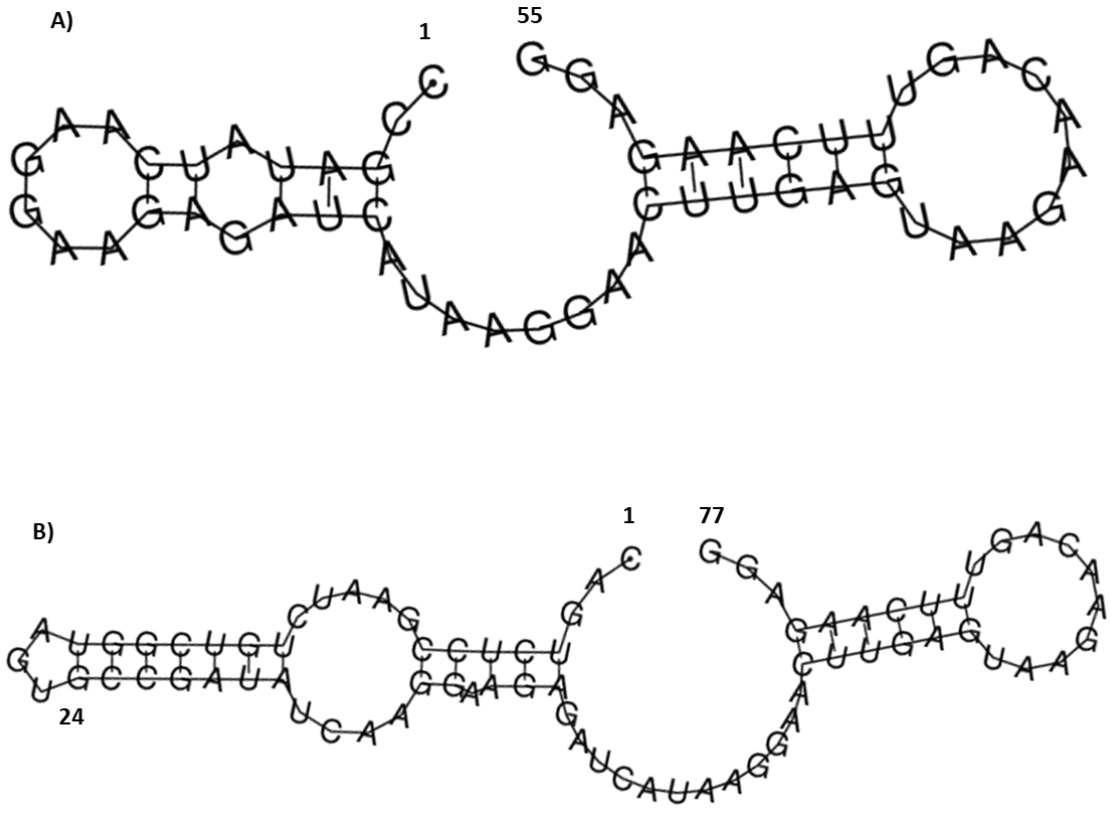

Figure 4.27 Predicted secondary structure of sRNA00203 (A) and tagged sRNA00203 (B). The numbers indicate the nucleotide positions in the mRNA, starting from the 5' end to the 3' end. The 1-24 nucleotide positions in Figure B indicate the tag.

4.10.3 Transcriptomic analysis of captured RNA interactome

4.10.3.1 Efficient capture of tagged sRNA using tag antisense probes

The constructed sRNA00203-overexpressing and tagged sRNA00203-expressing strains were used to capture the RNA interactome. Biofilm cell lysates from these strains were incubated with a 3' biotin-labelled tag antisense probe. Both RNA and DNA probes were utilized in the assay. The probes bound to the tagged sRNA and untagged associated RNAs, which were subsequently isolated using streptavidin-coated beads (Figure 4.28A). The result showed that the tagged sRNA was successfully captured from the mixture, indicating that the biotinylated probes interacted with the intended region. As expected, tagged sRNA was almost absent from the control. Both types of probes achieved comparable levels of enrichment (Figure 4.28B). The primer pair used for RT-qPCR was specific, as demonstrated by the presence of a single peak in Figure 4.27C.

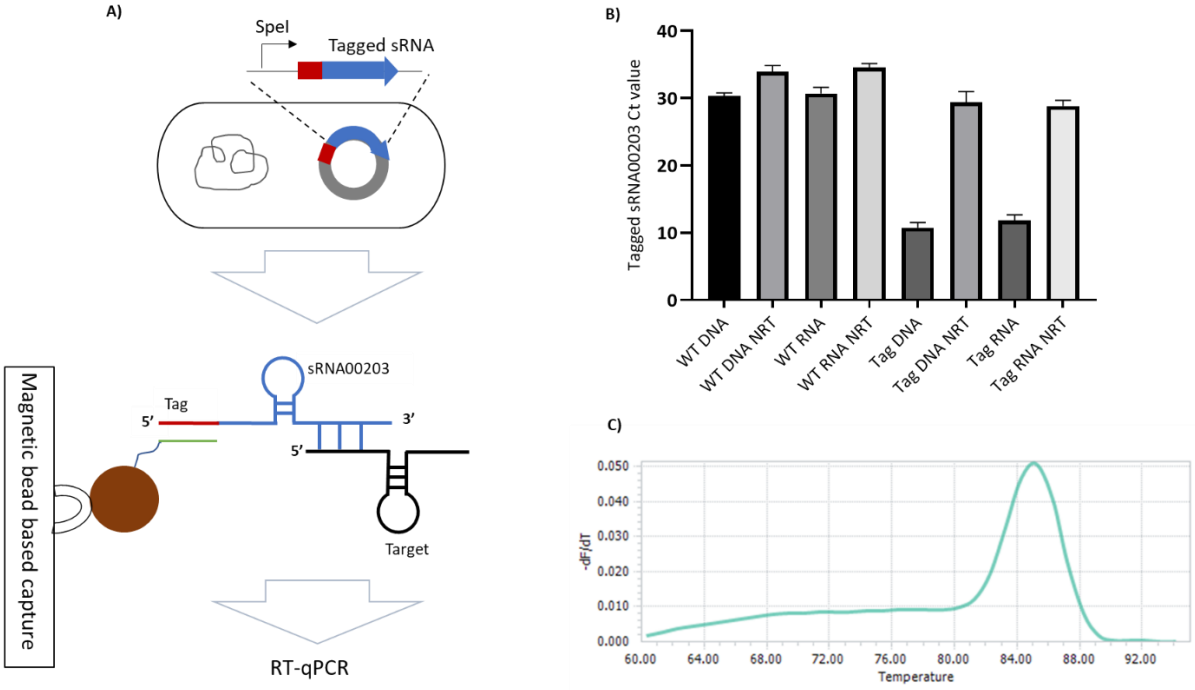

Figure 4.28 Detection of tagged sRNA from captured RNA samples.

(A) Tag-based RNA interactome experiment model. (B) Cycle threshold (Ct) values of tagged sRNA00203 in different samples using DNA and RNA antisense probe. WT: untagged RNA sample; Tag: tagged RNA RNA sample. The error bar was plotted using three independent experiments. (C) Melting curve analysis of tagged sRNA00203 amplicon obtained during RT-qPCR.

4.10.3.2 RNA sequencing of captured RNAs

To map the entire RNA interactome of the target RNA, we used 3' biotin-labelled tag antisense riboprobe capture followed by RNA-seq. The pooled RNA samples captured from the reaction tubes containing lysates of tagged sRNA00203-expressing and sRNA00203-overexpressing (control) biofilm cells were sequenced separately. The RNA sequencing generated ~4.5 million total mapped cDNA reads per library. Read quality was assessed using the Phred quality score, with Q30% of 91.98% for the experimental samples and 92.10% for the control samples. The observed high Q30 values attest to the accuracy of the sequencing data, ensuring the validity of downstream analyses.

Differential analysis revealed a total of 219 differentially enriched transcripts (DETs) in the experimental sample compared to the control sample, using a fold enrichment cut-off value of 2 and a p-value of < 0.05. To minimize the inclusion of spuriously bound genes, genes with FPKM values below 50 were also excluded. Of the filtered 219 DETS, 155 (70.8%) genes were upregulated and 64 genes were downregulated (Figure 4.29). The observed downregulation may suggest that the bead-based capture followed by the RNA-seq method can result in the detection of a number of non-specifically bound genes. Among the upregulated genes, 116 (74.8%) overlapped with the findings from transcriptomic and proteomic investigation of the sRNA00203-deleted strain. The identified genes were related to amino acid metabolism, secretion system, outer membrane protein, and iron acquisition system. Notably, the analysis also identified new candidate targets such as *lpxO* and E5A72_RS15655 (lipopolysaccharide assembly protein LapA encoding gene) that were not among the previously identified influenced genes. The list of the top identified putative primary targets is described in Table 4.9.

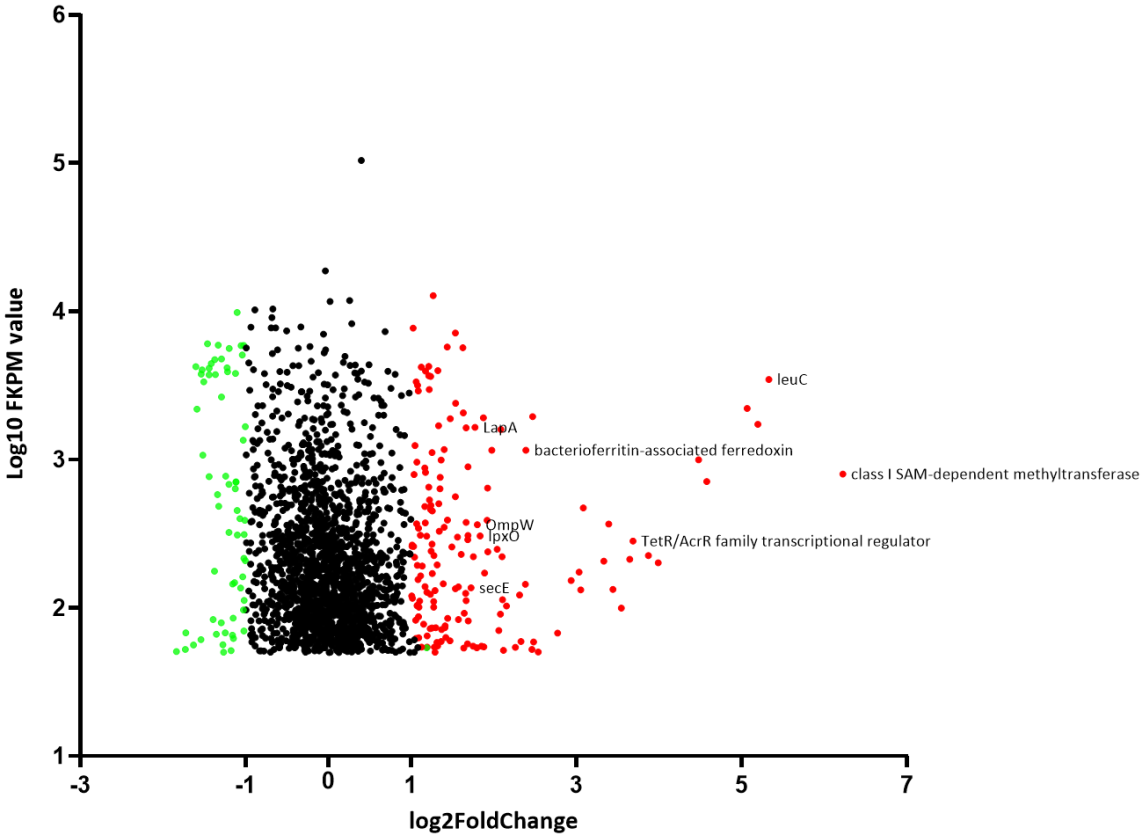

Figure 4.29 Volcano plot showing enriched genes in the tag-based captured RNA-seq. The volcano plot was constructed using genes detected in the tag-based capture assay, followed by RNA-seq that exhibited FPKM values of ≥ 50. The Y-axis represents the FPKM value of genes in the tagged sRNA00203-expressing RNA sample (experimental). Red dots represent genes with a fold change of ≥ 2 and greed dot represent gene with a fold change of ≤ -2 and a p-value of < 0.05. The labelled genes are among the DETs that overlapped with the combined omics study of the sRNA00203-deleted strain.

Table 4.9 Selected putative primary target genes of sRNA00203.

Gene ID	Description	$Log_2(FC^{\#})$	P-value
E5A72_RS16120	Class I SAM-dependent methyltransferase	6.22	7.71E-31
E5A72_RS09705	3-isopropylmalate dehydratase large subunit (*leuC*)	5.33	5.41E-27
E5A72_RS07330	TDT family transporter (Voltage-dependent anion channel)	5.19	9.55E-26
E5A72_RS02555	Hypothetical protein	2.94	4.87E-09
E5A72_RS08895	TetR/AcrR family transcriptional regulator	3.08	1.6E-11
E5A72_RS09035	Preprotein translocase subunit SecE	1.54	< 0.001
E5A72_RS00750	OmpW family protein	1.89	< 0.00001
E5A72_RS05275	Amino acid permease	1.69	< 0.00001
E5A72_RS00625	Multidrug efflux transcriptional repressor AdeL	1.61	< 0.001
E5A72_RS00620	ABC transporter substrate-binding protein	1.64	< 0.001
E5A72_RS09175	lipid A hydroxylase LpxO	1.84	3.50E-05
E5A72_RS15655	lipopolysaccharide assembly protein LapA	1.77	3.93E-05
E5A72_RS13770	Cold-shock protein	1.27	0.002
E5A72_RS04415	tRNA-Arg	2.11	0.003
E5A72_RS18725	LysR family transcriptional regulator	1.17	0.006
E5A72_RS19205	Csu fimbrial major subunit CsuAB	1.23	0.008
E5A72_RS15310	Fimbrial protein	1.10	0.015
E5A72_RS15945	TonB-dependent receptor	1.06	0.017

[#]-FC: Fold change.

4.6.3.3 RT-qPCR verification of primary targets

In the biofilm state, genes such as class I SAM-dependent methyltransferase (E5A72_RS16120), 3-isopropylmalate dehydratase large subunit (*leuC*), MFS transporter (E5A72_RS06620), 50S ribosomal protein L16 (*rplP*), Novel00134, and sRNA00056, which were confirmed by deletion and overexpression studies as influenced mRNAs, were selected for RT-qPCR analysis. Two of these genes (E5A72_RS16120 and *leuC*) were also identified in the RNA-seq of tag-based captured RNAs (Table 4.9). As illustrated in Figure 4.30, of the six genes, E5A72_RS16120, *leuC*, Novel00134, and sRNA00056 genes were verified as putative primary targets of sRNA00203 (Figure 4.30A, B, E, and F). However, Novel00134 and sRNA00056 genes were not detected in the RNA-seq data used for primary target search. This discrepancy may be due to inherent challenges in the prediction of novel genes and noncoding sRNAs.

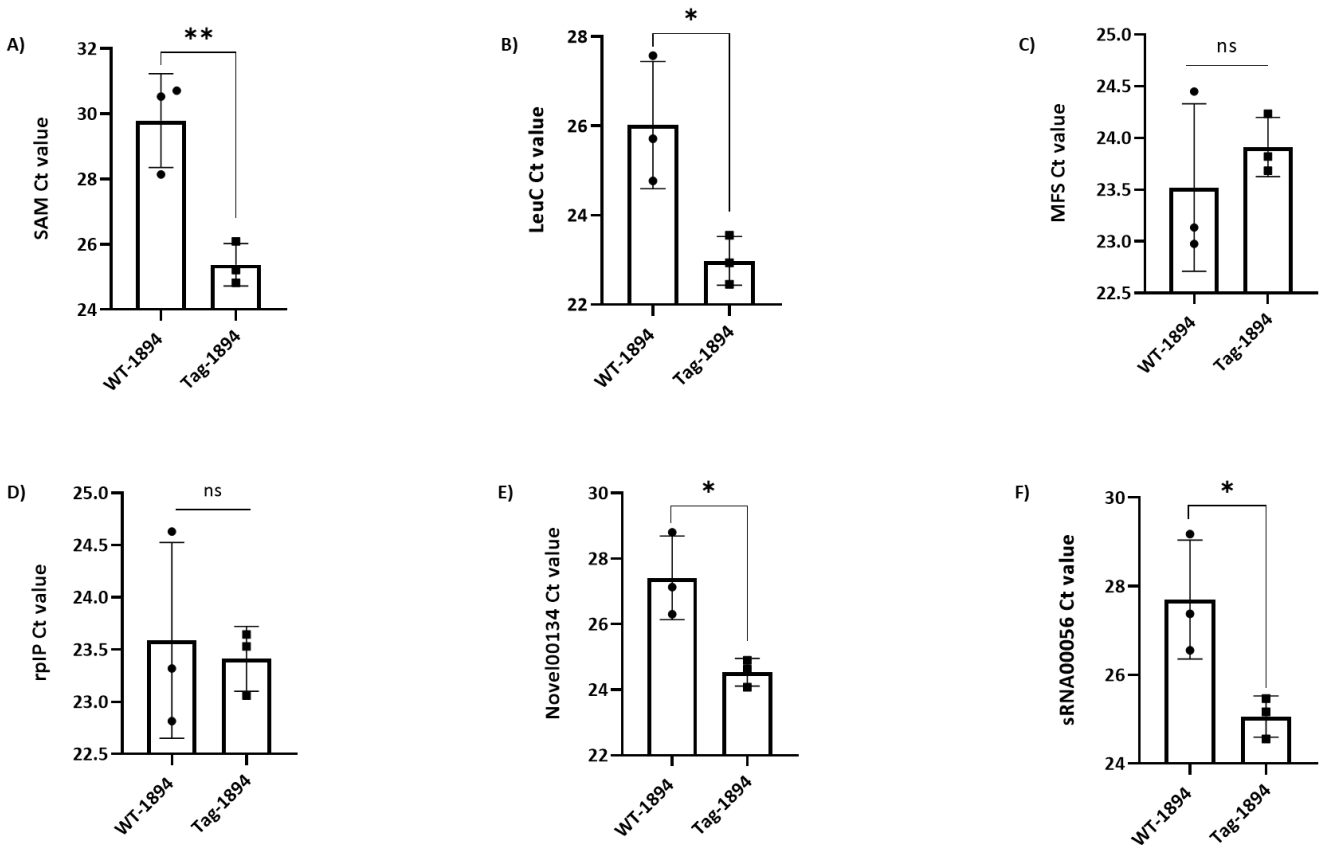

Figure 4.30 Detection level of potential primary targets of sRNA00203 in captured RNAs.

RT-qPCR was used to assess the mRNA level of genes identified in the tag-based captured RNA samples. An independent t-test was employed to compare the Ct value difference between tagged (Tag-1894) and untagged (WT-1894) RNA samples. *, $p < 0.05$. **, $p < 0.01$. SAM: Class I SAM-dependent methyltransferase; LeuC: 3-isopropylmalate dehydratase large subunit; rplP: 50S ribosomal protein L16.

4.11 Predicted binding motifs of sRNA and primary targets

We predicted the potential binding sites of sRNA00203 using IntaRNA and copraRNA software for the selected primary target transcripts identified in the tag-based capture. We found that the regulatory sRNA00203 could bind to the coding sequences or 5' untranslated region (UTR) of many of the putative target genes, as summarised in Table 4.10.

Table 4.10 Predicted binding sites of sRNA00203 on selected putative primary targets.

mRNA_ ID	Description	sRNA00203 position	mRNA position	Energy (kcal/mol)
E5A72_RS09035	Preprotein translocase subunit SecE	2–53	46–100	-16.01
E5A72_RS15655	lipopolysaccharide assembly protein LapA	24–53	82–111	-16.2
E5A72_RS09175	lipid A hydroxylase LpxO	10–53	849–887	-13.17
E5A72_RS15945	TonB-dependent receptor	13–40	320–345	-11.47
E5A72_RS00750	OmpW family protein	29–53	785–811	-9.85
Novel00134		2–26	8–38	-9.11
E5A72_RS08895	TetR/AcrR family transcriptional regulator	30–47	-94– (-111)	-9.02
E5A72_RS07330	TDT family transporter (Voltage-dependent anion channel)	15–44	172–201	-8.68
E5A72_RS16120	Class I SAM-dependent methyltransferase	25–34	444–453	-7.15
E5A72_RS02555	Hypothetical protein	9–27	46–63	-7.07
E5A72_RS09705	3-isopropylmalate dehydratase large subunit	31–41	43–53	-4.21

4.12 Verification of sRNA00203 and target interaction

Electrophoretic mobility shift assay (EMSA) was performed to validate the direct interaction between sRNA00203 and its putative primary mRNA targets, which were identified by the tag-based capture method. Targets involved in the secretion system (Preprotein translocase subunit SecE), cell wall synthesis (lipid A hydroxylase LpxO), or metabolism (Class I SAM-dependent methyltransferase) were selected for the assay. In vitro transcribed sRNA and portions of these target sequences that contain the predicted binding regions were incubated together under binding conditions. As a positive control, sRNA (Aar) and its confirmed target, CarO type III, as identified in *A. baumannii* (Hamrock et al., 2024) was incubated under similar condition. Either the target or sRNA mixed with binding buffer alone was used as a negative control. The formation of sRNA–mRNA complexes was assessed by running the mixtures on a 5% native polyacrylamide gel electrophoresis (PAGE).

As illustrated in Figure 4.30B, the EMSA results demonstrated a distinct shifted band when sRNA00203 was incubated with increasing concentrations of secE (2, 4, and 6 pmol). This indicates the formation of a stable sRNA-mRNA complex at the predicted region, spanning nucleotides 2 to 53 of sRNA00203 and 46 to 100 of *secE* (Figure 4.31A). Likewise, a shift was observed in the positive control reaction, confirming the ability of the assay to detect interactions. No shift was observed in either the target or sRNA mixed with binding buffer alone, confirming that the observed mobility shift in the experimental reactions was specific. The intensity of the shifted band increased with higher concentrations of *secE*, further supporting a dose-dependent binding between the sRNA and its target mRNA. Band density analysis of the gel revealed that, with a fixed concentration of sRNA (2 pmol), the amount of mRNA–sRNA complex formed at four pmol of *secE* was 3.7-fold higher than at two pmol of *secE*, and the complex formed at six pmol of *secE* showed a 1.6-fold increase compared to that at four pmol of *secE* (Figure 4.31B). Similar EMSA findings were also observed for the *lpxO* and E5A72_RS16120 target mRNAs (Figure 4.31D and F). These results provide further evidence that sRNA00203 regulates the expression of *secE*, *lpxO*, and E5A72_RS16120 through direct base-pairing interactions.

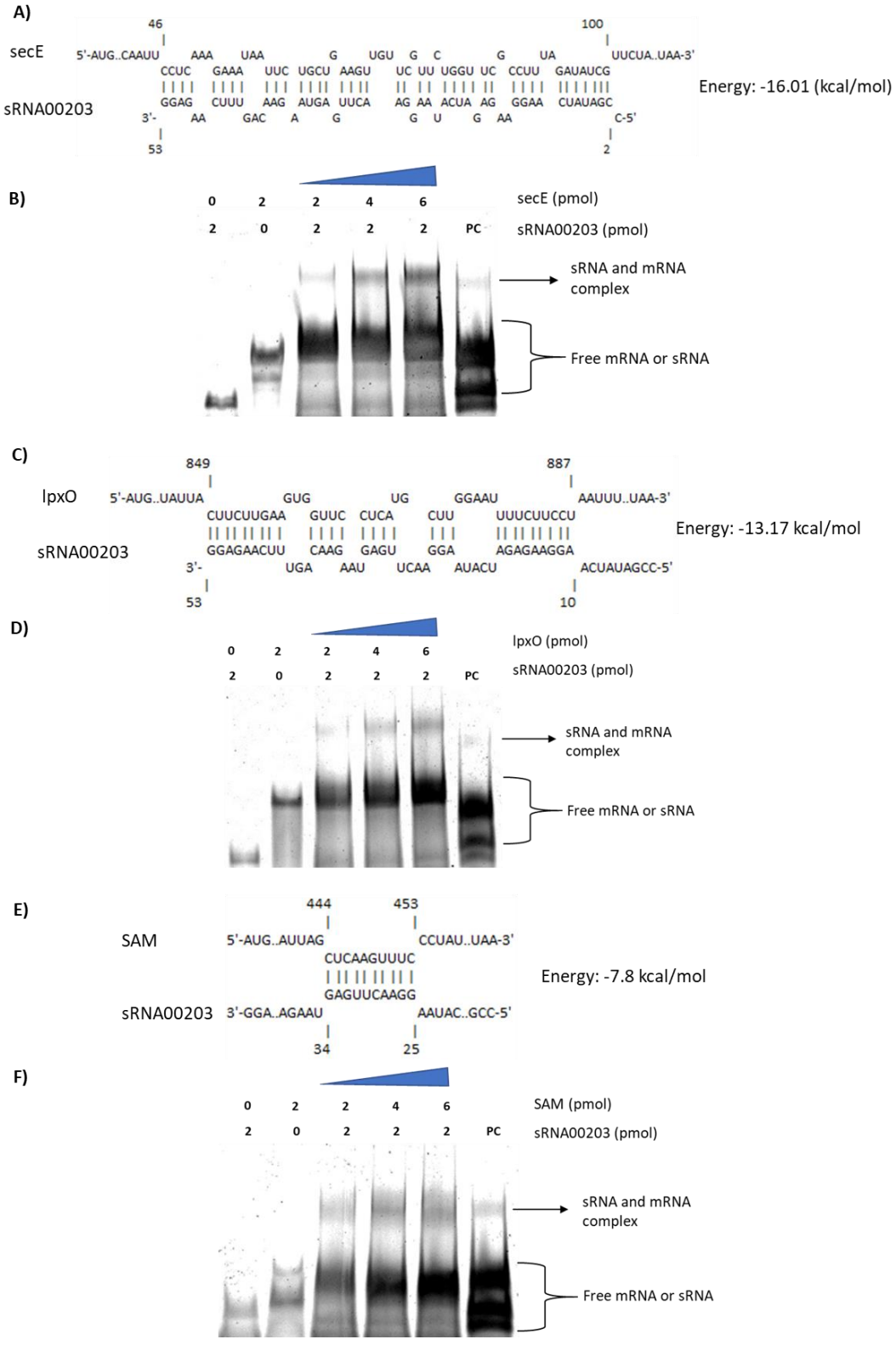

Figure 4.31 Detection of direct interaction between sRNA00203 and target mRNAs. Panels (A), (C), and (E) show the predicted binding regions of sRNA and target, whereas panels (B), (D), and (F) present the EMSA results. PC: positive control (2 pmol Aar sRNA mixed with two pmol *carO*).

4.13 Identification of sRNA00203 interacting proteins

Small RNAs (sRNAs) interact with a diverse class of proteins known as RNA-binding proteins (RBPs). In particular, binding to RNA chaperones such as Hfq, ProQ, and CsrA is crucial for regulating gene expression in bacteria. These proteins bind to sRNAs and mRNAs to facilitate structural changes that enhance sRNA-mRNA base pairing, stabilize RNA interactions, and accelerate the regulatory processes (Quendera et al., 2020). Given the importance of RBPs in facilitating sRNA function, we aimed to identify proteins that could potentially interact with sRNA00203 under biofilm conditions using the RNA-Protein pulldown assay. The reverse transcribed full length of sRNA00203 and control RNA were 3' biotinylated. In the presence of RNA-protein binding buffer, transcribed RNAs were separately incubated with equal amounts of biofilm cell lysate proteins in triplicate. Subsequently, ten microlitres of pulldown peptides were subjected to mass spectrometry analysis (Figure 4.31A).

The tryptic peptides detection by the Orbitrap Fusion™ Lumos™ mass spectrometer coupled with a Dionex UltiMate 3000 RSLCnano system was performed over a 90-minute gradient. The average fragmentation efficiency of peptides in the sRNA00203 samples (experimental) and control samples exceeded 65%. Additionally, percentage of missed cleavage of samples was comparable and remained below 10%, indicating efficient trypsin digestion. Label-free directDIA analysis using Spectronaut identified a total of 641 precursors and 605 peptides in the samples. The peptides were mapped to 155 proteins at a 1% FDR with a minimum of two unique peptides per protein. Specifically, an average of 126 proteins were identified in the experimental group and 64 proteins in the control group.

Differential enrichment analysis revealed 32 proteins exhibited significant changes in the sRNA00203 group compared to the control RNA group (fold-change ≥ 2 or ≤ -2 and q-value < 0.05). Of these differentially enriched proteins, only one protein (Large ribosomal subunit protein uL29) was down-regulated (Figure 4.32B). This finding demonstrates that random binding was substantially diminished. The 31 potential sRNA00203-binding proteins were broadly categorized as being related to transcription, translation, and metabolism. Fifteen of these proteins were ribosomal proteins, with nine belonging to the large ribosomal subunit and 6 to the small ribosomal subunit. Additionally, translation initiation factor, elongation factors, and DNA-directed RNA polymerase subunit alpha were also identified (Table 4.11).

Based on Gene Ontology classification, these proteins are recognized as RNA-binding proteins, confirming that our RNA-protein pulldown followed by mass spectrometry analysis was able to enrich for RNA-binding proteins.

Furthermore, proteins related to the TCA cycle, amino acid metabolism, fatty acid metabolism, and nucleotide metabolism were identified (Table 4.11). Beyond these metabolic categories, other proteins, such as the UPF0234 protein and the chaperone protein DnaK, were also identified among the top-ranked sRNA00203 interacting proteins (Figure 4.31B). Ontologically, the UPF0234 protein is classified as a nucleotide-binding protein. The chaperone protein DnaK, a member of the Hsp70 family, functions in protein folding under stressful conditions and may indirectly bind to RNA that is associated with proteins.

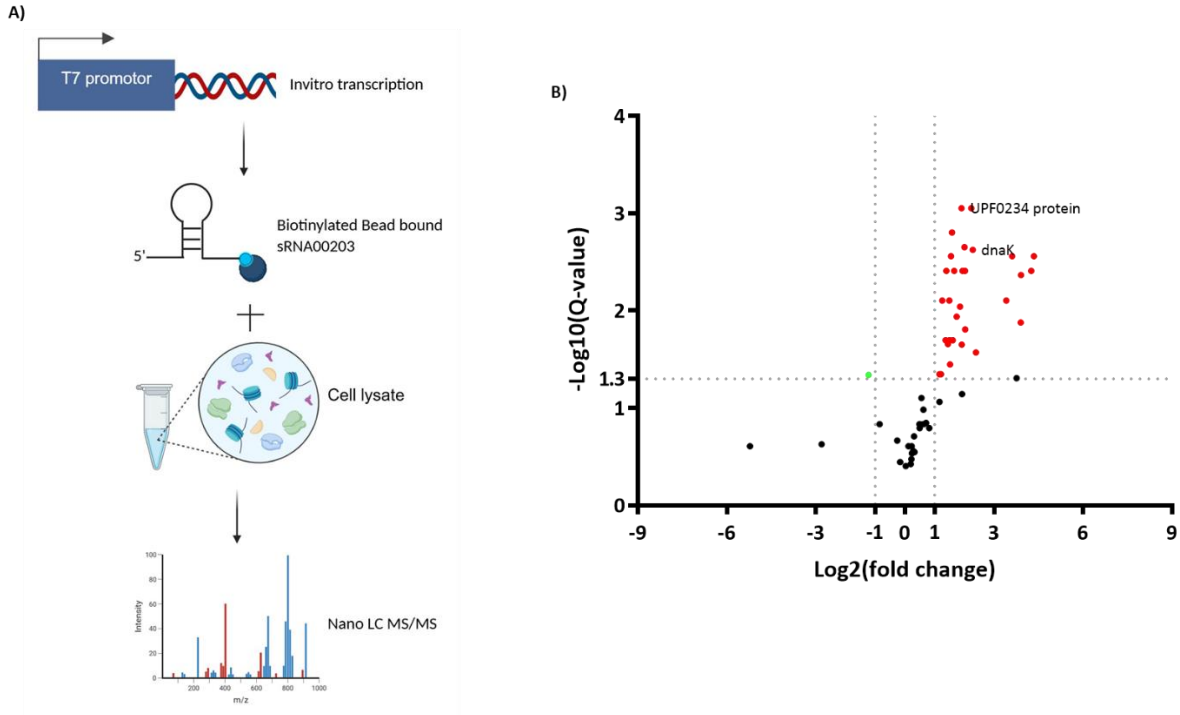

Figure 4.32 RNA-protein pulldown assay to identify sRNA00203-interacting protein in *A. baumannii*.

(A) Illustration of the method used to identify potential sRNA00203 binding proteins from biofilm cell lysate. The figure was created using BioRender. (B) Volcano plot showing all proteins quantified in the experimental and control groups after mass spectrometry data analysis. Red dots represent proteins with a fold change of ≥ 2, and green dot represent protein with a fold change of ≤ -2 and a q-value of < 0.05.

Table 4.11 Description of the putative sRNA00203-interacting proteins in biofilm cells.

UniProt ID	Protein name	$Log_2(FC^{\#})$	q-value
Ribosomal proteins			
A3M1G2	Large ribosomal subunit protein bL12	3.79	0.0036
A3M982	Large ribosomal subunit protein uL4	2.46	0.0086
A3M2X2	Large ribosomal subunit protein bL25	1.46	0.0098
B0V6W2	Small ribosomal subunit protein uS5	1.36	0.0119
A3M305	Small ribosomal subunit protein uS7	1.74	0.0172
Transcription and translation			
A3M750	Elongation factor Ts	2.06	0.0035
A3M7E3	Elongation factor P	2.13	0.0035
B0VSL8	Transcription elongation factor GreA	3.91	0.0043
A3M1T2	Translation initiation factor IF-1	1.84	0.0086
A3M959	DNA-directed RNA polymerase subunit alpha	1.24	0.0149
Metabolism			
A3M887	Succinate-CoA ligase [ADP-forming] subunit beta	2.33	0.0012
A3M140	ATP synthase subunit b	2.12	0.0028
A3M207	Nucleoside diphosphate kinase	4.43	0.0035
A3M3G1	Adenylate kinase	3.67	0.0035
A3M1J3	Pyrimidine/purine nucleoside phosphorylase	1.91	0.0137
B7GYR8	Acyl carrier protein	3.56	0.0172
A3M928	Malate dehydrogenase	1.52	0.0224
Others			
B0V634	UPF0234 protein	2.37	0.0020
A3M8W9	Chaperone protein DnaK	2.45	0.0035

[#]-FC: Fold change.

4.14 sRNA00203 may act independently of the known chaperone protein

Among the 31 differentially enriched putative sRNA00203-interacting proteins, the known chaperone proteins were not identified. In *A. baumannii*, Hfq has been identified as having a long glycine-rich C-terminal region (CTR), unlike in other bacteria, and the ability of its recombinant protein to bind to sRNA has been reported (A. Sharma et al., 2018). Indeed, Hfq protein was identified in our samples with 12% peptide coverage, confirming an acceptable level of identification in complex samples (Figure 4.33A). The quantitative analysis showed that the Hfq protein detection level was 1.5-fold higher in the sRNA00203 samples compared to the control RNA samples. However, this change was not statistically significant (q-value = 0.09) (Figure 4.33B). While further validation is necessary, this result tentatively implies that sRNA00203 could regulate its targets independently of the Hfq chaperone protein.

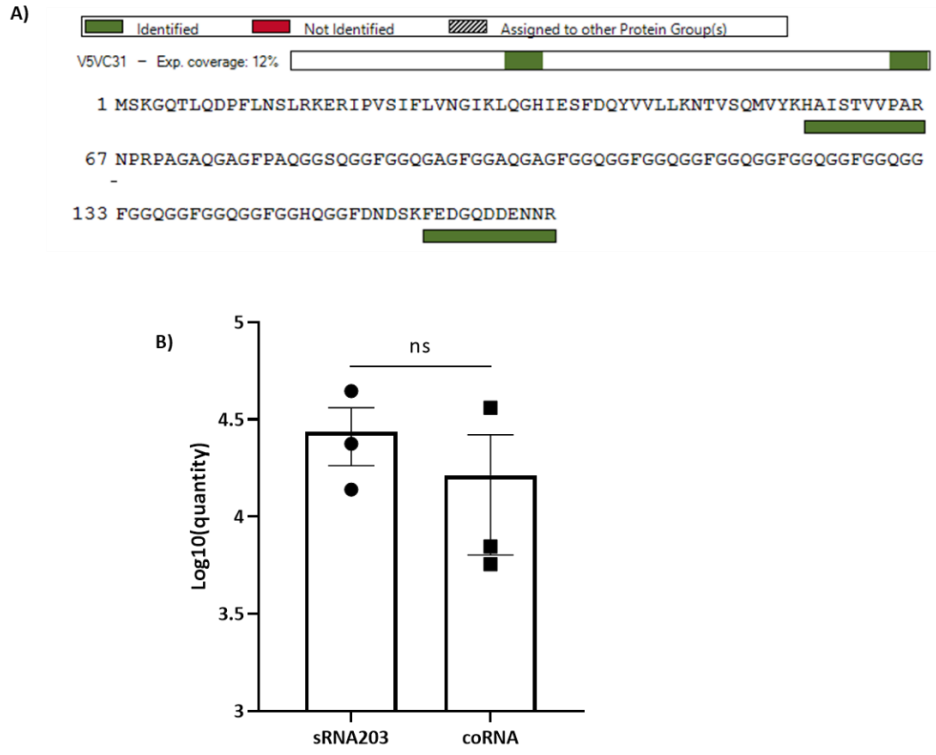

Figure 4.33 Detection status of RNA-binding protein Hfq in the RNA-protein pulldown. (A) Peptide coverage across the Hfq protein sequence**,** as measured by DIA label-free proteomics**.** The horizontal axis represents the amino acid sequence of the protein, while the colored bars indicate regions covered by identified peptides. (B) Quantified levels of Hfq protein in sRNA00203 and control RNAs (coRNA). Error bars indicate standard deviation (SD) across replicates (n = 3).

5. Discussion

5.1 Genome-wide influences of sRNA00203 on *Acinetobacter baumannii*

Bacterial non-coding small RNAs (sRNAs) are key regulatory molecules that govern gene expression to shape a wide range of physiological processes, including the modulation of stress responses and development of antimicrobial resistance (Khaledi et al., 2024). Previously, it was observed that novel sRNA00203, with a sequence length of 53 bp, was highly expressed in both untreated biofilm and imipenem-treated biofilm relative to its planktonic counterparts in *A. baumannii* ST1894 (Shenkutie et al., 2022). Consequently, deletion of the sRNA resulted in significant biofilm mass reduction and lower MBIC and MBEC (Shenkutie et al., 2023). Although the previous study also demonstrated the effect of sRNA00203 on a few biofilm and antibiotic-related genes, the majority of the influenced genes in the biofilm and planktonic growth forms remained unexplored. Thus, to comprehensively understand the genome-wide influences of the sRNA, we employed a combined transcriptome and proteome analysis of the deletion mutant and wild-type *A. baumannii* cells.

The sRNA was initially identified in a single *A. baumannii* strain. We showed in this study that it exhibits strong sequence and secondary structure conservation across *Acinetobacter* species with clinical significance. This supports the hypothesis that the regulatory influence of the sRNA on expression could be shared across the medically important members of the genus. The conservation pattern also provides a rational basis for studying the molecular mechanism of the sRNA00203 in the originally identified strain, which could be a representative.

Our combined omics studies of biological triplicates of biofilm cells revealed 816 differentially expressed genes and 600 differentially expressed proteins in the sRNA00203 deletion mutant relative to wild-type *A. baumannii* ST1894. Functionally, the influenced genes were annotated as encoding ribosomal proteins, Ade IJK efflux pumps, porin membrane proteins, MFS efflux pump, type IV pili, Csu pili, and iron acquisition systems. Likewise, regardless of the direction of change, the DEPs were classified into comparable functional categories. However, due to the role of sRNA, which is primarily involved in posttranscriptional regulation, we observed additional genes affected only at the protein

level. The proteins identified were related to secretion systems and cell wall synthesis. These concordant and discordant findings highlight the importance of integrating transcriptomic and proteomic investigations to unravel the regulatory roles of the sRNA in *A. baumannii.*

Several ribosomal proteins (r-proteins) coding genes, predominantly the 50s r-protein coding genes, were significantly upregulated in the sRNA00203 mutant biofilm cells (Figure 3.5). Conversely, proteomic analysis presented downregulation. In turn, in both studies, the translation pathway was significantly affected (Figures 4.2 and 4.13). Bacterial r-proteins are known building blocks of both the small (30s) and large (50s) ribosome subunits that orchestrate protein synthesis. The 30S subunit participates in the translation initiation by adhering to mRNA, and the 50S subunit is involved in the translocation process (Aseev et al., 2024). Therefore, likely due to defects in ribosome assembly as a consequence of reduced levels of r-proteins, mutant cells displayed growth retardation, which mimics the proteomics data. However, the upregulation at the transcript level may reflect a cellular response to compensate for this deficit. These findings may reflect the role of the small RNA in the post-transcriptional regulation of the r-protein, likely by translational initiation. In consequence, sRNA-dependent impairment of the r-proteins may contribute to increased sensitivity of the deletion mutant biofilm cells to aminoglycosides, macrolides, and tetracycline family of antimicrobials (Shirakawa et al., 2023).

Previously, we demonstrated lower inhibitory (1,024-fold) and eradication (128-fold) concentrations of imipenem for mutant biofilm cells compared to wild-type biofilm cells (Shenkutie et al., 2023). As one possible underlying mechanism for the higher susceptibility to imipenem, our follow-up RNA-seq and proteomic studies showed that sRNA00203 facilitated downregulation of porin proteins, including CarO type IV and OmpW family proteins. The outer membrane protein (OMP), CarO, a 25-29 kDa beta barrel-shaped protein, is associated with carbapenem nonsusceptibility in *A. baumanni* (Siroy et al., 2005). Reduced expression of CarO switched clinical isolates to carbapenem-resistant isolates (Limansky et al., 2002). This could be explained by the fact that this porin facilitates the influx of beta-lactam antibiotics, particularly carbapenems (Mussi et al., 2005). Structural investigation further supported CarO as a carbapenem influx agent by demonstrating its binding affinity to the antibiotics (Sariyer, 2022).

Similar to CarO, low expression of the OmpW protein was observed in carbapenem-resistant *A. baumannii* compared to *A. baumannii* reference strain (Tiwari et al., 2012). The diminished expression of OmpW was observed to promote outer membrane vesicle-mediated biofilm formation in *A. baumannii* (Park et al., 2021). We also demonstrated that sRNA00203 could primarily modulate the impairment of OmpW-encoding gene expression to enhance biofilm and associated antimicrobial resistance.

The virulence factor type IV pili exists in almost all *A. baumannii* strains (Harding et al., 2018). Loss of type IV pili led to biofilm reduction, absence of twitching motility, impairment of DNA uptake and adherence (Ronish et al., 2019; Vesel & Blokesch, 2021). Additionally, in our strain under investigation, it has been previously reported that type IV pili subunits were upregulated in biofilm cells relative to planktonic cells (Shenkutie et al., 2022). Following deletion of sRNA00203, our combined omics analysis demonstrated that several subunits essential for the biogenesis and assembly of the pili (PilB, PilG, and PilO) were repressed. As a result, the mutant appeared less pilated under transmission electron microscopy examination (Figure 4.15). Therefore, considering that biofilm formation and acquisition of resistant genes are primary contributing factors to *A. baumannii*'s status as a nosocomial pathogen, this sRNA could be regarded as a prominent virulence gene.

Unlike the type IV pili subunit influence, csu pili components such as CsuC and CsuAB showed opposite direction of regulation at the transcript and protein level, a pattern similar to that seen with ribosomal proteins. We speculated that the absence of the sRNA may lead to impaired translation or increased degradation of the CsuC and CsuAB proteins. The underlying mechanism could be alterations in ribosome binding, changes in mRNA secondary structure, or the involvement of other regulatory factors influenced by the sRNA00203. For instance, regulatory non-coding sRNAs, such as sRNA00056, which were found to be biofilm-associated (Table 4.7), were significantly influenced by sRNA00203. Since both the Csu pilus components are essential for biofilm development (Ahmad et al., 2023), their reduced protein levels in the sRNA deletion mutant are likely to be additional reasons for the biofilm reduction observed.

The sRNA00203 also influenced several genes involved in the iron acquisition system. In iron-limited conditions, *A. baumannii* produces siderophores to chelate iron from host iron storage proteins, enabling the pathogen to survive (Cook-Libin et al., 2022). In this study,

genes that are involved in acinetobactin synthesis (*basJ* and *basB*) and transporting the acinetobactin, which are embedded in the outer membrane (*bauF*) and inner membrane (E5A72_RS05910 and E5A72_RS05115) of the cell wall, were down-regulated in the mutant cells. Repression of TonB-dependent iron transporter expression was shown to impair iron uptake, which in turn led to a reduction in biofilm formation (Bao et al., 2022; N. Wang et al., 2022). Furthermore, another study showed that disruption of acinetobactin biosynthesis machinery and TonB3 in *A. baumannii* led to attenuation of virulence in an animal model (Runci et al., 2019; Sheldon & Skaar, 2020). These results imply that the survival rate of the sRNA00203 mutant in iron-restricted environments (human host) could be lower, possibly due to impairment of iron-dependent metabolic functions that are vital for biofilm resilience.

Expression of a plethora of efflux pumps plays a crucial role in the development of drug-resistant *A. baumannii* by extruding a wide range of antibiotics out of the cell (Zack et al., 2024). The first regulatory sRNA, AbsR25, was able to downregulate the MFS efflux pump (AbaF) upon exposure to Fosfomycin (A. Sharma et al., 2017). In contrast, our study revealed that the expression of sRNA00203 upregulated the efflux pump MFS (E5A72_RS06620) in the wild-type biofilm, which exhibited tolerant phenotypes to ciprofloxacin, unlike its planktonic and mutant biofilm counterparts. Beyond AMR, overexpression of MFS (BIT33_RS14560) has been shown to increase biofilm formation and virulence in *A. baumannii* (Yang et al., 2022). Indeed, considering the presence of diverse MFS efflux pumps in the pathogen's genome, further investigation of the identified MFS gene is warranted.

The effect of sRNA00203 was not limited to the biofilm growth. In the mutant planktonic cells, several genes within the *paa* operon were found to be repressed significantly. The KEGG analyses also revealed that the phenylalanine metabolism, which is modulated by this operon, was downregulated (Figure 4.7). *A. baumannii* utilizes phenylacetate as a carbon and energy source through the phenylacetate catabolism pathway and produces phenylacetic acid (PAA). This finally feeds into the Krebs cycle with the help of the *paa* operon (Ren & Palmer, 2023). In the *paaA* mutant of *A. baumannii*, accumulation of PAA was observed as a metabolic by-product during infection in the zebrafish model. This increased influx of neutrophils to the infection site led to reduced persistence of the pathogen (Bhuiyan et al., 2016). In addition, the phenylacetate catabolism pathway has

been implicated in oxidative stress response and antibiotic resistance (Hooppaw et al., 2022). In line with this observation, we found that two mM hydrogen peroxide exposure was able to retard the exponential growth phase of the deletion mutant. Altogether, although further study is needed, the observations provide a clue that the sRNA00203 mutant in the planktonic state may have a lower survival rate compared to the wild-type planktonic during infection.

All the issues discussed above, sections 5.3 and 5.4, are summarized by the proposed regulation model illustrated in Figure 5.1.

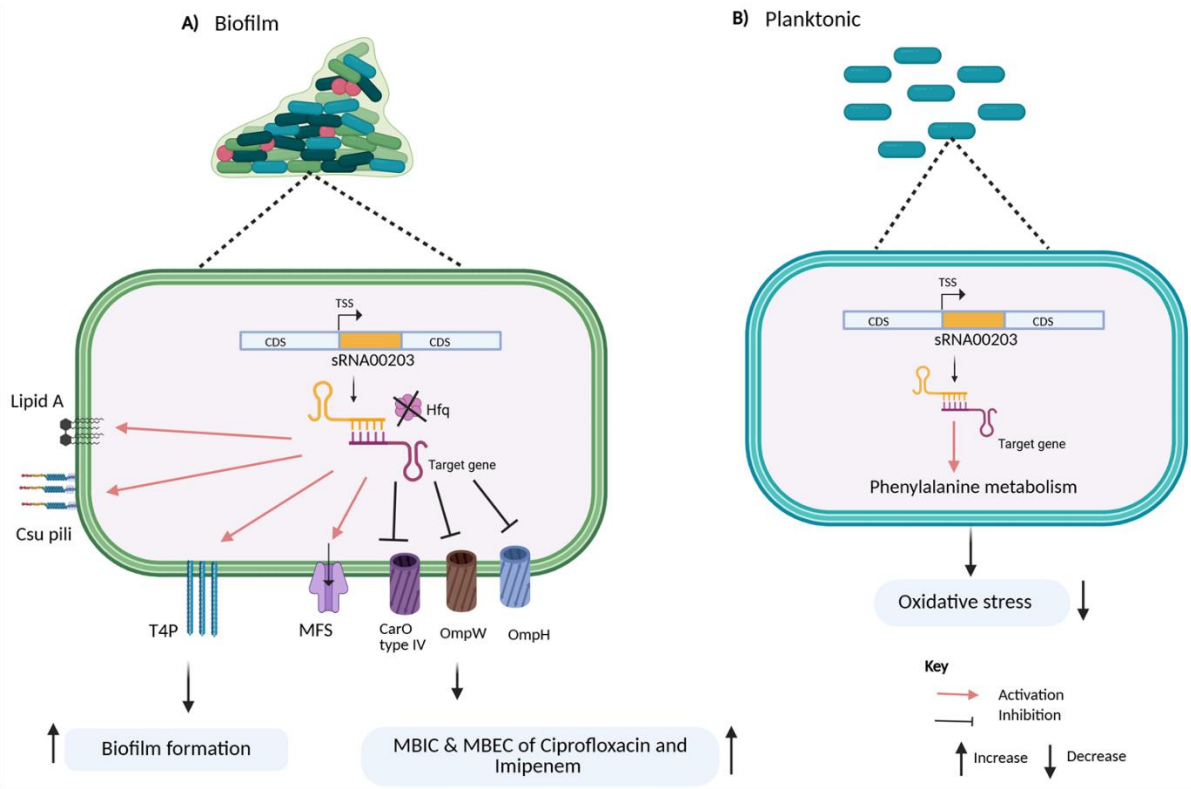

Figure 5.1 Proposed regulatory mechanism of sRNA00203 in *A. baumannii* ST1894.
(A) In the biofilm condition, transcription of sRNA00203 modulates the expression of multiple target genes, including those encoding major facilitator superfamily (MFS) transporters, porins (CarO type IV, OmpW, and OmpH), Lpx components of lipid A, and Csu pili. The regulation is potentially through Hfq-independent pathways. In turn, it promotes biofilm formation and increases antimicrobial resistance (elevated MBIC and MBEC values). (B) In the planktonic cells, expression of sRNA00203 mainly regulates genes involved in phenylalanine metabolism, leading to altered oxidative stress responses. T4P: type IV pili;

MBIC: minimum biofilm inhibitory concentration; MBEC: minimum biofilm eradication concentration; TSS: transcription start site; CDS: coding sequence.

5.2 Reconfirmation of the impact of sRNA00203 on biofilm formation

Combining the assessment of deletion mutants and overexpression strains with their respective controls enables a precise exploration of the function of sRNA in bacterial systems (Banerjee, 2025; Tong et al., 2023). Since the promoter region of sRNA00203 has not been experimentally validated, we utilized a constitutive plasmid promoter for the gain-of-function study. This choice was made because biofilm formation is a dynamic, continuous process rather than a single event, and we currently lack evidence regarding the timing of sRNA00203 expression during biofilm development. The overexpression resulted in more than a 350-fold change in the relative expression of the sRNA mRNA, a level that seems exceptionally high. For context, a previous overexpression study of coding gene in *A. baumannii* reported that, even when using a native promoter, relative mRNA levels were reached up to 311.5-fold in the ATCC 19606 strain and up to 619-fold in both the XAb50 and XAb53 strains, compared to the empty plasmid control (Yang et al., 2022).

The impact of sRNA00203 overexpression on biofilm formation was less pronounced than that of sRNA00203 deletion. Deletion of the sRNA resulted in a severe reduction (85%) of biofilm formation in the mutant (Shenkutie et al., 2023). Reversely, ectopic expression of sRNA00203 led to a modest increase in biofilm. The lower impact observed upon overexpression may be attributable to the naturally high concentration of sRNA00203 present in biofilm cells. Therefore, a further increase in sRNA expression did not produce a substantial change. On the other hand, the severe impairment of biofilm formation following the sRNA deletion could be explained by its activating role on several biofilm-related genes, as demonstrated by our combined omics analysis. For instance, *leuC* expression was 12.4-fold less in the mutant, whereas in the overexpressing strain, it was 7.8-fold higher. Unlike our findings, sRNAs play an inhibitory role, and their overexpression resulted in more phenotypic change than deletion (Coleman et al., 2020; Eyraud et al., 2014).

5.3 Primary targets of sRNA00203 in biofilm cells

A number of experimental and bioinformatics approaches have been used to map base-pairing targets of sRNA in bacteria. The prediction tools are efficient but frequently constrained by high false positive results (Tjaden, 2023). Although experimental methods are laborious, they can identify a high proportion of true sRNA targets. These methods can be Hfq-dependent approaches, such as RIL-seq (Melamed et al., 2016), and Hfq-independent methods, like GRIL-seq and MAPS (Han et al., 2016; Lalaouna et al., 2015). Given the lack of evidence for Hfq chaperone protein involvement in sRNA-mRNA interaction in *A. baumannii* in vivo (Hamrock et al., 2024) and the additional computational complexity of analyzing chimeric data from GRIL-seq, we chose to implement a modified MAPS method to map sRNA00203 primary targets at the genome scale of biofilm cells.

We replaced the MS2 aptamer used in the original MAPS method, which was fused to the sRNA, with a 24-nucleotide-long tag to minimize secondary structure deformation in sRNA00203 and to reduce sequence similarity of the MS2 aptamer within the genome of our strain. These modifications support capturing reliable targets through preserving the sRNA's native folding and binding capabilities. Additionally, to efficiently capture the low-abundance sRNA-mRNA complexes, we increased the expression level of the tagged sRNA fusion construct by using a high-copy plasmid promoter. Other changes, including those related to the binding and washing buffers, are also described in detail in Section 3.11.

The sRNA-mRNA complexes were captured using antisense tag riboprobe from tagged sRNA00203 expressing biofilm cell lysate, followed by RNA-seq. The sequencing identified 155 genes as candidate primary targets of the sRNA00203. Additional non-specific interactions were also enriched, indicating the method needs further blocking of these interactions. Longer duration of blocking may result in a very low amount of captured RNA, which will not be eligible for the standard RNA-seq workflow. It may demand a library preparation kit that requires very low input RNA. Although our modified method had this limitation, approximately 75% of the 155 targets were among the influenced genes, as demonstrated by the combined omics studies of the deletion mutant biofilm cells. Cell wall-related genes such as *lpxO* and E5A72_RS15655 (lipopolysaccharide assembly protein LapA encoding gene) were detected as new targets. Further, preliminary validation of three of the

targets by EMSA assay confirmed that our tag-based interactome capture approach successfully identified sRNA00203-mRNA interactions.

The genes involved in the synthesis of Lpx enzymes, such as UDP-3-O-acylglucosamine N-acyltransferase (*lpxD*) and Lipid-A-disaccharide synthase (*lpxB*), were positively influenced at the translation level by the sRNA00203; however, they were not enriched in the capture assay. Other related gene, *lpxO*, which encodes a dioxygenase involved in lipid A modification and considered a virulence factor (Bartholomew et al., 2019), was detected as a primary target. Upregulation of genes encoding Lpx enzymes was reported to be associated with biofilm formation through their possible contribution to the biofilm matrix synthesis (Shenkutie et al., 2022). The detection of *lpxO* in the capture assay, followed by EMSA confirmation of sRNA00203 binding at nucleotide positions 849–887, provides evidence of a direct regulatory interaction (Figure 4.30 C and D). The direction of regulation was likely positive, as transcriptomic data revealed a significant 1.5-fold downregulation in the mutant biofilm cells, even though the fold change did not pass the cut-off value. The observed binding around the 3' region suggests that sRNA00203 may stabilize *lpxO* mRNA. To confidently declare the proposed interplay, a rifampicin transcription inhibition assay is needed.

Similar to *lpxO*, the preprotein translocase subunit SecE encoding gene was found to be biofilm-associated, with its expression significantly elevated in biofilm cells compared to planktonic cells (Table 4.7). This aligns with the observed biofilm impairment in the sRNA00203 deletion mutant. The *SecE* encoding protein is a component of the Sec translocase complex, which facilitates the translocation of proteins across the cytoplasmic membrane in bacteria (Crane & Randall, 2017). In *A. baumannii*, the specific role of the Sec pathway remains underexplored. A study in other bacteria demonstrates its importance in exporting proteins necessary for adherence and biofilm formation (Huang et al., 2008). Hereby, we demonstrate that sRNA00203 positively regulates *SecE* at the translational level by specifically binding to nucleotides 40–100, as confirmed by EMSA data. The direct interaction may lead to stabilizing *secE* mRNA or enhance its translation, potentially by relieving the secondary structure on the upstream region. This kind of underlying mechanism has been observed in other positive regulation by sRNAs like DsrA in *E. coli* (McCullen et al., 2010) and phrS in *P. aeruginosa* (Sonnleitner et al., 2011).

The third in vitro confirmed primary target was class I SAM-dependent methyltransferase (E5A72_RS16120). This indicates that sRNA00203 may be involved in the regulation of epigenetic control. Among the various mechanisms of epigenetic regulation, DNA methylation has been implicated in promoting persister cell formation in *A. baumannii* through the activity of the DNA adenine methyltransferase (Dam) enzyme (H. Kim et al., 2022). Persisters are reported to be subpopulations of biofilm cells that contribute to the antimicrobial tolerance conferred by biofilms in *E. coli* (Keren et al., 2004). By implication, the sRNA could facilitate this phenomenon in *A. baumannii* biofilm through DNA methylation.

5.4 Potential sRNA00203 binding proteins

Our transcriptomics, proteomics, and tag-based primary target investigation revealed that sRNA00203 significantly influences a diverse array of genes in *A. baumannii* biofilm cells. To explore the question of how the sRNA had such a broad impact, we hypothesized that sRNA00203 might require protein partners, such as chaperone proteins or other proteins. RNA-binding proteins (RBPs) are fundamental to nearly all cellular processes. They orchestrate the fate of most of the RNA molecules in a bacterial cell (Holmqvist & Vogel, 2018). Therefore, to identify the candidate sRNA00203 binding proteins, we used RNA-Protein pull-down followed by mass spectrometry. We found that small and large ribosomal subunit proteins, elongation factors, RNA polymerase subunit, TCA cycle-related, and other metabolism enzyme-related proteins were overrepresented. These known RNA-binding proteins and metabolism-related proteins were also identified in other bacteria through different approaches (Stenum et al., 2023; Zhu et al., 2024). This implies the reliability of our method for the intended purpose. Identification of the metabolism proteins indicated their participation as RBPs in diverse bacteria, beyond their primary roles.

In many bacterial pathogens, RNA chaperones mediate sRNA-dependent regulation of virulence gene expression (Djapgne & Oglesby, 2021). The chaperones, like host factor Q (Hfq) and FinO family member ProQ, facilitate RNA-RNA interactions and stabilize sRNA-mRNA complexes (Quendera et al., 2020). In *A. baumannii*, deletion of Hfq caused reduced biofilm formation and virulence, but its role as a chaperone protein has not been confirmed. Only its recombinant form in vitro binding with sRNA, AbsR25, has been reported (A. Sharma et al., 2018). In the present study, Hfq was not among the significantly associated

proteins with sRNA00203. Other RNA-binding proteins that may play analogous roles in the pathogen were enriched. Chaperone protein DnaK and UPF0234 protein were among the top overrepresented proteins.

DnaK, the molecular chaperone protein, has a core function to fold nascent proteins and refold aggregated proteins during stressful conditions (Mayer & Bukau, 2005). In our study, the DnaK protein was detected as sRNA00203-associated protein from biofilm cell lysate. This finding could be interpreted in two ways. First, considering its contribution to curli-mediated biofilm formation (Sugimoto et al., 2018), the protein could be sequestered by the sRNA as a target for biofilm development. Second, although no studies have reported DnaK to bind with sRNA and mediate its regulation, we speculate that it could bind sRNA00203 to modulate several biofilm-related genes influenced by the sRNA. In support of this hypothesis, structurally, DnaK has a nucleotide-binding domain at the N-terminal side (Mayer & Bukau, 2005). Additionally, DnaK was reported as a putative RBP in *E. coli* (Stenum et al., 2023). The other protein significantly bound to the sRNA00203 was UPF0234. Similar to DnaK, ontologically, it is a nucleotide-binding protein, and YajQ, a member of the UPF0234 protein family, was also found to be an RBP in *E. coli* (Stenum et al., 2023). The orthologous YajQ protein was recognized as a receptor of cyclic di-GMP, which is an essential secondary messenger in the development of biofilm and also contributed to virulence (An et al., 2014). Altogether, we infer that both DnaK and UPF0234 protein could mediate biofilm formation in association with sRNA00203 in *A. baumannii*, but this warrants further functional and binding verification.

6. Conclusions and future directions

Most of the *A. baumannii* clinical isolates are biofilm formers. The ability to form biofilm is one of the main factors that enable the pathogen to be endemic in the health care institutions and to resist a broad range of antimicrobials (Gedefie et al., 2023). Since biofilm formation is a process under critical regulation, insights gained from studying this regulatory hub could be leveraged to control the burden associated with biofilms. Regulatory sRNAs are reported to significantly impact biofilm in *A. baumannii*. However, the comprehensive regulatory circuits of the sRNAs remained unexplored. Thus, the current study aimed to bridge this gap through multiomics, modified MAPS, and RNA-Protein pull-down investigations. The previously sRNA00203-deleted strain, the sRNA00203 overexpressing strain, and tagged sRNA00203 expressing strains constructed in the present study, and the wild-type *A. baumannii* ST1894 strain were used for the investigations.

The current study confirms that overexpression of sRNA00203 is a positive modulator of biofilm formation, but the impact on biofilm compared to the deletion of sRNA00203 was substantially lower. It was a 20.7% biofilm mass increase upon overexpression and an 85% reduction following deletion. Therefore, to fully unleash the regulatory influences of the sRNA, we performed comparative transcriptome and proteome analysis of the deletion mutant and wild-type *A. baumannii* ST1894. Accordingly, 20.4% of genes and 16.3 % of proteins of the genome were modulated by the sRNA at the biofilm state. Proteins that encode the AdeK efflux pump and OMPs were negatively regulated. In contrast, proteins that code ribosomal proteins, type IV pili, csu pili, iron acquisition system, Lpx components, sec pathway-related, and MFS were positively regulated. These proteins are essential for biofilm formation, which aligns with the reduction observed in biofilm and biofilm-related antimicrobial resistance in the sRNA-deleted strain.

In the sRNA overexpressing *A. baumannii* ST1894 strain, the biofilm-associated genes such as class I SAM-dependent methyltransferase (E5A72_RS16120), 3-isopropylmalate dehydratase large subunit (*leuC*), MFS transporter (E5A72_RS06620), 50S ribosomal protein L16 (*rplP*), Novel00134, and sRNA00056 showed significantly higher expression. The expression impact was similar to that observed in the sRNA-deleted strain, but with a lower degree of impact, indicating an activating role of the sRNA.

Of the genes and proteins influenced, 116 were identified as putative primary targets of sRNA00203 by the tag-based capture. The sRNA has predicted binding sites on the 5' untranslated region (UTR) or within the coding region of the targets. Three genes from different functional categories, namely preprotein translocase subunit SecE, lipid A hydroxylase LpxO, and class I SAM-dependent methyltransferase, were further confirmed to bind at the predicted region by EMSA. The finding highlights that the majority of the genes influenced by sRNA could be modulated through other mechanisms. One of these mechanisms could involve proteins, such as the UPF0234 protein and the chaperone protein DnaK, rather than the major chaperone protein Hfq.

Overall, our data further support the idea that sRNA00203 harbours characteristics of regulating diverse biological processes, including biofilm formation and biofilm-specific antibiotic resistance, and suggest that it could also contribute to virulence in *A. baumannii*. In turn, targeting the sRNA or the systems influenced by it will contribute to minimizing the *A. baumannii* biofilm-related burden occurring in healthcare.

This study had some limitations. A few of which are addressed in the discussion section; here, I will explain the remaining ones. First, for the overexpression study, we used the plasmid promoter. Although we were able to generate valuable data, the use of its native promoter may be better to recapitulate the physiological regulation of sRNA00203. Second, the study was limited to a single strain. Indeed, we confirmed the presence of the sRNA in various clinical strains collected from different anatomical sites through Oxford Nanopore sequencing followed by gel detection.

Therefore, to extrapolate the influences of sRNA00203 to *A. baumannii* strains, it will be necessary to investigate multiple strains with diverse genetic backgrounds in future research. Future studies should also focus on experimental verification of additional primary targets from the identified putative primary targets. This is recommended to solidify the evidence for the regulatory mechanism of sRNA00203 and to generate data that could also strengthen evidence about tag-based interactome capture, which could serve as an alternative, valuable tool. Additionally, EMSA is needed to confirm the binding of the chaperone protein DnaK and the UPF0234 protein with the sRNA. Furthermore, a functional investigation of these proteins in *A. baumannii* could yield new insights regarding the interplay between the sRNA and its associated proteins.

7. References

Abdi, S. N., Ghotaslou, R., Ganbarov, K., Mobed, A., Tanomand, A., Yousefi, M., Asgharzadeh, M., & Kafil, H. S. (2020). *Acinetobacter baumannii* Efflux Pumps and Antibiotic Resistance. *Infection and Drug Resistance*, *13*, 423. https://doi.org/10.2147/IDR.S228089

Ahmad, I., Nadeem, A., Mushtaq, F., Zlatkov, N., Shahzad, M., Zavialov, A. V., Wai, S. N., & Uhlin, B. E. (2023). Csu pili dependent biofilm formation and virulence of *Acinetobacter baumannii*. *Npj Biofilms and Microbiomes*, *9*(1). https://doi.org/10.1038/s41522-023-00465-6

Alkasir, R., Ma, Y., Liu, F., Li, J., Lv, N., Xue, Y., Hu, Y., & Zhu, B. (2018). Characterization and transcriptome analysis of *Acinetobacter baumannii* persister cells. *Microbial Drug Resistance*, *24*(10), 1466–1474. https://doi.org/10.1089/mdr.2017.0341

Álvarez-Fraga, L., Rumbo-Feal, S., Pérez, A., Gómez, M. J., Gayoso, C., Vallejo, J. A., Ohneck, E. J., Valle, J., Actis, L. A., Beceiro, A., Bou, G., & Poza, M. (2017). Global assessment of small RNAs reveals a non-coding transcript involved in biofilm formation and attachment in *Acinetobacter baumannii* ATCC 17978. *PLoS ONE*, *12*(8), e0182084. https://doi.org/10.1371/journal.pone.0182084

Amaral, L., Martins, A., Spengler, G., & Molnar, J. (2014). Efflux pumps of Gram-negative bacteria: What they do, how they do it, with what and how to deal with them. In *Frontiers in Pharmacology: Vol. 4 JAN* (p. 168). Frontiers Research Foundation. https://doi.org/10.3389/fphar.2013.00168

An, S. qi, Caly, D. L., McCarthy, Y., Murdoch, S. L., Ward, J., Febrer, M., Dow, J. M., & Ryan, R. P. (2014). Novel Cyclic di-GMP Effectors of the YajQ Protein Family Control Bacterial Virulence. *PLoS Pathogens*, *10*(10). https://doi.org/10.1371/journal.ppat.1004429

Anderson, S. E., Chin, C. Y., Weiss, D. S., & Rather, P. N. (2020). Copy number of an integron-encoded antibiotic resistance locus regulates a virulence and opacity switch in *Acinetobacter baumannii* AB5075. *MBio*, *11*(5), 1–19. https://doi.org/10.1128/mBio.02338-20

Antunes, L. C. S., Visca, P., & Towner, K. J. (2014). *Acinetobacter baumannii*: Evolution of a

global pathogen. In *Pathogens and Disease* (Vol. 71, Issue 3, pp. 292–301). https://doi.org/10.1111/2049-632X.12125

Ardebili, A., Lari, A. R., Beheshti, M., & Lari, E. R. (2015). Association between mutations in gyrA and parC genes of *Acinetobacter baumannii* clinical isolates and ciprofloxacin resistance. *Iranian Journal of Basic Medical Sciences*, *18*(6), 623–626.

Arroyo, L. A., Herrera, C. M., Fernandez, L., Hankins, J. V., Trent, M. S., & Hancock, R. E. W. (2011). The pmrCAB operon mediates polymyxin resistance in *Acinetobacter baumannii* ATCC 17978 and clinical isolates through phosphoethanolamine modification of lipid A. *Antimicrobial Agents and Chemotherapy*, *55*(8), 3743–3751. https://doi.org/10.1128/AAC.00256-11

Aseev, L. V., Koledinskaya, L. S., & Boni, I. V. (2024). Extraribosomal Functions of Bacterial Ribosomal Proteins—An Update, 2023. *International Journal of Molecular Sciences*, *25*(5). https://doi.org/10.3390/ijms25052957

Bagge, N., Hentzer, M., Andersen, J. B., Ciofu, O., Givskov, M., & Høiby, N. (2004). Dynamics and Spatial Distribution of β-Lactamase Expression in Pseudomonas aeruginosa Biofilms. *Antimicrobial Agents and Chemotherapy*, *48*(4), 1168–1174. https://doi.org/10.1128/AAC.48.4.1168-1174.2004

Banerjee, R. (2025). Tiny but Mighty: Small RNAs—The Micromanagers of Bacterial Survival, Virulence, and Host–Pathogen Interactions. *Non-Coding RNA*, *11*(3), 36. https://doi.org/10.3390/ncrna11030036

Bao, J., Xie, L., Ma, Y., An, R., Gu, B., & Wang, C. (2022). Proteomic and Transcriptomic Analyses Indicate Reduced Biofilm-Forming Abilities in Cefiderocol-Resistant *Klebsiella pneumoniae*. *Frontiers in Microbiology*, *12*(January), 1–15. https://doi.org/10.3389/fmicb.2021.778190

Barraud, N., Kjelleberg, S., & Rice, S. A. (2015). Dispersal from Microbial Bio fi lms. *Microbiol Spectrum*, *3*(6), MB-0015-2014. https://doi.org/10.1128/microbiolspec.MB-0015-2014.Correspondence

Bartholomew, T. L., Kidd, T. J., Pessoa, J. S., Álvarez, R. C., & Bengoechea, J. A. (2019). 2-Hydroxylation of *Acinetobacter baumannii* Lipid a Contributes To Virulence. *Infection*

and Immunity, *87*(4), 1–17. https://doi.org/10.1128/IAI.00066-19

Beceiro, A., Llobet, E., Aranda, J., Bengoechea, J. A., Doumith, M., Hornsey, M., Dhanji, H., Chart, H., Bou, G., Livermore, D. M., & Woodford, N. (2011). Phosphoethanolamine modification of lipid A in colistin-resistant variants of *Acinetobacter baumannii* mediated by the pmrAB two-component regulatory system. *Antimicrobial Agents and Chemotherapy*, *55*(7), 3370–3379. https://doi.org/10.1128/AAC.00079-11

Beisel, C. L., & Storz, G. (2010). Base pairing small RNAs and their roles in global regulatory networks. In *FEMS Microbiology Reviews* (Vol. 34, Issue 5, pp. 866–882). Oxford Academic. https://doi.org/10.1111/j.1574-6976.2010.00241.x

Bhuiyan, M. S., Ellett, F., Murray, G. L., Kostoulias, X., Cerqueira, G. M., Schulze, K. E., Maifiah, M. H. M., Li, J., Creek, D. J., Lieschke, G. J., & Peleg, A. Y. (2016). *Acinetobacter baumannii* phenylacetic acid metabolism influences infection outcome through a direct effect on neutrophil chemotaxis. *Proceedings of the National Academy of Sciences of the United States of America*, *113*(34), 9599–9604. https://doi.org/10.1073/pnas.1523116113

Bianco, A., Quirino, A., Giordano, M., Marano, V., Rizzo, C., Liberto, M. C., Focà, A., & Pavia, M. (2016). Control of carbapenem-resistant *Acinetobacter baumannii* outbreak in an intensive care unit of a teaching hospital in Southern Italy. *BMC Infectious Diseases*, *16*(1), 1–7. https://doi.org/10.1186/s12879-016-2036-7

Bjånes, E., Koh, T., Qayum, T., Zurich, R., Mccabe, S., Hampel, K., Cartwright, L., & Nizet, V. (2024). *Exploring Roles of the Polysaccharide Capsule in Pathogenesis of Hypervirulent Acinetobacter baumannii Clinical Isolate Lac-4*.

Cafiso, V., Stracquadanio, S., Lo Verde, F., Dovere, V., Zega, A., Pigola, G., Aranda, J., & Stefani, S. (2020). COLR *Acinetobacter baumannii* sRNA Signatures: Computational Comparative Identification and Biological Targets. *Frontiers in Microbiology*, *10*, 3075. https://doi.org/10.3389/fmicb.2019.03075

Cao, B., Christophersen, L., Kolpen, M., Jensen, P. Ø., Sneppen, K., Høiby, N., Moser, C., & Sams, T. (2016). Diffusion retardation by binding of tobramycin in an alginate biofilm model. *PLoS ONE*, *11*(4), 1–11. https://doi.org/10.1371/journal.pone.0153616

Cao, B., Christophersen, L., Thomsen, K., Sønderholm, M., Bjarnsholt, T., Jensen, P. Ø., Høiby, N., & Moser, C. (2015). Antibiotic penetration and bacterial killing in a Pseudomonas aeruginosa biofilm model. *Journal of Antimicrobial Chemotherapy*, *70*(7), 2057–2063. https://doi.org/10.1093/jac/dkv058

Carrier, M. C., Lalaouna, D., & Massé, E. (2018). Broadening the Definition of Bacterial Small RNAs: Characteristics and Mechanisms of Action. In *Annual Review of Microbiology* (Vol. 72, pp. 141–161). Annual Reviews. https://doi.org/10.1146/annurev-micro-090817-062607

Casadevall, A., & Pirofski, L. A. (2009). Virulence factors and their mechanisms of action: The view from a damage-response framework. *Journal of Water and Health*, *7*(SUPPL. 1), 2–18. https://doi.org/10.2166/wh.2009.036

Casella, L. G., Torres, N. J., Tomlinson, B. R., Shepherd, M., & Shaw, L. N. (2023). The novel two-component system AmsSR governs alternative metabolic pathway usage in *Acinetobacter baumannii*. *Frontiers in Microbiology*, *14*(April), 1–17. https://doi.org/10.3389/fmicb.2023.1139253

Casella, L. G., Weiss, A., Pérez-Rueda, E., Antonio Ibarra, J., & Shaw, L. N. (2017). Towards the complete proteinaceous regulome of *Acinetobacter baumannii*. *Microbial Genomics*, *3*(3). https://doi.org/10.1099/mgen.0.000107

Cayô, R., Rodríguez, M. C., Espinal, P., Fernández-Cuenca, F., Ocampo-Sosa, A. A., Pascual, Á., Ayala, J. A., Vila, J., & Martínez-Martínez, L. (2011). Analysis of genes encoding penicillin-binding proteins in clinical isolates of *Acinetobacter baumannii*. *Antimicrobial Agents and Chemotherapy*, *55*(12), 5907–5913. https://doi.org/10.1128/AAC.00459-11

Cerqueira, G. M., Kostoulias, X., Khoo, C., Aibinu, I., Qu, Y., Traven, A., & Peleg, A. Y. (2014). A global virulence regulator in *Acinetobacter baumannii* and its control of the phenylacetic acid catabolic pathway. *Journal of Infectious Diseases*, *210*(1), 46–55. https://doi.org/10.1093/infdis/jiu024

Chambers, J. R., & Sauer, K. (2013). Small RNAs and their role in biofilm formation. In *Trends in Microbiology* (Vol. 21, Issue 1, pp. 39–49). https://doi.org/10.1016/j.tim.2012.10.008

Chapartegui-González, I., Lázaro-Díez, M., Bravo, Z., Navas, J., Icardo, J. M., & Ramos-Vivas,

J. (2018). *Acinetobacter baumannii* maintains its virulence after long-time starvation. *PLoS ONE*, *13*(8), 1–14. https://doi.org/10.1371/journal.pone.0201961

Charretier, Y., Diene, S. M., Baud, D., Chatellier, S., Santiago-Allexant, E., Van Belkum, A., Guigon, G., & Schrenzel, J. (2018). Colistin heteroresistance and involvement of the PmrAB regulatory system in *Acinetobacter baumannii*. *Antimicrobial Agents and Chemotherapy*, *62*(9). https://doi.org/10.1128/AAC.00788-18

Chen, W. (2020). Host Innate Immune Responses to *Acinetobacter baumannii* Infection. *Frontiers in Cellular and Infection Microbiology*, *10*(September), 1–16. https://doi.org/10.3389/fcimb.2020.00486

Chin, C. Y., Tipton, K. A., Farokhyfar, M., Burd, E. M., Weiss, D. S., & Rather, P. N. (2018). A high-frequency phenotypic switch links bacterial virulence and environmental survival in *Acinetobacter baumannii*. *Nature Microbiology*, *3*(5), 563–569. https://doi.org/10.1038/s41564-018-0151-5

Choi, C. H., Lee, E. Y., Lee, Y. C., Park, T. I., Kim, H. J., Hyun, S. H., Kim, S. A., Lee, S. K., & Lee, J. C. (2005). Outer membrane protein 38 of *Acinetobacter baumannii* localizes to the mitochondria and induces apoptosis of epithelial cells. *Cellular Microbiology*, *7*(8), 1127–1138. https://doi.org/10.1111/j.1462-5822.2005.00538.x

Chukamnerd, A., Saipetch, N., Singkhamanan, K., Ingviya, N., Assanangkornchai, N., Surachat, K., & Chusri, S. (2024). Association of biofilm formation, antimicrobial resistance, clinical characteristics, and clinical outcomes among *Acinetobacter baumannii* isolates from patients with ventilator-associated pneumonia. *Clinical Respiratory Journal*, *18*(1), 1–10. https://doi.org/10.1111/crj.13732

Ciofu, O., Moser, C., Jensen, P. Ø., & Høiby, N. (2022). Tolerance and resistance of microbial biofilms. *Nature Reviews Microbiology*, *20*(10), 621–635. https://doi.org/10.1038/s41579-022-00682-4

Coleman, S. R., Smith, M. L., Spicer, V., Lao, Y., Mookherjee, N., & Hancock, R. E. W. (2020). Overexpression of the Small RNA PA0805.1 in Pseudomonas aeruginosa Modulates the Expression of a Large Set of Genes and Proteins, Resulting in Altered Motility, Cytotoxicity, and Tobramycin Resistance. *MSystems*, *5*(3).

https://doi.org/10.1128/MSYSTEMS.00204-20/SUPPL_FILE/MSYSTEMS.00204-20-ST005.DOCX

Conde-Pérez, K., Vázquez-Ucha, J. C., Álvarez-Fraga, L., Ageitos, L., Rumbo-Feal, S., Martínez-Guitián, M., Trigo-Tasende, N., Rodríguez, J., Bou, G., Jiménez, C., Beceiro, A., & Poza, M. (2021). In-Depth Analysis of the Role of the Acinetobactin Cluster in the Virulence of *Acinetobacter baumannii*. *Frontiers in Microbiology*, *12*(October). https://doi.org/10.3389/fmicb.2021.752070

Cook-Libin, S., Sykes, E. M. E. E., Kornelsen, V., & Kumar, A. (2022). Iron Acquisition Mechanisms and Their Role in the Virulence of *Acinetobacter baumannii*. *Infection and Immunity*, *90*(10). https://doi.org/10.1128/iai.00223-22

Coyne, S., Rosenfeld, N., Lambert, T., Courvalin, P., & Périchon, B. (2010). Overexpression of resistance-nodulation-cell division pump AdeFGH confers multidrug resistance in *Acinetobacter baumannii*. *Antimicrobial Agents and Chemotherapy*, *54*(10), 4389–4393. https://doi.org/10.1128/AAC.00155-10

Crane, J. M., & Randall, L. L. (2017). The Sec System: Protein Export in *Escherichia coli* . *EcoSal Plus*, *7*(2). https://doi.org/10.1128/ecosalplus.esp-0002-2017

Cress, B. F., Englaender, J. A., He, W., Kasper, D., Linhardt, R. J., & Koffas, M. A. G. (2014). Masquerading microbial pathogens: Capsular polysaccharides mimic host-tissue molecules. *FEMS Microbiology Reviews*, *38*(4), 660–697. https://doi.org/10.1111/1574-6976.12056

Damier-Piolle, L., Magnet, S., Brémont, S., Lambert, T., & Courvalin, P. (2008). AdeIJK, a resistance-nodulation-cell division pump effluxing multiple antibiotics in *Acinetobacter baumannii*. *Antimicrobial Agents and Chemotherapy*, *52*(2), 557–562. https://doi.org/10.1128/AAC.00732-07

Daniel, C., Haentjens, S., Bissinger, M. C., & Courcol, R. J. (1999). Characterization of the *Acinetobacter baumannii* Fur regulator: Cloning and sequencing of the fur homolog gene. *FEMS Microbiology Letters*, *170*(1), 199–209. https://doi.org/10.1016/S0378-1097(98)00533-3

Davies, D. (2003). Understanding biofilm resistance to antibacterial agents. *Nature Reviews*

Drug Discovery, *2*(2), 114–122. https://doi.org/10.1038/nrd1008

Del Pozo, J. L. (2018). Biofilm-related disease. *Expert Review of Anti-Infective Therapy*, *16*(1), 51–65. https://doi.org/10.1080/14787210.2018.1417036

Dexter, C., Murray, G. L., Paulsen, I. T., & Peleg, A. Y. (2015). Community-acquired *Acinetobacter baumannii*: Clinical characteristics, epidemiology and pathogenesis. *Expert Review of Anti-Infective Therapy*, *13*(5), 567–573. https://doi.org/10.1586/14787210.2015.1025055

Djapgne, L., & Oglesby, A. G. (2021). Impacts of Small RNAs and Their Chaperones on Bacterial Pathogenicity. *Frontiers in Cellular and Infection Microbiology*, *11*(July), 1–12. https://doi.org/10.3389/fcimb.2021.604511

Djeribi, R., Bouchloukh, W., Jouenne, T., & Menaa, B. (2012). Characterization of bacterial biofilms formed on urinary catheters. *American Journal of Infection Control*, *40*(9), 854–859. https://doi.org/10.1016/j.ajic.2011.10.009

Doi, Y., Wachino, J. ichi, & Arakawa, Y. (2016). Aminoglycoside Resistance: The Emergence of Acquired 16S Ribosomal RNA Methyltransferases. *Infectious Disease Clinics of North America*, *30*(2), 523–537. https://doi.org/10.1016/j.idc.2016.02.011

Donlan, R. M., & Costerton, J. W. (2002). Biofilms: Survival mechanisms of clinically relevant microorganisms. *Clinical Microbiology Reviews*, *15*(2), 167–193. https://doi.org/10.1128/CMR.15.2.167-193.2002

Dutcher, H. A., & Raghavan, R. (2018). Origin, Evolution, and Loss of Bacterial Small RNAs. *Microbiology Spectrum*, *6*(2). https://doi.org/10.1128/microbiolspec.rwr-0004-2017

Dutta, T., & Srivastava, S. (2018). Small RNA-mediated regulation in bacteria: A growing palette of diverse mechanisms. *Gene*, *656*, 60–72. https://doi.org/10.1016/j.gene.2018.02.068

Eyraud, A., Tattevin, P., Chabelskaya, S., & Felden, B. (2014). A small RNA controls a protein regulator involved in antibiotic resistance in Staphylococcus aureus. *Nucleic Acids Research*, *42*(8), 4892–4905. https://doi.org/10.1093/nar/gku149

Eze, E. C., Chenia, H. Y., & El Zowalaty, M. E. (2018). *Acinetobacter baumannii* biofilms:

Effects of physicochemical factors, virulence, antibiotic resistance determinants, gene regulation, and future antimicrobial treatments. In *Infection and Drug Resistance* (Vol. 11, pp. 2277–2299). Dove Press. https://doi.org/10.2147/IDR.S169894

Farshadzadeh, Z., Taheri, B., Rahimi, S., Shoja, S., Pourhajibagher, M., Haghighi, M. A., & Bahador, A. (2018). Growth rate and biofilm formation ability of clinical and laboratory-evolved colistin-resistant strains of *Acinetobacter baumannii*. *Frontiers in Microbiology*, *9*(FEB). https://doi.org/10.3389/FMICB.2018.00153/FULL

Felden, B., & Augagneur, Y. (2021). Diversity and Versatility in Small RNA-Mediated Regulation in Bacterial Pathogens. *Frontiers in Microbiology*, *12*, 2273. https://doi.org/10.3389/FMICB.2021.719977

Feng, S. H., Stojadinovic, A., Izadjoo, M., Jackson, H. M., Program, I., & Services, U. (2013). Distinctive stages and strain variations of. *J Wound Care*, *22*(4), 173–174, 176–178, 180–181. https://doi.org/10.12968/jowc.2013.22.4.173

Fernandez-Garcia, L., Ambroa, A., Blasco, L., Bleriot, I., López, M., Alvarez-Marin, R., Fernández-Cuenca, F., Martinez-Martinez, L., Vila, J., Rodríguez-Baño, J., Garnacho-Montero, J., Cisneros, J. M., Pascual, A., Pachón, J., Bou, G., Smani, Y., & Tomás, M. (2018). Relationship between the Quorum network (sensing/quenching) and clinical features of pneumonia and bacteraemia caused by A. Baumannii. *Frontiers in Microbiology*, *9*(December), 1–11. https://doi.org/10.3389/fmicb.2018.03105

Ferreira, T. de O., Koto, R. Y., Leite, G. F. da C., Klautau, G. B., Nigro, S., Silva, C. B. da, Souza, A. P. I. da F., Mimica, M. J., Cesar, R. G., & Salles, M. J. C. (2016). Microbial investigation of biofilms recovered from endotracheal tubes using sonication in intensive care unit pediatric patients. *Brazilian Journal of Infectious Diseases*, *20*(5), 468–475. https://doi.org/10.1016/j.bjid.2016.07.003

Figueiredo, S., Poirel, L., Papa, A., Koulourida, V., & Nordmann, P. (2009). Overexpression of the naturally occurring blaOXA-51 gene in *Acinetobacter baumannii* mediated by novel insertion sequence ISAba9. *Antimicrobial Agents and Chemotherapy*, *53*(9), 4045–4047. https://doi.org/10.1128/AAC.00292-09

Flemming, H. C., Wingender, J., Szewzyk, U., Steinberg, P., Rice, S. A., & Kjelleberg, S. (2016).

Biofilms: An emergent form of bacterial life. *Nature Reviews Microbiology*, *14*(9), 563–575. https://doi.org/10.1038/nrmicro.2016.94

Foong, W. E., Wilhelm, J., Tam, H. K., & Pos, K. M. (2020). Tigecycline efflux in *Acinetobacter baumannii* is mediated by TetA in synergy with RND-type efflux transporters. *Journal of Antimicrobial Chemotherapy*, *75*(5), 1135–1139. https://doi.org/10.1093/jac/dkaa015

Gaddy, J. A., Tomaras, A. P., & Actis, L. A. (2009). The *Acinetobacter baumannii* 19606 OmpA protein plays a role in biofilm formation on abiotic surfaces and in the interaction of this pathogen with eukaryotic cells. *Infection and Immunity*, *77*(8), 3150–3160. https://doi.org/10.1128/IAI.00096-09

García-Patiño, M. G., García-Contreras, R., & Licona-Limón, P. (2017). The immune response against *Acinetobacter baumannii*, an emerging pathogen in nosocomial infections. *Frontiers in Immunology*, *8*(APR). https://doi.org/10.3389/fimmu.2017.00441

Garrett, T. R., Bhakoo, M., & Zhang, Z. (2008). Bacterial adhesion and biofilms on surfaces. *Progress in Natural Science*, *18*(9), 1049–1056. https://doi.org/10.1016/j.pnsc.2008.04.001

Gedefie, A., Alemayehu, E., Mohammed, O., Bambo, G. M., Kebede, S. S., & Kebede, B. (2023). Prevalence of biofilm producing *Acinetobacter baumannii* clinical isolates: A systematic review and meta-analysis. *PLoS ONE*, *18*(11 November), 1–16. https://doi.org/10.1371/journal.pone.0287211

Geisinger, E., Huo, W., Hernandez-Bird, J., & Isberg, R. R. (2019). *Acinetobacter baumannii*: Envelope determinants that control drug resistance, virulence, and surface variability. In *Annual Review of Microbiology* (Vol. 73, pp. 481–506). Annual Reviews. https://doi.org/10.1146/annurev-micro-020518-115714

Geisinger, E., & Isberg, R. R. (2015). Antibiotic Modulation of Capsular Exopolysaccharide and Virulence in *Acinetobacter baumannii*. *PLOS Pathogens*, *11*(2), e1004691. https://doi.org/10.1371/JOURNAL.PPAT.1004691

Girija, A. S. S., Vijayashree Priyadharsini, J., & Paramasivam, A. (2019). Plasmid-encoded resistance to trimethoprim/sulfamethoxazole mediated by dfrA1, dfrA5, sul1 and sul2 among *Acinetobacter baumannii* isolated from urine samples of patients with severe

urinary tract infection. *Journal of Global Antimicrobial Resistance*, *17*, 145–146. https://doi.org/10.1016/j.jgar.2019.04.001

Govindarajan, S., & Amster-Choder, O. (2017). The bacterial Sec system is required for the organization and function of the MreB cytoskeleton. *PLoS Genetics*, *13*(9), 1–27. https://doi.org/10.1371/journal.pgen.1007017

Grygiel, I., Bajrak, O., Wójcicki, M., Krusiec, K., Jończyk-Matysiak, E., Górski, A., Majewska, J., & Letkiewicz, S. (2024). Comprehensive Approaches to Combatting *Acinetobacter baumannii* Biofilms: From Biofilm Structure to Phage-Based Therapies. *Antibiotics*, *13*(11), 1–35. https://doi.org/10.3390/antibiotics13111064

Guilhen, C., Forestier, C., & Balestrino, D. (2017). Biofilm dispersal: multiple elaborate strategies for dissemination of bacteria with unique properties. *Molecular Microbiology*, *105*(2), 188–210. https://doi.org/10.1111/mmi.13698

Guillier, M., Gottesman, S., & Storz, G. (2006). Modulating the outer membrane with small RNAs. *Genes & Development*, *20*(17), 2338–2348. https://doi.org/10.1101/GAD.1457506

Gupta, G., Chauhan, P. S., Jha, P. N., Verma, R. K., Singh, S., Yadav, V. K., Sahoo, D. K., & Patel, A. (2024). Secretory molecules from secretion systems fine-tune the host-beneficial bacteria (PGPRs) interaction. *Frontiers in Microbiology*, *15*(February), 1–17. https://doi.org/10.3389/fmicb.2024.1355750

Haider, S., & Pal, R. (2013). Integrated Analysis of Transcriptomic and Proteomic Data. *Current Genomics*, *14*(2), 91–110. https://doi.org/10.2174/1389202911314020003

Hamrock, F. J., Ryan, D., Shaibah, A., Ershova, A. S., Mogre, A., Sulimani, M. M., Ben Taarit, S., Reichardt, S., Hokamp, K., Westermann, A. J., & Kröger, C. (2024). Global analysis of the RNA–RNA interactome in *Acinetobacter baumannii* AB5075 uncovers a small regulatory RNA repressing the virulence-related outer membrane protein CarO . *Nucleic Acids Research*, *August*, 11283–11300. https://doi.org/10.1093/nar/gkae668

Han, K., Tjaden, B., & Lory, S. (2016). GRIL-seq provides a method for identifying direct targets of bacterial small regulatory RNA by in vivo proximity ligation. *Nature Microbiology*, *2*(December). https://doi.org/10.1038/nmicrobiol.2016.239

Harding, C. M., Hennon, S. W., & Feldman, M. F. (2018). Uncovering the mechanisms of *Acinetobacter baumannii* virulence. In *Nature Reviews Microbiology* (Vol. 16, Issue 2, pp. 91–102). https://doi.org/10.1038/nrmicro.2017.148

Hausner, M., & Wuertz, S. (1999). High rates of conjugation in bacterial biofilms as determined by quantitative in situ analysis. *Applied and Environmental Microbiology*, *65*(8), 3710–3713. https://doi.org/10.1128/aem.65.8.3710-3713.1999

He, X., Lu, F., Yuan, F., Jiang, D., Zhao, P., Zhu, J., Cheng, H., Cao, J., & Lu, G. (2015). Biofilm formation caused by clinical *Acinetobacter baumannii* isolates is associated with overexpression of the AdeFGH efflux pump. *Antimicrobial Agents and Chemotherapy*, *59*(8), 4817–4825. https://doi.org/10.1128/AAC.00877-15

Holmqvist, E., & Vogel, J. (2018). RNA-binding proteins in bacteria. *Nature Reviews Microbiology*, *16*(10), 601–615. https://doi.org/10.1038/s41579-018-0049-5

Hooppaw, A. J., McGuffey, J. C., Venanzio, G. Di, Ortiz-Marquez, J. C., Weber, B. S., Lightly, T. J., van Opijnen, T., Scott, N. E., Cardona, S. T., & Feldman, M. F. (2022). The Phenylacetic Acid Catabolic Pathway Regulates Antibiotic and Oxidative Stress Responses in Acinetobacter. *MBio*, *13*(3). https://doi.org/10.1128/mbio.01863-21

Hör, J., Matera, G., Vogel, J., Gottesman, S., & Storz, G. (2020). Trans-Acting Small RNAs and Their Effects on Gene Expression in *Escherichia coli* and Salmonella enterica. *EcoSal Plus*, *9*(1). https://doi.org/10.1128/ecosalplus.esp-0030-2019

Howard, A., O'Donoghue, M., Feeney, A., & Sleator, R. D. (2012). *Acinetobacter baumannii* An emerging opportunistic pathogen. *Virulence*, *3*(3), 5. https://doi.org/10.4161/viru.19700

Hrenovic, J., Durn, G., Goic-Barisic, I., & Kovacic, A. (2014). Occurrence of an environmental *Acinetobacter baumannii* strain similar to a clinical isolate in paleosol from Croatia. *Applied and Environmental Microbiology*, *80*(9), 2860–2866. https://doi.org/10.1128/AEM.00312-14

Hu, L., Shi, Y., Xu, Q., Zhang, L., He, J., Jiang, Y., Liu, L., Leptihn, S., Yu, Y., Hua, X., & Zhou, Z. (2020). Capsule Thickness, Not Biofilm Formation, Gives Rise to Mucoid *Acinetobacter baumannii* Phenotypes That are More Prevalent in Long-Term Infections: A Study of

Clinical Isolates from a Hospital in China. *Infection and Drug Resistance*, *13*, 99. https://doi.org/10.2147/IDR.S230178

Huang, M. J., Meng, L. Y., Fan, M. W., Hu, P., & Bian, Z. (2008). Effect of biofilm formation on virulence factor secretion via the general secretory pathway in Streptococcus mutans. *Archives of Oral Biology*, *53*(12), 1179–1185. https://doi.org/10.1016/j.archoralbio.2008.07.007

Jacobs, A. C., Hood, I., Boyd, K. L., Olson, P. D., Morrison, J. M., Carson, S., Sayood, K., Iwen, P. C., Skaar, E. P., & Dunman, P. M. (2010). Inactivation of phospholipase D diminishes *Acinetobacter baumannii* pathogenesis. *Infection and Immunity*, *78*(5), 1952–1962. https://doi.org/10.1128/IAI.00889-09

Jahan, M. I., Rahaman, M. M., Hossain, M. A., & Sultana, M. (2021). Draft genome sequence of a carbapenem-resistant clinical *Acinetobacter baumannii* revealing co-existence of four classes of β-lactamases. *Journal of Global Antimicrobial Resistance*, *27*, 329–331. https://doi.org/10.1016/j.jgar.2021.11.002

Jahn, C. E., Charkowski, A. O., & Willis, D. K. (2008). Evaluation of isolation methods and RNA integrity for bacterial RNA quantitation. *Journal of Microbiological Methods*, *75*(2), 318–324. https://doi.org/10.1016/j.mimet.2008.07.004

Jamal, M., Ahmad, W., Andleeb, S., Jalil, F., Imran, M., Nawaz, M. A., Hussain, T., Ali, M., Rafiq, M., & Kamil, M. A. (2018). Bacterial biofilm and associated infections. *Journal of the Chinese Medical Association*, *81*(1), 7–11. https://doi.org/10.1016/j.jcma.2017.07.012

Jamali, H., Akrami, F., Layeghkhavidaki, H., & Bouakkaz, S. (2025). Bacterial protein secretion systems: Mechanisms, functions, and roles in virulence. *Microbial Pathogenesis*, *206*(May), 107790. https://doi.org/10.1016/j.micpath.2025.107790

Jean B. Patel, Melvin P. Weinstein, George M. Eliopoulos, Stephen G. Jenkins, Stephen G. Jenkins, J. S. L. I. (2017). *Performance Standards for Antimicrobial Susceptibility Testing*.

Jia, T., Liu, B., Mu, H., Qian, C., Wang, L., Li, L., Lu, G., Zhu, W., Guo, X., Yang, B., Huang, D., Feng, L., & Liu, B. (2021). A novel small rna promotes motility and virulence of enterohemorrhagic *Escherichia coli* o157:H7 in response to ammonium. *MBio*, *12*(2), 1–

19. https://doi.org/10.1128/mBio.03605-20

Jon Beckwith. (2013). The Sec-dependent pathway. *Res Microbiol.*, *164*(6), 497–504. https://doi.org/10.1016/j.resmic.2013.03.007.The

Jouybari, M. A., Ahanjan, M., Mirzaei, B., & Goli, H. R. (2021). Role of aminoglycoside-modifying enzymes and 16s rRNA methylase (ArmA) in resistance of *Acinetobacter baumannii* clinical isolates against aminoglycosides. *Revista Da Sociedade Brasileira de Medicina Tropical*, *54*, 1–10. https://doi.org/10.1590/0037-8682-0599-2020

Kaplan, J. B. (2010). Biofilm Dispersal: Mechanisms, Clinical Implications, and Potential Therapeutic Uses. *Journal of Dental Research*, *89*(3), 205–218. https://doi.org/10.1177/0022034509359403

Kareem, S. M., Al-Kadmy, I. M. S., Al-Kaabi, M. H., Aziz, S. N., & Ahmad, M. (2017). *Acinetobacter baumannii* virulence is enhanced by the combined presence of virulence factors genes phospholipase C (plcN) and elastase (lasB). *Microbial Pathogenesis*, *110*, 568–572. https://doi.org/10.1016/j.micpath.2017.08.001

Keren, I., Shah, D., Spoering, A., Kaldalu, N., & Lewis, K. (2004). Specialized persister cells and the mechanism of multidrug tolerance in *Escherichia coli*. *Journal of Bacteriology*, *186*(24), 8172–8180. https://doi.org/10.1128/JB.186.24.8172-8180.2004

Khaledi, M., Khatami, M., Hemmati, J., Bakhti, S., Hoseini, S. A., & Ghahramanpour, H. (2024). Role of Small Non-Coding RNA in Gram-Negative Bacteria: New Insights and Comprehensive Review of Mechanisms, Functions, and Potential Applications. *Molecular Biotechnology*, *0123456789*. https://doi.org/10.1007/s12033-024-01248-w

Kim, H., Kim, J. H., Cho, H., & Ko, K. S. (2022). Overexpression of a DNA Methyltransferase Increases Persister Cell Formation in *Acinetobacter baumannii*. *Microbiology Spectrum*, *10*(6). https://doi.org/10.1128/spectrum.02655-22

Kim, J., Lee, J. Y., Lee, H., Choi, J. Y., Kim, D. H., Wi, Y. M., Peck, K. R., & Ko, K. S. (2017). Microbiological features and clinical impact of the type VI secretion system (T6SS) in *Acinetobacter baumannii* isolates causing bacteremia. *Virulence*, *8*(7), 1378–1389. https://doi.org/10.1080/21505594.2017.1323164/SUPPL_FILE/KVIR_A_1323164_SM4980.ZIP

Ko, S. Y., Kim, N., Park, S. Y., Kim, S. Y., Shin, M., & Lee, J. C. (2023). *Acinetobacter baumannii* under Acidic Conditions Induces Colistin Resistance through PmrAB Activation and Lipid A Modification. *Antibiotics*, *12*(5). https://doi.org/10.3390/antibiotics12050813

Kröger, C., Kary, S. C., Schauer, K., & Cameron, A. D. S. (2017). Genetic regulation of virulence and antibiotic resistance in *Acinetobacter baumannii*. In *Genes* (Vol. 8, Issue 1, p. 12). Multidisciplinary Digital Publishing Institute. https://doi.org/10.3390/genes8010012

Kröger, C., MacKenzie, K. D., Alshabib, E. Y., Kirzinger, M. W. B., Suchan, D. M., Chao, T. C., Akulova, V., Miranda-CasoLuengo, A. A., Monzon, V. A., Conway, T., Sivasankaran, S. K., Hinton, J. C. D., Hokamp, K., & Cameron, A. D. S. (2018). The primary transcriptome, small RNAs and regulation of antimicrobial resistance in *Acinetobacter baumannii* ATCC 17978. *Nucleic Acids Research*, *46*(18), 9684–9698. https://doi.org/10.1093/nar/gky603

Kuo, H. Y., Chao, H. H., Liao, P. C., Hsu, L., Chang, K. C., Tung, C. H., Chen, C. H., Liou, M. L., Sharma, A., Dubey, V., Sharma, R., Devnath, K., Gupta, V. K., Akhter, J., Bhando, T., Verma, A., Ambatipudi, K., Sarkar, M., & Pathania, R. (2017). Functional characterization of *Acinetobacter baumannii* Lacking the RNA chaperone Hfq. *Frontiers in Microbiology*, *8*(OCT), 2068. https://doi.org/10.3389/fmicb.2017.02068

Kurcik-Trajkovska, B. (2009). Acinetobacter spp. - A serious enemy threatening hospitals worldwide. *Macedonian Journal of Medical Sciences*, *2*(2), 157–162. https://doi.org/10.3889/MJMS.1857-5773.2009.0043

Kyriakidis, I., Vasileiou, E., Pana, Z. D., & Tragiannidis, A. (2021). *Acinetobacter baumannii* antibiotic resistance mechanisms. In *Pathogens* (Vol. 10, Issue 3, p. 373). Multidisciplinary Digital Publishing Institute. https://doi.org/10.3390/pathogens10030373

Lade, H., Paul, D., & Kweon, J. H. (2014). N -Acyl Homoserine Lactone-Mediated Quorum Sensing with Special Reference to Use of Quorum Quenching Bacteria in Membrane Biofouling Control. *BioMed Research International*, *2014*. https://doi.org/10.1155/2014/162584

Lalaouna, D., Carrier, M. C., Semsey, S., Brouard, J. S., Wang, J., Wade, J. T., & Massé, E.

(2015). A 3’ external transcribed spacer in a tRNA transcript acts as a sponge for small RNAs to prevent transcriptional noise. *Molecular Cell*, *58*(3), 393–405. https://doi.org/10.1016/j.molcel.2015.03.013

Law, S. K. K., & Tan, H. S. (2022). The role of quorum sensing, biofilm formation, and iron acquisition as key virulence mechanisms in *Acinetobacter baumannii* and the corresponding anti-virulence strategies. *Microbiological Research*, *260*(March), 127032. https://doi.org/10.1016/j.micres.2022.127032

Lee, C. R., Lee, J. H., Park, M., Park, K. S., Bae, I. K., Kim, Y. B., Cha, C. J., Jeong, B. C., & Lee, S. H. (2017). Biology of *Acinetobacter baumannii*: Pathogenesis, antibiotic resistance mechanisms, and prospective treatment options. *Frontiers in Cellular and Infection Microbiology*, *7*(MAR), 55. https://doi.org/10.3389/fcimb.2017.00055

Lewis, K. (2001). Riddle of biofilm resistance. In *Antimicrobial Agents and Chemotherapy* (Vol. 45, Issue 4, pp. 999–1007). https://doi.org/10.1128/AAC.45.4.999-1007.2001

Li, F. J., Starrs, L., & Burgio, G. (2018). Tug of war between *Acinetobacter baumannii* and host immune responses. In *Pathogens and disease* (Vol. 76, Issue 9, p. 4). https://doi.org/10.1093/femspd/ftz004

Li, P., Zhang, S., Wang, J., Al-Shamiri, M. M., Han, B., Chen, Y., Han, S., & Han, L. (2023). Uncovering the Secretion Systems of *Acinetobacter baumannii*: Structures and Functions in Pathogenicity and Antibiotic Resistance. *Antibiotics*, *12*(2). https://doi.org/10.3390/antibiotics12020195

Limansky, A. S., Mussi, M. A., & Viale, A. M. (2002). Loss of a 29-kilodalton outer membrane protein in *Acinetobacter baumannii* is associated with imipenem resistance. *Journal of Clinical Microbiology*, *40*(12), 4776–4778. https://doi.org/10.1128/JCM.40.12.4776-4778.2002

Lin, L., Tan, B., & Pantapalangkoor, P. (2012). Inhibition of LpxC Protects Mice from Resistant *Acinetobacter baumannii* by Modulating Inflammation and Enhancing Phagocytosis. *MBio*, *3*(5), 23–29. https://doi.org/10.1128/mBio.00312-12

Lin, M.-F. (2014). Antimicrobial resistance in *Acinetobacter baumannii* : From bench to bedside . *World Journal of Clinical Cases*, *2*(12), 787.

https://doi.org/10.12998/wjcc.v2.i12.787

Lin, M. F., Lin, Y. Y., & Lan, C. Y. (2015). The role of the two-component system BaeSR in disposing chemicals through regulating transporter systems in *Acinetobacter baumannii*. *PLoS ONE*, *10*(7), 1–15. https://doi.org/10.1371/journal.pone.0132843

Lin, M. F., Lin, Y. Y., Yeh, H. W., & Lan, C. Y. (2014). Role of the BaeSR two-component system in the regulation of *Acinetobacter baumannii* adeAB genes and its correlation with tigecycline susceptibility. *BMC Microbiology*, *14*(1), 1–12. https://doi.org/10.1186/1471-2180-14-119

Lin, M. F., Tsai, P. W., Chen, J. Y., Lin, Y. Y., & Lan, C. Y. (2015). OmpA Binding Mediates the Effect of Antimicrobial Peptide LL-37 on *Acinetobacter baumannii*. *PLOS ONE*, *10*(10), e0141107. https://doi.org/10.1371/JOURNAL.PONE.0141107

Livak, K. J., & Schmittgen, T. D. (2001). Analysis of relative gene expression data using real-time quantitative PCR and the 2-ΔΔCT method. *Methods*, *25*(4), 402–408. https://doi.org/10.1006/meth.2001.1262

López-Martín, M., Dubern, J. F., Alexander, M. R., & Williams, P. (2021). Abam regulates quorum sensing, biofilm formation, and virulence in *Acinetobacter baumannii*. *Journal of Bacteriology*, *203*(8), 1–13. https://doi.org/10.1128/JB.00635-20

Lowe, M., Ehlers, M. M., Ismail, F., Peirano, G., Becker, P. J., Pitout, J. D. D., & Kock, M. M. (2018). *Acinetobacter baumannii*: Epidemiological and beta-lactamase data from two tertiary academic hospitals in Tshwane, South Africa. *Frontiers in Microbiology*, *9*(JUN), 1–9. https://doi.org/10.3389/fmicb.2018.01280

Lucidi, M., Visaggio, D., Migliaccio, A., Capecchi, G., Visca, P., Imperi, F., & Zarrilli, R. (2023). Pathogenicity and virulence of *Acinetobacter baumannii*: Factors contributing to the fitness in healthcare settings and the infected host. *Virulence*, *15*(1), 1–28. https://doi.org/10.1080/21505594.2023.2289769

Magill, S. S., Edwards, J. R., Bamberg, W., Beldavs, Z. G., Dumyati, G., Kainer, M. A., Lynfield, R., Maloney, M., Mcallister-Hollod, L., Nadle, J., Ray, S. M., Thompson, D. L., Wilson, L. E., & Fridkin, S. K. (2014). Multistate Point-Prevalence Survey of Health Care–Associated Infections. *The New England Journal of Medicine*, *37013370*(27), 1198–

1208. https://doi.org/doi:10.1056/NEJMoa1306801.

Mah, T. F. C., & O'Toole, G. A. (2001). Mechanisms of biofilm resistance to antimicrobial agents. *Trends in Microbiology*, *9*(1), 34–39. https://doi.org/10.1016/S0966-842X(00)01913-2

Mahendran, G., Jayasinghe, O. T., Thavakumaran, D., Arachchilage, G. M., & Silva, G. N. (2022). Key players in regulatory RNA realm of bacteria. In *Biochemistry and Biophysics Reports* (Vol. 30). Elsevier B.V. https://doi.org/10.1016/j.bbrep.2022.101276

Man Hwan Oh, K. H. (2020). AbaR is a LuxR type regulator essential for motility and the formation of biofilm and pellicle in *Acinetobacter baumannii*. *Genes Genomics*, *42*(11), 1339–1346.

Mayer, M. P., & Bukau, B. (2005). Hsp70 chaperones: Cellular functions and molecular mechanism. *Cellular and Molecular Life Sciences*, *62*(6), 670–684. https://doi.org/10.1007/s00018-004-4464-6

McClure, R., Balasubramanian, D., Sun, Y., Bobrovskyy, M., Sumby, P., Genco, C. A., Vanderpool, C. K., & Tjaden, B. (2013). Computational analysis of bacterial RNA-Seq data. *Nucleic Acids Research*, *41*(14), e140–e140. https://doi.org/10.1093/nar/gkt444

McCullen, C. A., Benhammou, J. N., Majdalani, N., & Gottesman, S. (2010). Mechanism of positive regulation by DsrA and RprA small noncoding RNAs: Pairing increases translation and protects rpoS mRNA from degradation. *Journal of Bacteriology*, *192*(21), 5559–5571. https://doi.org/10.1128/JB.00464-10

Mea, H. J., Yong, P. V. C., & Wong, E. H. (2021). An overview of *Acinetobacter baumannii* pathogenesis: Motility, adherence and biofilm formation. In *Microbiological Research* (Vol. 247, p. 126722). Urban & Fischer. https://doi.org/10.1016/j.micres.2021.126722

Mediati, D. G., Wu, S., Wu, W., & Tree, J. J. (2021). Networks of Resistance: Small RNA Control of Antibiotic Resistance. In *Trends in Genetics* (Vol. 37, Issue 1, pp. 35–45). Elsevier Current Trends. https://doi.org/10.1016/j.tig.2020.08.016

Melamed, S., Peer, A., Faigenbaum-Romm, R., Gatt, Y. E., Reiss, N., Bar, A., Altuvia, Y., Argaman, L., & Margalit, H. (2016). Global Mapping of Small RNA-Target Interactions in

Bacteria. *Molecular Cell*, *63*(5). https://doi.org/10.1016/J.MOLCEL.2016.07.026

Melamed, S., Zhang, A., Jarnik, M., Mills, J., Silverman, A., Zhang, H., & Storz, G. (2023). σ28-dependent small RNA regulation of flagella biosynthesis. *ELife*, *12*, 1–36. https://doi.org/10.7554/eLife.87151

Metzger, G. A., Ridenhour, B. J., France, M., Gliniewicz, K., Millstein, J., Settles, M. L., Forney, L. J., Stalder, T., & Top, E. M. (2022). Biofilms preserve the transmissibility of a multi-drug resistance plasmid. *Npj Biofilms and Microbiomes*, *8*(1), 1–10. https://doi.org/10.1038/s41522-022-00357-1

Michaelis, C., & Grohmann, E. (2023). Horizontal Gene Transfer of Antibiotic Resistance Genes in Biofilms. *Antibiotics*, *12*(2). https://doi.org/10.3390/antibiotics12020328

Miller, B. K., Zulauf, K. E., & Braunstein, M. (2017). The sec pathways and exportomes of Mycobacterium tuberculosis. *Tuberculosis and the Tubercle Bacillus: Second Edition*, *type VII*, 607–625. https://doi.org/10.1128/9781555819569.ch28

Mishra, S. K., Baidya, S., Bhattarai, A., Shrestha, S., Homagain, S., Rayamajhee, B., Hui, A., & Willcox, M. (2024). Bacteriology of endotracheal tube biofilms and antibiotic resistance: a systematic review. *Journal of Hospital Infection*, *147*, 146–157. https://doi.org/10.1016/j.jhin.2024.03.004

Moffatt, J. H., Harper, M., Harrison, P., Hale, J. D. F., Vinogradov, E., Seemann, T., Henry, R., Crane, B., St. Michael, F., Cox, A. D., Adler, B., Nation, R. L., Li, J., & Boyce, J. D. (2010). Colistin resistance in *Acinetobacter baumannii* is mediated by complete loss of lipopolysaccharide production. *Antimicrobial Agents and Chemotherapy*, *54*(12), 4971–4977. https://doi.org/10.1128/AAC.00834-10

Mohammed, M. A., Salim, M. T. A., Anwer, B. E., Aboshanab, K. M., & Aboulwafa, M. M. (2021). Impact of target site mutations and plasmid associated resistance genes acquisition on resistance of *Acinetobacter baumannii* to fluoroquinolones. *Scientific Reports*, *11*(1), 1–16. https://doi.org/10.1038/s41598-021-99230-y

Mohd Sazlly Lim, S., Zainal Abidin, A., Liew, S. M., Roberts, J. A., & Sime, F. B. (2019). The global prevalence of multidrug-resistance among *Acinetobacter baumannii* causing hospital-acquired and ventilator-associated pneumonia and its associated mortality: A

systematic review and meta-analysis. *Journal of Infection*, *79*(6), 593–600. https://doi.org/10.1016/j.jinf.2019.09.012

Montanaro, L., Poggi, A., Visai, L., Ravaioli, S., Campoccia, D., Speziale, P., & Arciola, C. R. (2011). Extracellular DNA in biofilms. *International Journal of Artificial Organs*, *34*(9), 824–831. https://doi.org/10.5301/ijao.5000051

Morris, F. C., Dexter, C., Kostoulias, X., Uddin, M. I., & Peleg, A. Y. (2019). The Mechanisms of Disease Caused by *Acinetobacter baumannii*. *Frontiers in Microbiology*, *10*(JULY), 1601. https://doi.org/10.3389/FMICB.2019.01601/XML/NLM

Moscardini, A., Di Pietro, S., Signore, G., Parlanti, P., Santi, M., Gemmi, M., & Cappello, V. (2020). Uranium-free X solution: a new generation contrast agent for biological samples ultrastructure. *Scientific Reports*, *10*(1), 1–11. https://doi.org/10.1038/s41598-020-68405-4

Murray, C. J., Ikuta, K. S., Sharara, F., Swetschinski, L., Robles Aguilar, G., Gray, A., Han, C., Bisignano, C., Rao, P., Wool, E., Johnson, S. C., Browne, A. J., Chipeta, M. G., Fell, F., Hackett, S., Haines-Woodhouse, G., Kashef Hamadani, B. H., Kumaran, E. A. P., McManigal, B., … Collaborators, A. R. (2022). Global burden of bacterial antimicrobial resistance in 2019: a systematic analysis. *The Lancet*, *399*(10325), 629–655. https://doi.org/10.1016/S0140-6736(21)02724-0

Mussi, M. A., Limansky, A. S., & Viale, A. M. (2005). Acquisition of resistance to carbapenems in multidrug-resistant clinical strains of *Acinetobacter baumannii*: Natural insertional inactivation of a gene encoding a member of a novel family of β-barrel outer membrane proteins. *Antimicrobial Agents and Chemotherapy*, *49*(4), 1432–1440. https://doi.org/10.1128/AAC.49.4.1432-1440.2005

Na, S. H., Jeon, H., Oh, M. H., Kim, Y. J., Chu, M., Lee, I. Y., & Lee, J. C. (2021). Therapeutic effects of inhibitor of ompA expression against carbapenem-resistant *Acinetobacter baumannii* strains. *International Journal of Molecular Sciences*, *22*(22), 12257. https://doi.org/10.3390/ijms222212257

Niu, C., Clemmer, K. M., Bonomo, R. A., & Rather, P. N. (2008). Isolation and characterization of an autoinducer synthase from *Acinetobacter baumannii*. *Journal of Bacteriology*,

190(9), 3386–3392. https://doi.org/10.1128/JB.01929-07

Novović, K., & Jovčić, B. (2023). Colistin Resistance in *Acinetobacter baumannii*: Molecular Mechanisms and Epidemiology. *Antibiotics*, *12*(3), 516. https://doi.org/10.3390/antibiotics12030516

Palethorpe, S., Farrow, J. M., Wells, G., Milton, M. E., Actis, L. A., Cavanagh, J., & Pesci, E. C. (2022). *Acinetobacter baumannii* Regulates Its Stress Responses via the BfmRS Two-Component Regulatory System. *Journal of Bacteriology*, *204*(2), 1–20. https://doi.org/10.1128/jb.00494-21

Park, J., Kim, M., Shin, B., Kang, M., Yang, J., Lee, T. K., & Park, W. (2021). A novel decoy strategy for polymyxin resistance in *Acinetobacter baumannii*. *ELife*, *10*, 1–29. https://doi.org/10.7554/eLife.66988

Parra-Millán, R., Vila-Farrés, X., Ayerbe-Algaba, R., Varese, M., Sánchez-Encinales, V., Bayó, N., Pachón-Ibáñez, M. E., Teixidó, M., Vila, J., Pachón, J., Giralt, E., & Smani, Y. (2018). Synergistic activity of an OmpA inhibitor and colistin against colistin-resistant *Acinetobacter baumannii*: Mechanistic analysis and in vivo efficacy. *Journal of Antimicrobial Chemotherapy*, *73*(12), 3405–3412. https://doi.org/10.1093/jac/dky343

Peleg, A. Y., Seifert, H., & Paterson, D. L. (2008). *Acinetobacter baumannii*: Emergence of a successful pathogen. *Clinical Microbiology Reviews*, *21*(3), 538–582. https://doi.org/10.1128/CMR.00058-07

Pelletier, M. R., Casella, L. G., Jones, J. W., Adams, M. D., Zurawski, D. V., Hazlett, K. R. O., Doi, Y., & Ernst, R. K. (2013). Unique structural modifications are present in the lipopolysaccharide from colistin-resistant strains of *Acinetobacter baumannii*. *Antimicrobial Agents and Chemotherapy*, *57*(10), 4831–4840. https://doi.org/10.1128/AAC.00865-13

Périchon, B., Goussard, S., Walewski, V., Krizova, L., Cerqueira, G., Murphy, C., Feldgarden, M., Wortman, J., Clermont, D., Nemec, A., & Courvalin, P. (2014). Identification of 50 class D β-lactamases and 65 Acinetobacter-derived cephalosporinases in Acinetobacter spp. *Antimicrobial Agents and Chemotherapy*, *58*(2), 936–949. https://doi.org/10.1128/AAC.01261-13

Petrova, O. E., & Sauer, K. (2012). Sticky situations: Key components that control bacterial surface attachment. *Journal of Bacteriology*, *194*(10), 2413–2425. https://doi.org/10.1128/JB.00003-12

Piepenbrink, K. H., Lillehoj, E., Harding, C. M., Labonte, J. W., Zuo, X., Rapp, C. A., Munson, R. S., Goldblum, S. E., Feldman, M. F., Gray, J. J., & Sundberg, E. J. (2016). Structural diversity in the type IV Pili of multidrug-resistant Acinetobacter. *Journal of Biological Chemistry*, *291*(44), 22924–22935. https://doi.org/10.1074/jbc.M116.751099

Pompilio, A., Scribano, D., Sarshar, M., Di Bonaventura, G., Palamara, A. T., & Ambrosi, C. (2021). Gram-negative bacteria holding together in a biofilm: The *Acinetobacter baumannii* way. *Microorganisms*, *9*(7), 1–33. https://doi.org/10.3390/microorganisms9071353

Powers, M. J., & Trent, M. S. (2018). Expanding the paradigm for the outer membrane: *Acinetobacter baumannii* in the absence of endotoxin. *Molecular Microbiology*, *107*(1), 47–56. https://doi.org/10.1111/mmi.13872

Qin, J., Feng, Y., Lü, X., & Zong, Z. (2021). Precise Species Identification for Acinetobacter: a Genome-Based Study with Description of Two Novel Acinetobacter Species. *MSystems*, *6*(3). https://doi.org/10.1128/msystems.00237-21

Queenan, A. M., & Bush, K. (2007). Carbapenemases: The versatile β-lactamases. *Clinical Microbiology Reviews*, *20*(3), 440–458. https://doi.org/10.1128/CMR.00001-07

Quendera, A. P., Seixas, A. F., dos Santos, R. F., Santos, I., Silva, J. P. N., Arraiano, C. M., & Andrade, J. M. (2020). RNA-Binding Proteins Driving the Regulatory Activity of Small Non-coding RNAs in Bacteria. *Frontiers in Molecular Biosciences*, *7*(May), 1–9. https://doi.org/10.3389/fmolb.2020.00078

Rabih O. Darouiche, M. D. (2004). Treatment of infections associated with surgical implants. 2004;350:1422-9. *N Engl J Med*, *350*(14), 1422–1429.

Ren, X., & Palmer, L. D. (2023). Acinetobacter Metabolism in Infection and Antimicrobial Resistance. *Infection and Immunity*, *91*(6). https://doi.org/10.1128/iai.00433-22

Ribera, A., Ruiz, J., & Vila, J. (2003). Presence of the tet M determinant in a clinical isolate of

Acinetobacter baumannii. *Antimicrobial Agents and Chemotherapy*, *47*(7), 2310–2312. https://doi.org/10.1128/AAC.47.7.2310-2312.2003

Richmond, G. E., Evans, L. P., Anderson, M. J., Wand, M. E., Bonney, L. C., Ivens, A., Chua, K. L., Webber, M. A., Mark Sutton, J., Peterson, M. L., & Piddock, L. J. V. (2016). The *Acinetobacter baumannii* two-component system aders regulates genes required for multidrug efflux, biofilm formation, and virulence in a strain-specific manner. *MBio*, *7*(2). https://doi.org/10.1128/mBio.00430-16

Ronish, L. A., Lillehoj, E., Fields, J. K., Sundberg, E. J., & Piepenbrink, K. H. (2019). The structure of PilA from *Acinetobacter baumannii* AB5075 suggests a mechanism for functional specialization in Acinetobacter type IV pili. *Journal of Biological Chemistry*, *294*(1), 218–230. https://doi.org/10.1074/jbc.RA118.005814

Rosenfeld, N., Bouchier, C., Courvalin, P., & Périchon, B. (2012). Expression of the resistance-nodulation-cell division pump AdeIJK in *Acinetobacter baumannii* is regulated by AdeN, a TetR-type regulator. *Antimicrobial Agents and Chemotherapy*, *56*(5), 2504–2510. https://doi.org/10.1128/AAC.06422-11

Roy, S., Chowdhury, G., Mukhopadhyay, A. K., Dutta, S., & Basu, S. (2022). Convergence of Biofilm Formation and Antibiotic Resistance in *Acinetobacter baumannii* Infection. In *Frontiers in Medicine* (Vol. 9, p. 793615). https://doi.org/10.3389/fmed.2022.793615

Runci, F., Gentile, V., Frangipani, E., Rampioni, G., Leoni, L., Lucidi, M., Visaggio, D., Harris, G., Chen, W., Stahl, J., Averhoff, B., & Visca, P. (2019). Contribution of active iron uptake to *Acinetobacter baumannii* pathogenicity. *Infection and Immunity*, *87*(4), 1–16. https://doi.org/10.1128/IAI.00755-18

Saipriya, K., Swathi, C. H., Ratnakar, K. S., & Sritharan, V. (2020). Quorum-sensing system in *Acinetobacter baumannii*: a potential target for new drug development. *Journal of Applied Microbiology*, *128*(1), 15–27. https://doi.org/10.1111/jam.14330

Saleh, N. M., Saad, S. I., El-Sayed, M., El-Sayyad, G. S., & Abo Safe, F. A. (2023). Contribution of different mechanisms to aminoglycoside resistance in clinical isolates of *Acinetobacter baumannii*. *Microbial Pathogenesis*, *182*(July), 106255. https://doi.org/10.1016/j.micpath.2023.106255

Sariyer, E. (2022). The role of *Acinetobacter baumannii* CarO outer membrane protein in carbapenems influx. *Research in Microbiology*, *173*(6–7), 103966. https://doi.org/10.1016/j.resmic.2022.103966

Sauer, K., Camper, A. K., Ehrlich, G. D., Costerton, J. W., & Davies, D. G. (2002). Pseudomonas aeruginosa displays multiple phenotypes during development as a biofilm. *Journal of Bacteriology*, *184*(4), 1140–1154. https://doi.org/10.1128/jb.184.4.1140-1154.2002

Sauer, K., Stoodley, P., Goeres, D. M., Hall-Stoodley, L., Burmølle, M., Stewart, P. S., & Bjarnsholt, T. (2022). The biofilm life cycle: expanding the conceptual model of biofilm formation. *Nature Reviews Microbiology*, *20*(10), 608–620. https://doi.org/10.1038/s41579-022-00767-0

Savage, V. J., Chopra, I., & O'Neill, A. J. (2013). Staphylococcus aureus biofilms promote horizontal transfer of antibiotic resistance. *Antimicrobial Agents and Chemotherapy*, *57*(4), 1968–1970. https://doi.org/10.1128/AAC.02008-12

Schilling, D., Findei, S., Richter, A. S., Taylor, J. A., & Gerischer, U. (2010). The small RNA Aar in Acinetobacter baylyi: A putative regulator of amino acid metabolism. *Archives of Microbiology*, *192*(9), 691–702. https://doi.org/10.1007/s00203-010-0592-6

Serio, A. W., Keepers, T., Andrews, L., & Krause, K. M. (2018). Aminoglycoside Revival: Review of a Historically Important Class of Antimicrobials Undergoing Rejuvenation. *EcoSal Plus*, *8*(1). https://doi.org/10.1128/ecosalplus.esp-0002-2018

Shapiro, J. A., & Wencewicz, T. A. (2016). Acinetobactin Isomerization Enables Adaptive Iron Acquisition in *Acinetobacter baumannii* through pH-Triggered Siderophore Swapping. *ACS Infectious Diseases*, *2*(2), 157–168. https://doi.org/10.1021/acsinfecdis.5b00145

Sharma, A., Dubey, V., Sharma, R., Devnath, K., Gupta, V. K., Akhter, J., Bhando, T., Verma, A., Ambatipudi, K., Sarkar, M., & Pathania, R. (2018). The unusual glycine-rich C terminus of the *Acinetobacter baumannii* RNA chaperone Hfq plays an important role in bacterial physiology. *The Journal of Biological Chemistry*, *293*(35), 13377–13388. https://doi.org/10.1074/JBC.RA118.002921

Sharma, A., Sharma, R., Bhattacharyya, T., Bhando, T., & Pathania, R. (2017). Fosfomycin

resistance in *Acinetobacter baumannii* is mediated by efflux through a major facilitator superfamily (MFS) transporter—AbaF. *Journal of Antimicrobial Chemotherapy*, *72*(1), 68–74. https://doi.org/10.1093/JAC/DKW382

Sharma, R., Arya, S., Patil, S. D., Sharma, A., Jain, P. K., Navani, N. K., & Pathania, R. (2014). Identification of novel regulatory small RNAs in *Acinetobacter baumannii*. *PLoS ONE*, *9*(4), e93833. https://doi.org/10.1371/journal.pone.0093833

Sheldon, J. R., & Skaar, E. P. (2020). *Acinetobacter baumannii* can use multiple siderophores for iron acquisition, but only acinetobactin is required for virulence. In *PLoS Pathogens* (Vol. 16, Issue 10). https://doi.org/10.1371/journal.ppat.1008995

Shenkutie, A. M., Gebrelibanos, D., Yao, M., Hundie, G. B., Chow, F. W. N., & Leung, P. H. M. (2023). Impairment of novel non-coding small RNA00203 inhibits biofilm formation and reduces biofilm-specific antibiotic resistance in *Acinetobacter baumannii*. *International Journal of Antimicrobial Agents*, *62*, 106889. https://doi.org/10.1016/j.ijantimicag.2023.106889

Shenkutie, A. M., Yao, M. Z., Siu, G. K. H., Wong, B. K. C., & Leung, P. H. M. (2020). Biofilm-induced antibiotic resistance in clinical *Acinetobacter baumannii* isolates. *Antibiotics*, *9*(11), 1–15. https://doi.org/10.3390/antibiotics9110817

Shenkutie, A. M., Zhang, J., Yao, M., Asrat, D., Chow, F. W. N., & Leung, P. H. M. (2022). Effects of Sub-Minimum Inhibitory Concentrations of Imipenem and Colistin on Expression of Biofilm-Specific Antibiotic Resistance and Virulence Genes in *Acinetobacter baumannii* Sequence Type 1894. *International Journal of Molecular Sciences*, *23*(20), 12705. https://doi.org/10.3390/ijms232012705

Shimoni, Y., Friedlander, G., Hetzroni, G., Niv, G., Altuvia, S., Biham, O., & Margalit, H. (2007). Regulation of gene expression by small non-coding RNAs: A quantitative view. *Molecular Systems Biology*, *3*(1), 138. https://doi.org/10.1038/msb4100181

Shirakawa, R., Ishikawa, K., Furuta, K., & Kaito, C. (2023). Knockout of ribosomal protein RpmJ leads to zinc resistance in *Escherichia coli*. *PLoS ONE*, *18*(3 March), 1–14. https://doi.org/10.1371/journal.pone.0277162

Singh, R., Pérez-Varela, M., Colquhoun, J. M., Kröger, C., Hamrock, F. J., Shaibah, A., Neidle,

E. L., & Rather, P. N. (2025). CsrA-mediated regulation of a virulence switch in *Acinetobacter baumannii*. *MBio*, *16*(4). https://doi.org/10.1128/mbio.04058-24

Siroy, A., Molle, V., Lemaître-Guillier, C., Vallenet, D., Pestel-Caron, M., Cozzone, A. J., Jouenne, T., & Dé, E. (2005). Channel formation by CarO, the carbapenem resistance-associated outer membrane protein of *Acinetobacter baumannii*. *Antimicrobial Agents and Chemotherapy*, *49*(12), 4876–4883. https://doi.org/10.1128/AAC.49.12.4876-4883.2005

Sonnleitner, E., Gonzalez, N., Sorger-Domenigg, T., Heeb, S., Richter, A. S., Backofen, R., Williams, P., Hüttenhofer, A., Haas, D., & Bläsi, U. (2011). The small RNA PhrS stimulates synthesis of the Pseudomonas aeruginosa quinolone signal. *Molecular Microbiology*, *80*(4), 868–885. https://doi.org/10.1111/j.1365-2958.2011.07620.x

Soper, T., Mandin, P., Majdalani, N., Gottesman, S., & Woodson, S. A. (2010). Positive regulation by small RNAs and the role of Hfq. *Proceedings of the National Academy of Sciences of the United States of America*, *107*(21), 9602–9607. https://doi.org/10.1073/pnas.1004435107

Stahl, J., Bergmann, H., Göttig, S., Ebersberger, I., & Averhoff, B. (2015). *Acinetobacter baumannii* virulence is mediated by the concerted action of three phospholipases D. *PLoS ONE*, *10*(9), 1–19. https://doi.org/10.1371/journal.pone.0138360

Stenum, T. S., Kumar, A. D., Sandbaumhüter, F. A., Kjellin, J., Jerlström-Hultqvist, J., AndrCrossed D Sign©n, P. E., Koskiniemi, S., Jansson, E. T., & Holmqvist, E. (2023). RNA interactome capture in *Escherichia coli* globally identifies RNA-binding proteins. *Nucleic Acids Research*, *51*(9), 4572–4587. https://doi.org/10.1093/nar/gkad216

Storz, G., Vogel, J., & Wassarman, K. M. (2011). Regulation by Small RNAs in Bacteria: Expanding Frontiers. *Molecular Cell*, *43*(6), 880–891. https://doi.org/10.1016/j.molcel.2011.08.022

Sugimoto, S., Arita-Morioka, K. ichi, Terao, A., Yamanaka, K., Ogura, T., & Mizunoe, Y. (2018). Multitasking of Hsp70 chaperone in the biogenesis of bacterial functional amyloids. *Communications Biology*, *1*(1), 2–15. https://doi.org/10.1038/s42003-018-0056-0

Tamura, K., Stecher, G., & Kumar, S. (2021). *MEGA11 : Molecular Evolutionary Genetics*

Analysis Version 11. *38*(7), 3022–3027. https://doi.org/10.1093/molbev/msab120

Tang, J., Chen, Y., Wang, X., Ding, Y., Sun, X., & Ni, Z. (2020). Contribution of the abaI/abaR quorum sensing system to resistance and virulence of *Acinetobacter baumannii* clinical strains. *Infection and Drug Resistance*, *13*, 4273–4281. https://doi.org/10.2147/IDR.S276970

Taylor, E., Jauneikaite, E., Sriskandan, S., Woodford, N., & Hopkins, K. L. (2022). Novel 16S rRNA methyltransferase RmtE3 in *Acinetobacter baumannii* ST79. *Journal of Medical Microbiology*, *71*(5), 1–6. https://doi.org/10.1099/jmm.0.001531

Tiku, V. (2022). *Acinetobacter baumannii*: Virulence Strategies and Host Defense Mechanisms. *DNA and Cell Biology*, *41*(1), 43–48. https://doi.org/10.1089/dna.2021.0588

Tipton, K. A., Chin, C. Y., Farokhyfar, M., Weiss, D. S., & Rathera, P. N. (2018). Role of capsule in resistance to disinfectants, host antimicrobials, and desiccation in *Acinetobacter baumannii*. *Antimicrobial Agents and Chemotherapy*, *62*(12). https://doi.org/10.1128/AAC.01188-18

Tipton, K. A., & Rather, P. N. (2017). An ompRenvZ two-component system ortholog regulates phase variation, osmotic tolerance, motility, and virulence in *Acinetobacter baumannii* strain AB5075. *Journal of Bacteriology*, *199*(3), 1–16. https://doi.org/10.1128/JB.00705-16

Tiwari, V., Vashistt, J., Kapil, A., & Moganty, R. R. (2012). Comparative proteomics of inner membrane fraction from Carbapenem-resistant *Acinetobacter baumannii* with a reference strain. *PLoS ONE*, *7*(6). https://doi.org/10.1371/journal.pone.0039451

Tjaden, B. (2023). TargetRNA3: predicting prokaryotic RNA regulatory targets with machine learning. *Genome Biology*, *24*(1), 1–13. https://doi.org/10.1186/s13059-023-03117-2

Tomaras, A. P., Flagler, M. J., Dorsey, C. W., Gaddy, J. A., & Actis, L. A. (2008). Characterization of a two-component regulatory system from *Acinetobacter baumannii* that controls biofilm formation and cellular morphology. *Microbiology*, *154*(11), 3398–3409. https://doi.org/10.1099/mic.0.2008/019471-0

Tong, C., Liang, Y., Zhang, Z., Wang, S., Zheng, X., Liu, Q., & Song, B. (2023). Review of knockout technology approaches in bacterial drug resistance research. *PeerJ*, *11*. https://doi.org/10.7717/peerj.15790

Trapnell, C., Williams, B. A., Pertea, G., Mortazavi, A., Kwan, G., van Baren, M. J., Salzberg, S. L., Wold, B. J., & Pachter, L. (2011). Transcript assembly and abundance estimation from RNA-Seq reveals thousands of new transcripts and switching among isoforms. *Nature Biotechnology*, *28*(5), 511–515. https://doi.org/10.1038/nbt.1621.Transcript

Tucker, A. T., Nowicki, E. M., Boll, J. M., Knauf, G. A., Burdis, N. C., Stephen Trent, M., & Davies, B. W. (2014). Defining gene-phenotype relationships in *Acinetobacter baumannii* through one-step chromosomal gene inactivation. *MBio*, *5*(4), 1–9. https://doi.org/10.1128/mBio.01313-14

Uppalapati, S. R., Sett, A., & Pathania, R. (2020). The Outer Membrane Proteins OmpA, CarO, and OprD of *Acinetobacter baumannii* Confer a Two-Pronged Defense in Facilitating Its Success as a Potent Human Pathogen. *Frontiers in Microbiology*, *11*(October), 2441. https://doi.org/10.3389/fmicb.2020.589234

Vashist, J., Tiwari, V., Das, R., Kapil, A., & Rajeswari, M. R. (2011). Analysis of penicillin-binding proteins (PBPs) in carbapenem resistant *Acinetobacter baumannii*. *Indian Journal of Medical Research*, *133*(3), 332–338.

Vesel, N., & Blokesch, M. (2021). Pilus production in *Acinetobacter baumannii* is growth phase dependent and essential for natural transformation. *Journal of Bacteriology*, *203*(8). https://doi.org/10.1128/JB.00034-21

Vijayakumar, S., Biswas, I., & Veeraraghavan, B. (2019). Accurate identification of clinically important Acinetobacter spp.: An update. *Future Science OA*, *5*(7). https://doi.org/10.2144/fsoa-2018-0127

Wang, N., Gao, J., Xiao, S., & Zhuang, G. (2022). Overexpression of pdeR promotes biofilm formation of *Paracoccus denitrificans* by promoting ATP production and iron acquisition. *Frontiers in Microbiology*, *13*(August), 1–12. https://doi.org/10.3389/fmicb.2022.966976

Wang, Y., Wang, Z., & Ji, Q. (2020). CRISPR-Cas9-Based Genome Editing and Cytidine Base

Editing in *Acinetobacter baumannii*. *STAR Protocols*, *1*(1), 100025. https://doi.org/10.1016/j.xpro.2020.100025

Waters, S. A., McAteer, S. P., Kudla, G., Pang, I., Deshpande, N. P., Amos, T. G., Leong, K. W., Wilkins, M. R., Strugnell, R., Gally, D. L., Tollervey, D., & Tree, J. J. (2017). Small RNA interactome of pathogenic *Escherichia coli* revealed through crosslinking of RN ase E. *The EMBO Journal*, *36*(3), 374–387. https://doi.org/10.15252/embj.201694639

Weber, B. S., Kinsella, R. L., Harding, C. M., & Feldman, M. F. (2017). The Secrets of Acinetobacter Secretion. *Trends in Microbiology*, *25*(7), 532–545. https://doi.org/10.1016/j.tim.2017.01.005

Weiss, A., Broach, W. H., Lee, M. C., & Shaw, L. N. (2016). Towards the complete small RNome of *Acinetobacter baumannii*. *Microbial Genomics*, *2*(3), 1–18. https://doi.org/10.1099/mgen.0.000045

Whitehead, N. A., Barnard, A. M. L., Slater, H., Simpson, N. J. L., & Salmond, G. P. C. (2001). Quorum-sensing in Gram-negative bacteria. *FEMS Microbiol Rev* ., *25*.

WHO. (2024). WHO bacterial priority pathogens list. https://scholar.google.com/scholar_lookup?title=WHO bacterial priority pathogens list&publication_year=2024&

Winkler, K., Karner, A., Horner, A., Hannesschlaeger, C., Knyazev, D., Siligan, C., Zimmermann, M., Kuttner, R., Pohl, P., & Preiner, J. (2020). Interaction of the motor protein SecA and the bacterial protein translocation channel SecYEG in the absence of ATP. *Nanoscale Advances*, *2*(8), 3431–3443. https://doi.org/10.1039/d0na00427h

Wong, D., Nielsen, T. B., Bonomo, R. A., Pantapalangkoor, P., Luna, B., & Spellberg, B. (2017). Clinical and pathophysiological overview of Acinetobacter infections: A century of challenges. *Clinical Microbiology Reviews*, *30*(1), 409–447. https://doi.org/10.1128/CMR.00058-16

Wong, M. H. yin, Chan, B. K. wai, Chan, E. W. chi, & Chen, S. (2019). Over-Expression of ISAba1-Linked Intrinsic and Exogenously Acquired OXA Type Carbapenem-Hydrolyzing-Class D-ß-Lactamase-Encoding Genes Is Key Mechanism Underlying Carbapenem Resistance in *Acinetobacter baumannii*. *Frontiers in Microbiology*, *10*(December), 1–9.

https://doi.org/10.3389/fmicb.2019.02809

World Health Organization (WHO). (2017). Prioritization of Pathogens to Guide Discovery, Research and Development of New Antibiotics for Drug-Resistant Bacterial Infections, Including Tuberculosis. In *WHO Bulletin* (Vol. 13, Issue 1). https://apps.who.int/iris/handle/10665/311820

Xiong, L., Yi, F., Yu, Q., Huang, X., Ao, K., Wang, Y., & Xie, Y. (2022). Transcriptomic analysis reveals the regulatory role of quorum sensing in the *Acinetobacter baumannii* ATCC 19606 via RNA-seq. *BMC Microbiology*, *22*(1), 1–12. https://doi.org/10.1186/S12866-022-02612-Z/TABLES/3

Yang, R., Lai, B., Liao, K., Liu, B., Huang, L., Li, S., Gu, J., Lin, Z., Chen, Y., Wang, S., Qiu, Y., Deng, J., Chen, S., Zhuo, C., & Zhou, Y. (2022). Overexpression of BIT33_RS14560 Enhances the Biofilm Formation and Virulence of *Acinetobacter baumannii*. *Frontiers in Microbiology*, *13*(April), 867770. https://doi.org/10.3389/fmicb.2022.867770

Yoon, E. J., Chabane, Y. N., Goussard, S., Snesrud, E., Courvalin, P., Dé, E., & Grillot-Courvalin, C. (2015). Contribution of resistance-nodulation-cell division efflux systems to antibiotic resistance and biofilm formation in *Acinetobacter baumannii*. *MBio*, *6*(2). https://doi.org/10.1128/mBio.00309-15

Yoon, E. J., Courvalin, P., & Grillot-Courvalin, C. (2013). RND-type efflux pumps in multidrug-resistant clinical isolates of *Acinetobacter baumannii*: Major role for AdeABC overexpression and aders mutations. *Antimicrobial Agents and Chemotherapy*, *57*(7), 2989–2995. https://doi.org/10.1128/AAC.02556-12

Zack, K. M., Sorenson, T., & Joshi, S. G. (2024). Types and Mechanisms of Efflux Pump Systems and the Potential of Efflux Pump Inhibitors in the Restoration of Antimicrobial Susceptibility, with a Special Reference to *Acinetobacter baumannii*. *Pathogens*, *13*(3), 197. https://doi.org/10.3390/pathogens13030197

Zahn, M., D'Agostino, T., Eren, E., Baslé, A., Ceccarelli, M., & Van Berg, B. Den. (2015). Small-molecule transport by CarO, an abundant eight-stranded β-barrel outer membrane protein from *Acinetobacter baumannii*. *Journal of Molecular Biology*, *427*(14), 2329–2339. https://doi.org/10.1016/j.jmb.2015.03.016

Zapun, A., Contreras-Martel, C., & Vernet, T. (2008). Penicillin-binding proteins and β-lactam resistance. *FEMS Microbiology Reviews*, *32*(2), 361–385. https://doi.org/10.1111/j.1574-6976.2007.00095.x

Zeighami, H., Valadkhani, F., Shapouri, R., Samadi, E., & Haghi, F. (2019). Virulence characteristics of multidrug resistant biofilm forming *Acinetobacter baumannii* isolated from intensive care unit patients. *BMC Infectious Diseases*, *19*(1), 1–9. https://doi.org/10.1186/s12879-019-4272-0

Zhang, A., Wassarman, K. M., Rosenow, C., Tjaden, B. C., Storz, G., & Gottesman, S. (2003). Global analysis of small RNA and mRNA targets of Hfq. *Molecular Microbiology*, *50*(4), 1111–1124. https://doi.org/10.1046/j.1365-2958.2003.03734.x

Zhao, A., Sun, J., & Liu, Y. (2023). Understanding bacterial biofilms: From definition to treatment strategies. *Frontiers in Cellular and Infection Microbiology*, *13*(April), 1–23. https://doi.org/10.3389/fcimb.2023.1137947

Zhu, Y., Ponath, F., Cosi, V., & Vogel, J. (2024). A global survey of small RNA interactors identifies KhpA and KhpB as major RNA-binding proteins in Fusobacterium nucleatum. *Nucleic Acids Research*, *52*(7), 3950–3970. https://doi.org/10.1093/nar/gkae010